THÈSE

Présentée devant l'Université de Lorraine

pour l'obtention du grade de

DOCTEUR DE L'UNIVERSITÉ DE LORRAINE

Ecole doctorale EMMA

Spécialité: Chimie du Solide

par

Weigang ZHAO

SYNTHÈSE ET CARACTÉRISATION DE MATÉRIAUX CARBONÉS MICROPOREUX POUR LE STOCKAGE DE L'HYDROGÈNE

Sous la responsabilité d'Alain CELZARD et Vanessa FIERRO

Soutenue publiquement le 9 octobre 2012 devant la Commission d'examen

Rapporteurs :

M. Phillip LLEWELLYN, Directeur de Recherches CNRS

M. Roger GADIOU, Maître de Conférences, Université de Haute Alsace

Examinateurs:

M. Michel LATROCHE, Directeur de Recherches CNRS

Mme Maria Teresa IZQUIERDO, Chargée de Recherches, Université de Saragosse

Mme Vanessa FIERRO, Chargée de Recherches CNRS

M. Alain CELZARD, Professeur, Université de Lorraine

Thèse préparée à l'Institut Jean Lamour – UMR CNRS 7198, sur le Campus Fibres d'Epinal.

Remerciements

This thesis could not have been finished without the full support and assistance from advisors, colleagues, friends and family members.

First, I would like to express my deep sense of gratitude to my advisors, Prof. Alain CELZARD and Dr. Vanessa FIERRO for giving me the opportunity to do this project, also giving me great personal support especially when I arrived in France. They brought me to the wholly new research area of hydrogen storage. They demonstrated that persistence and hard work are the basic requirements to accomplish a research goal. Their broad knowledge of science and creative thoughts in research has inspired me throughout my study.

Special thanks go to Prof. Guanben DU, who is the advisor for my master diploma, and also to Prof. Antonio Pizzi and Dr. G Tondi. The value of their assistance is inestimable.

Thanks to my Friends: Andrzej, Paola and Jerome, Cesar and Karin, Gisele, Flavia, Hong, Xinjun, Xiaojian. It was a pleasure to meet you in ENSTIB.

Last, but not least, I thank my beloved family: my parents, my wife and my sisters, for their love, full support, and encouragement over these years. It would not have been possible to finish my Ph.D. without their support.

Table des matières

Introduction

L'hydrogène est un élément remarquable en ce que la molécule H_2 est un vecteur énergétique potentiel non polluant pour les applications automobiles et stationnaires. Sa combustion dans l'air ne produit en effet que de la vapeur d'eau. Ce gaz nécessite néanmoins, avant de pouvoir devenir l'élément clé d'un modèle économique futur, le développement d'une infrastructure particulière. Cette dernière est constituée de cinq éléments : production, distribution, stockage, conversion et application, qui sont à des stades inégaux de développement et de maîtrise technologique. La problématique du stockage qui nous intéresse ici est d'une importance cruciale pour l'établissement d'une économie basée sur l'hydrogène. En effet, l'hydrogène a un potentiel énergétique qui est très élevé s'il est exprimé par unité de masse mais très faible par unité de volume, environ trois fois plus et quatre fois moins, respectivement, que celui des combustibles liquides traditionnels. Il est donc essentiel de pouvoir stocker suffisamment d'hydrogène dans le plus petit volume possible, tout en veillant à la sécurité. Lorsque les applications transport sont visées, il faut en plus minimiser le poids du système de stockage.

Ces dernières années, différentes méthodes pour stocker l'hydrogène ont été développées et évaluées, telles que la liquéfaction, la compression de gaz, la formation d'hydrures métalliques ou complexes, et l'adsorption sur des matériaux hautement poreux (nanostructures carbonées, réseaux métallo-organiques (metal-organic frameworks : MOFs), zéolithes et polymères poreux). Cependant, aucune d'entre elles n'a montré de vrai potentiel pour atteindre la cible définie par le Département Américain à l'Energie (US DOE) de 5.5% massique et 40 kg/L. Le charbon actif pourrait être un adsorbant convenable en raison de son aire spécifique très élevée et de sa porosité pouvant être tout à la fois contrôlable et extrêmement étroite. Par ailleurs, les capacités d'adsorption augmentent significativement quand la température est abaissée, par exemple à 77K.

Dans cette thèse, la thématique du stockage d'hydrogène sur des charbons actifs optimises pour cette application est abordée. Les matériaux adsorbants ont été

préparés, caractérisés et optimisés dans l'équipe de l'IJL installée à Epinal, dans les locaux de l'ENSTIB. La détermination des capacités d'adsorption d'hydrogène de ces matériaux a été faite dans deux autres laboratoires : d'une part à l'ICMPE – Thiais avec une méthode volumétrique à 77K et 298K, d'autre part à l'ICB – Saragosse avec une méthode gravimétrique à 77K. Pour ce faire, une partie des échantillons a été envoyée dans chacun de ces deux laboratoires, mais plusieurs stages ont été faits à l'ICMPE afin de nous familiariser avec les techniques utilisées et étudier nous-mêmes nos matériaux. Ces derniers sont essentiellement issus d'un même précurseur, l'anthracite chinois Taisi, en raison de sa disponibilité commerciale, de son faible coût, et de son excellent comportement en activation chimique. Des charbons actifs hautement microporeux et ayant des surfaces BET apparentes de plus de 3 000 m^2/g peuvent ainsi être obtenus, a priori favorables pour bien adsorber l'hydrogène et par conséquent s'approcher de la cible de l'US DOE.

Ce travail a été réalisé en quatre étapes principales:

(1) Etude et compréhension des conditions expérimentales de préparation des charbons actifs dérivés d'anthracite Taisi sur leur porosité. Dans ce but, les agents d'activation NaOH et KOH ont été particulièrement étudiés en termes de rapport massique hydroxyde / anthracite (variant de 1.5 à 7), de température de traitement (entre 973 et 1073 K), et de vitesse de chauffe (1, 3 et 5 K/min). L'analyse statistique a été utilisée pour déterminer quels paramètres expérimentaux sont vraiment significatifs.

(2) Optimisation de la texture poreuse des charbons actifs pour le stockage d'hydrogène. A partir des précédents résultats, les conditions expérimentales permettant de préparer les matériaux présentant les plus hautes surfaces spécifiques et/ou les volumes microporeux les plus développés ont été identifiées. Des maxima de textures poreuses ont pu être mis en évidence en fonction des paramètres de synthèse, à partir desquels les adsorbants correspondants ont été sélectionnés pour être testés en stockage d'hydrogène.

(3) Etude des corrélations entre capacité de stockage d'hydrogène et paramètres texturaux des charbons actifs. Cette partie s'est intéressée à l'impact de l'aire spécifique, des volumes microporeux et des distributions de tailles de pores sur les capacités de stockage d'hydrogène mesurées dans différentes conditions. Nous avons mis en œuvre des méthodes statistiques pour évaluer l'effet des deux principales variables de synthèse, la température et le rapport massique hydroxyde/anthracite, pour prédire les capacités de stockage des adsorbants résultants.

(4) Etude du dopage des charbons actifs par de l'azote et de nanoparticules métalliques de Pd, de manière à essayer d'en améliorer les performances en stockage de d'hydrogène.

Ce mémoire est donc présenté « par articles ». Cette manière de procéder présente des avantages et quelques inconvénients. Elle permet de présenter un travail abouti et concis, allant à l'essentiel, et déjà jugé « par les pairs » puisque les publications ont déjà été pour la plupart acceptées dans des revues de rang A avec comité de lecture. Elle permet donc de réduire considérablement le nombre de pages à rédiger, afin d'éviter les redondances. Par contre, elle ne rend nécessairement bien compte du travail fourni, puisque les articles ne présentent que les résultats les plus marquants, sans faire allusion ni aux développements implicites qu'il a fallu faire, ni aux résultats de moindre importance, mais néanmoins intéressants, qui ont été obtenus.

Ce mémoire est organisé comme suit. Après cette introduction, un résumé d'une vingtaine de pages est donné. Il permet au lecteur d'entrevoir toute la démarche intellectuelle et expérimentale de la thèse. Les chapitres suivants sont rédigés en anglais. Le Chapitre 1 fait l'état de l'art sur le stockage de l'hydrogène, les charbons actifs en général, et leur application à l'adsorption d'hydrogène en particulier. Il présente les concepts de base qui seront utilisés dans la suite du mémoire, et notamment dans les publications scientifiques. Le Chapitre 2 décrit les méthodes expérimentales mises en œuvre dans cette thèse, en ce qui concerne la préparation des adsorbants et la caractérisation de leur porosité et de leurs capacités de stockage. Le

Chapitre 3 regroupe les publications parues ou soumises, en anglais toujours. Elles sont néanmoins précédées d'un résumé d'une page en français. Le mémoire se termine par la liste des références bibliographiques et par une conclusion générale.

Résumé de la thèse

Cette partie du mémoire résume quelle démarche a été la notre au cours de cette thèse, et résume les principaux résultats obtenus.

Ce travail est le résultat d'une collaboration fructueuse entre trois laboratoires : un laboratoire espagnol, l'Instituto de Carboquimica (ICB-CSIC) à Saragosse (Espagne), et deux laboratoires français, l'Institut de Chimie et des Matériaux Paris-Est (ICMPE – UMR CNRS 7182) et l'Institut Jean Lamour (IJL – UMR CNRS 7198) sur le site de l'ENSTIB à Epinal. L'IJL a apporté son expertise dans la synthèse et la caractérisation de charbons actifs hautement microporeux préparés par activation d'anthracites avec des hydroxydes alcalins. L'ICB et l'ICMPE ont apporté leur expertise dans la mesure des capacités de stockage d'hydrogène mais aussi dans d'autres types de caractérisations qui n'existent pas à l'IJL.

Le stockage de l'hydrogène par adsorption a fait l'objet de nombreuses études dans toutes sortes de matériaux carbonés. Des capacités très diverses, parfois contradictoires, ont été rapportées. Nous avons utilisé un anthracite d'origine chinoise, « Taisi », comme précurseur de charbons dont nous avons essayé d'optimiser la microporosité pour le stockage d'hydrogène. Les anthracites sont des matériaux naturels dont l'activation chimique par des hydroxydes alcalins conduit à des charbons actifs hautement microporeux. Leurs performances exceptionnelles en termes de stockage du méthane par adsorption avaient fait l'objet d'un certain nombre de publications par notre groupe à Nancy. Tout portait alors à croire que ces matériaux pourraient également convenir, moyennant une adaptation de leur procédé d'activation, à l'adsorption d'hydrogène.

L'activation est le procédé par lequel la porosité d'un solide carboné est à la fois ouverte et développée. Le matériau résultant, dit charbon actif, peut présenter une surface spécifique jusqu'à environ 3000 m^2/g. C'est en général un excellent adsorbant qui est utilisé comme tel dans de nombreux procédés industriels. Si le précurseur est déjà un carbone, les pores peuvent être créés par gazéification contrôlée, en faisant passer un gaz oxydant sur le matériau à haute température. On parle alors d'activation physique, le gaz étant du CO_2 ou de la vapeur d'eau. Si le précurseur est un matériau organique ou un charbon minéral, il peut être imprégné d'un agent qui sera à la fois déshydratant et oxydant à haute température. On parle alors d'activation chimique, l'agent activant étant NaOH ou H_3PO_4, par exemple. Les deux types d'activation ne

conduisent pas au même type de porosité, d'où leur intérêt, selon le résultat souhaité. La Figure 1 montre un modèle de structure de carbone activé, avec le classement des pores selon leurs tailles et tel que défini par l'IUPAC.

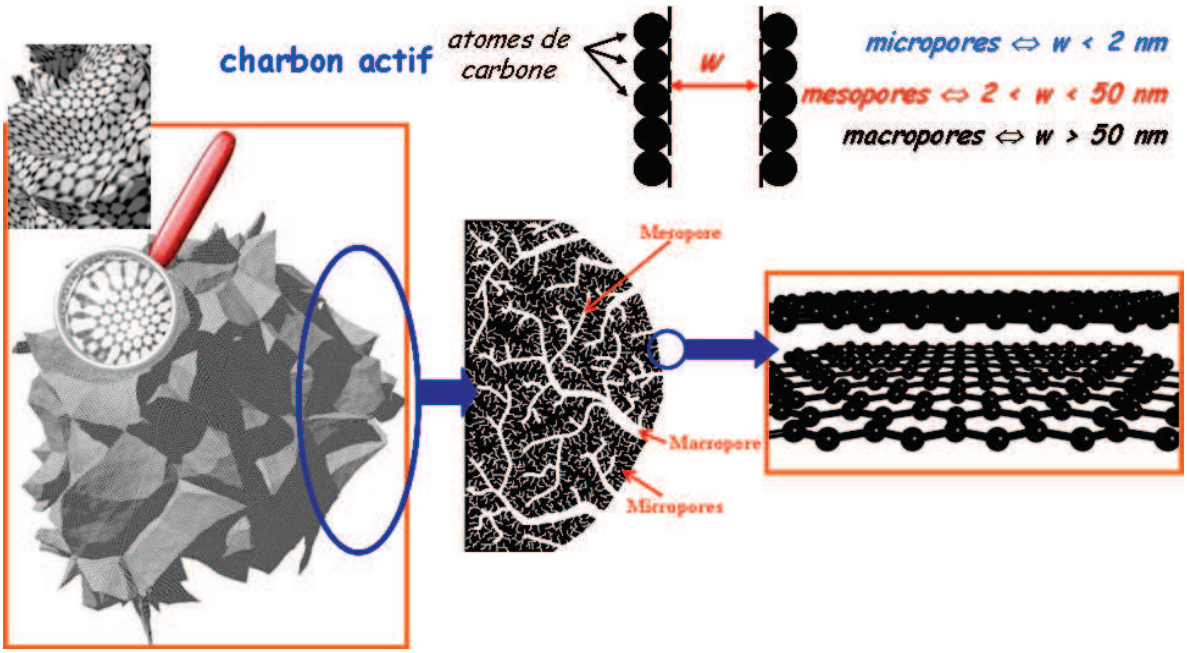

Fig. 1 : Modèle dit « du papier froissé », décrivant la structure poreuse hiérarchisée d'un charbon actif.

Le contexte de l'étude étant posé, et ces quelques rappels étant faits, nous allons maintenant résumer les différents résultats obtenus, publication par publication.

- **Contributions de l'adsorption et de la compression à la capacité de stockage d'hydrogène des anthracites activés (article 1)**

Nous avons réalisé une étude systématique de l'effet des conditions d'activation de l'anthracite chinois « Taisi » sur sa structure poreuse et sa capacité de stockage de l'hydrogène. En augmentant la température d'activation, l'aire spécifique BET, S_{BET}, la microporosité et la capacité de stockage d'hydrogène augmentent également. Le même phénomène est observé lorsqu'on augmente le rapport activant/anthracite de 1.5 à 2.5. KOH est meilleur activant est NaOH. La Figure 2 montre une corrélation directe entre la capacité de stockage par adsorption de H_2 à 77K et la S_{BET} jusqu'à la valeur théorique de 2630 m^2/g. On peut aussi observer qu'il est possible d'obtenir des charbons plus performants par activation avec du KOH.

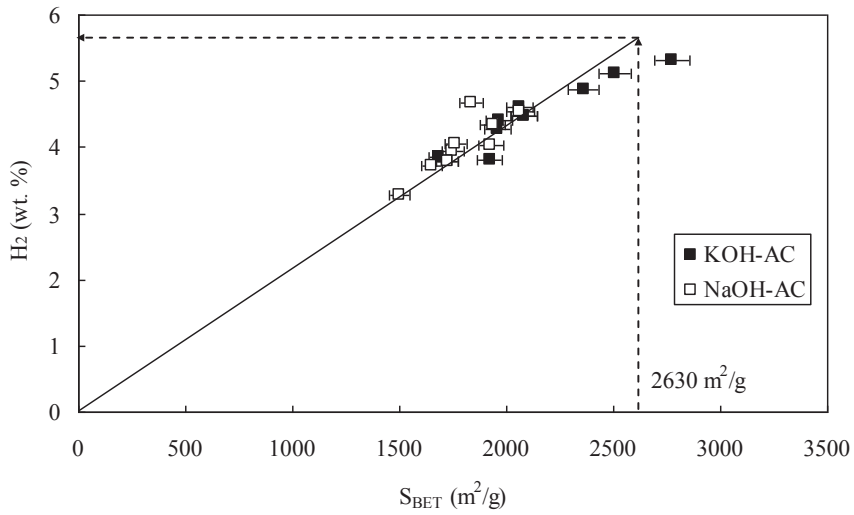

Fig. 2 : Variation de la capacité de stockage d'hydrogène à 77K en fonction de la S_{BET}.

De cette étude, nous avons pu aussi conclure que le stockage de H_2 à très haute pression et à 77K présente peu d'intérêt. Les Figures 3 et 4 présentent, sur le même type de graphe, à 298K et à 77K respectivement: la quantité de H_2 adsorbé, la quantité de H_2 qui serait stocké par compression dans le même volume vide, et le pourcentage de capacité de stockage ainsi gagné par la présence du charbon. A 298K, le gain maximal par rapport à la seule compression est de 30% à 3 MPa. A 77K, le gain maximal est d'environ 3000% à une pression inférieure à 1MPa.

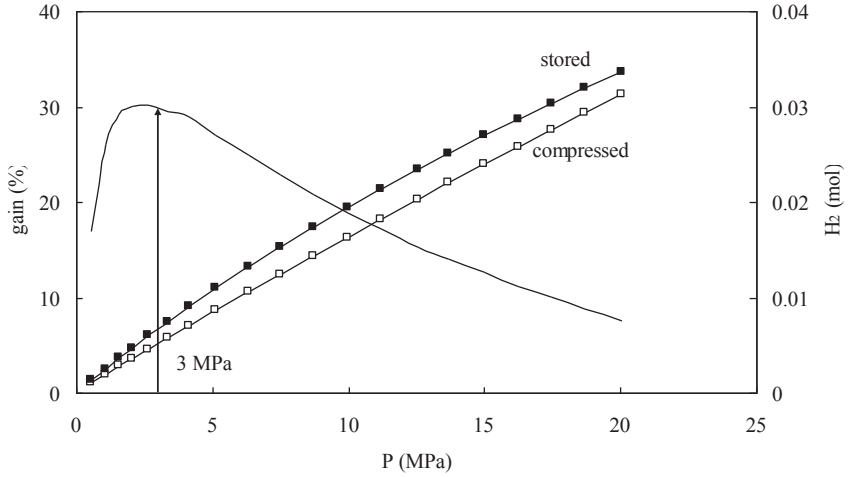

Fig. 3 : Variation de la quantité de H_2 stocké (■) et comprimé (□) dans le réservoir à 298K avec la pression. La ligne continue montre le pourcentage de H_2 gagné par adsorption.

La quantité d'hydrogène adsorbé à 77K est maximale à 4MPa, et le gain à cette pression est encore de 100%. En augmentant la pression au-delà de 4MPa, on

n'augmente que la quantité de H_2 stocké par compression, d'où une perte rapide du gain. Il est même nettement désavantageux d'utiliser du charbon aux pressions supérieures à 7 – 8 MPa.

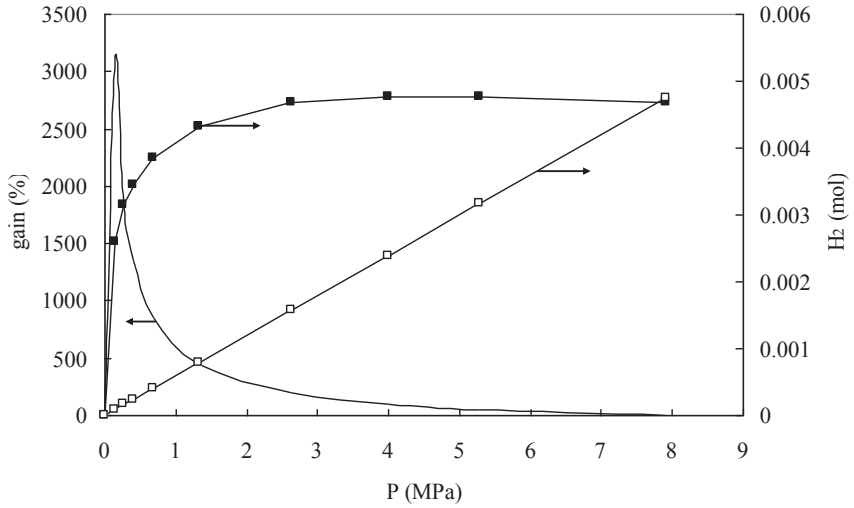

Fig. 4 : Variation de la quantité de H_2 stocké (■) et comprimé (□) dans le réservoir à 77K avec la pression. La ligne continue montre le pourcentage de H_2 gagné par adsorption.

- **Charbons actifs avec une distribution de pores adéquate pour le stockage de l'hydrogène (articles 2 et 3)**

Nous avons comparé les capacités de stockage de quelques-uns de nos charbons à celles d'autres charbons actifs bien connus : (i) trois charbons microporeux de Kansai Coke and Chemicals Co., Ltd. (Japon): MAXSORB-3 (connu auparavant sous le nom d'AX21), MAXSORB-30 and MSC 25; (ii) deux charbons mésoporeux: Black Pearls 71 (BP71) et CXV de CECA (filiale d'Arkema, France); et (iii) un tamis moléculaire de Takeda Chem. Ind. (Japan): CMS 4A.

La Figure 5 montre la corrélation entre S_{BET} et la capacité de stockage d'hydrogène à 77K et 4MPa. Nos charbons sont toujours meilleurs pour une S_{BET} équivalente. Les performances de nos carbones activés peuvent être expliquées par une distribution de pores (PSD) plus adéquate pour des S_{BET} équivalentes.

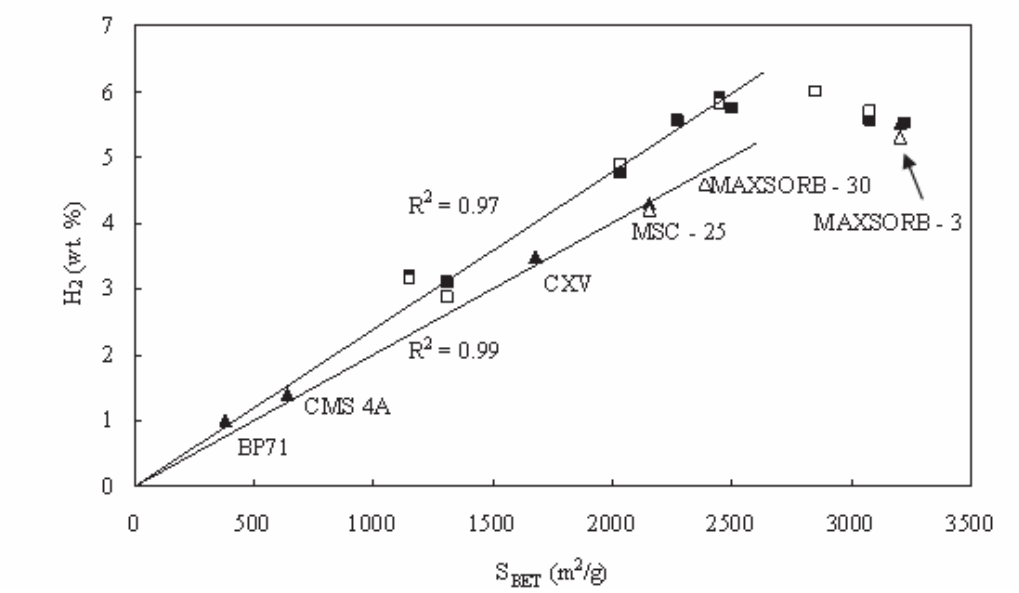

Fig. 5 : Capacité de stockage d'hydrogène en excès pour les six charbons commerciaux (triangles) et neuf de nos charbons (carrés) à 77K et 4MPa, en fonction de la S_{BET}. Les symboles pleins et vides correspondent aux mesures faites sur le dispositif gravimétrique et volumétrique respectivement.

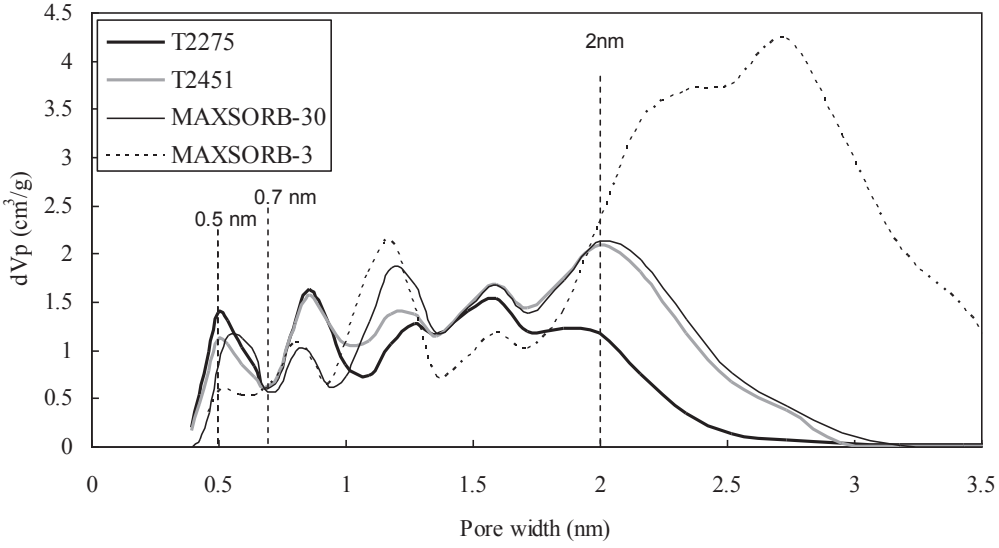

Fig. 6 : Distribution de tailles de pores pour deux de nos charbons (T2275 et T2451) et pour deux charbons commerciaux (MAXSORB-3 et MAXSORB-30).

La Figure 6 présente les PSD obtenues par application du modèle DFT aux isothermes de N_2 pour les charbons T2275 (2275 m^2/g), T2451 (2451 m^2/g) et MAXSORB-30 (2387 m^2/g). Les deux charbons T2275 et T2451ont été choisis parce qu'ils ont des surfaces similaires à celle du MAXSORB-30, ce dernier ayant une surface intermédiaire. La PSD du charbon MAXSORB-3 (3203 m^2/g), qui a la capacité de stockage d'hydrogène la plus élevée des charbons commerciaux, a été

aussi représentée. La Figure 6 montre que nos charbons actifs ont la plus grande proportion de pores ayant un diamètre autour de 0.85 nm. La PSD du MAXSORB-3 est plus déplacée vers les diamètres de pores plus larges que celle du MAXSORB-30. Malgré cela, l'adsorption d'hydrogène sur le MAXSORB-3 est plus élevée que sur le MAXSORB-30.

Plusieurs auteurs ont suggéré qu'il existe un diamètre optimal pour le stockage d'hydrogène: 0.5-0.7 nm, 0.68 nm, 0.7 nm or 0.71 nm. Nous avons trouvé que les charbons qui ont la plus haute capacité pour le stockage d'hydrogène n'ont pas une PSD centrée sur 0.7nm, mais cela ne veut pas dire que ce ne soit pas le diamètre optimal. Ce fait suggère que les pores plus grands contribuent aussi au stockage d'hydrogène. Pour prouver cela, nous avons premièrement calculé le volume de pores dans quatre intervalles de diamètres : < 0.5 nm (ultramicropores); 0.5-0.7 nm (ultramicropores); 0.7-2 nm (supermicropores) and 2-50 nm (mesopores). Nous avons décidé de diviser l'intervalle d'ultramicropores en deux pour étudier l'effet du diamètre de pore optimal. Ensuite, la contribution de chaque intervalle de diamètres à la capacité de stockage totale a été estimée en ajustant les données d'adsorption à l'expression linéaire suivante:

$$\mathrm{H_2\ excessuptake} = \sum_i x_i\, V_i$$

où x_i (wt. % g cm^{-3}) et V_i (cm^3 g^{-1}) sont le coefficient de pondération et le volume des pores dans le i^{ème} intervalle de largeur de pore, respectivement. En utilisant $i = 4$ (voir précédemment), cette équation a été utilisée pour corréler les données de tous les charbons utilisés dans ce travail. La Figure 7 montre qu'il existe un très bon accord entre les capacités de stockage mesurées et ainsi prédites.

Les coefficients de pondération donnés dans la Figure 7 permettent de calculer la contribution de chaque intervalle de pore à la capacité totale de stockage par excès. Ces contributions sont montrées dans la Figure 8. On peut observer que : (i) quoique la taille de pores optimale soit voisine de 0.7nm, il faut, pour réussir à obtenir des capacités de stockage supérieures à 4%, avoir des pores avec un diamètre plus large que 0.7nm ; (ii) le développement de l'aire spécifique est toujours accompagné par un élargissement du diamètre des pores mais nos charbons activés montrent des capacités de stockage d'hydrogène supérieures parce que, pour des S_{BET} similaires, ils ont une PSD plus étroite; (iii) des charbons actifs avec des PSD plus déplacées vers les pores

plus larges peuvent avoir des capacités de stockage d'hydrogène supérieures s'ils conservent un volume de micropores élevé.

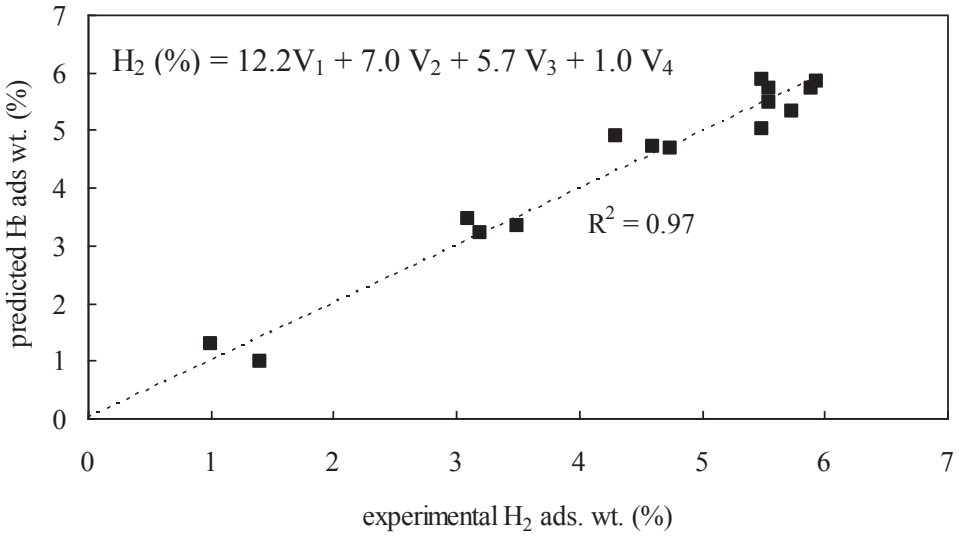

Fig. 7 : Corrélation entre les capacités de stockage d'hydrogène mesurées et prédites par l'équation qui est donnée dans la figure.

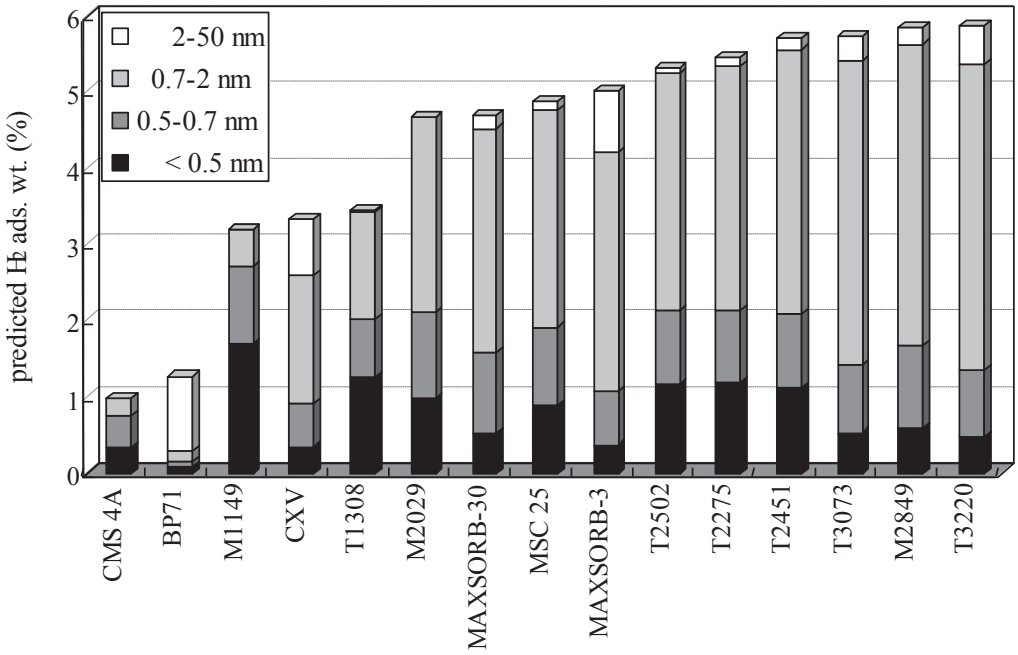

Fig. 8 : Contribution de chaque intervalle de tailles de pores (< 0.5, 0.5-0.7, 0.7-2, 2-50 nm) à la capacité de stockage en excès prédite.

En conclusion, nous avons pu montrer la supériorité de nos charbons actifs par rapport aux charbons commerciaux bien connus comme le MAXSORB-3. Leurs meilleures performances à S_{BET} donnée sont dues à une distribution de taille de pores plus adaptée.

- **Optimisation des charbons actifs pour l'adsorption d'hydrogène (article 4)**

Nous avons utilisé la méthodologie de la surface de réponse (RSM) pour étudier l'effet de la température d'activation (T) et du rapport massique activant/anthracite (R) sur la capacité de stockage d'hydrogène des anthracites activés chimiquement. Nous avons utilisé un plan d'expériences centré avec variation de T entre 725 et 775°C et variation de R entre 2 et 3. Chaque point du plan d'expériences est caractérisé par une paire de conditions expérimentales (T, W), le point central étant défini par la paire (750, 2.5). La Figure 9 montre de manière schématique le plan d'expériences.

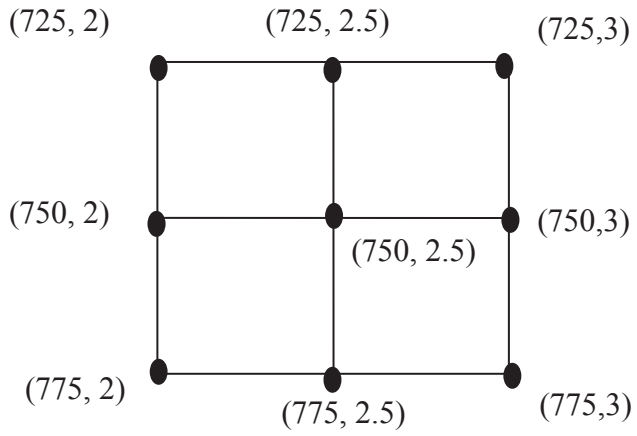

Fig. 9 : Schéma des points expérimentaux du plan d'expériences.

Le Tableau 1 montre la S_{BET} et la capacité de stockage de H_2 (absolue et en excès) pour tous les charbons préparés pour appliquer le modèle de surface de réponse. Avec ces expériences et le software Design Expert 7.0 (STAT-EASE Inc., Minneapolis, USA), nous avons pu proposer une équation polynomiale qui tient compte de l'effet de W, pour prédire la capacité de stockage d'hydrogène en excès :

$$H_2 \text{ (wt. \%)} = -1.39 + 3.82 \times W - 0.46 \times W^2$$

Ce modèle a été validé par une analyse de variance (ANOVA) qui a montré aussi que les termes T, T^2 et TW n'étaient pas significatifs. La Figure 10 montre la surface de réponse pour la capacité de stockage d'hydrogène en excès. La capacité de stockage de H_2 la plus haute est située dans la zone rouge. L'effet de W sur la capacité de stockage d'hydrogène est beaucoup plus important que l'effet de T dans l'intervalle de T et W de cette étude.

Tab. 1 : Matrice d'expériences pour le modèle centré et réponses en termes de S_{BET} et capacité de stockage d'hydrogène.

Experiment	Actual Values		Responses		
	T (°C)	W	S_{BET} (m^2/g)	H_2 wt% Absolute	H_2 wt% Excess
1	750	2.5	2702	6.2 ± 0.1	5.8 ± 0.1
2	725	3	2955	6.0 ± 0.1	5.5 ± 0.1
3	775	2.5	2651	5.9 ± 0.1	5.6 ± 0.1
4	725	2.5	2343	5.3 ± 0.1	4.9 ± 0.1
5	750	2.5	2899	6.3 ± 0.1	5.9 ± 0.1
6	775	3	2978	6.0 ± 0.1	5.7 ± 0.1
7	750	2.5	2632	6.0 ± 0.1	5.6 ± 0.1
8	750	2	2011	4.6 ± 0.1	4.3 ± 0.1
9	775	2	1973	4.3 ± 0.1	4.1 ± 0.1
10	750	2.5	2702	5.8 ± 0.1	5.4 ± 0.1
11	725	2	1657	4.0 ± 0.1	3.9 ± 0.1
12	750	3	2748	5.9 ± 0.1	5.5 ± 0.1

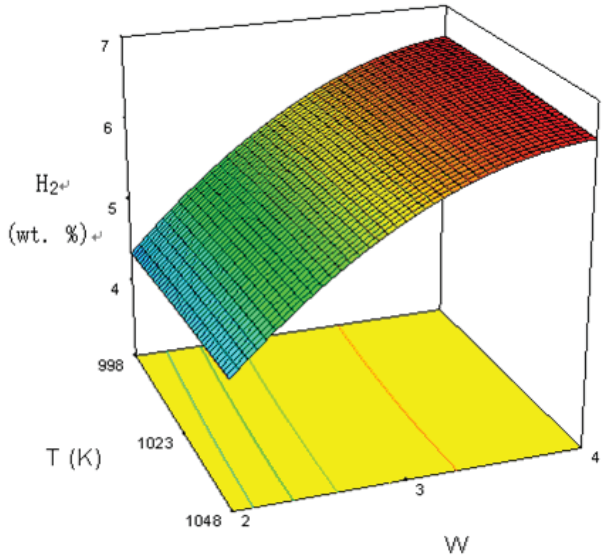

Fig. 10 : Représentation tridimensionnelle de la capacité de stockage d'hydrogène en excès par rapport à la variation de T et de W.

Grâce au plan d'expériences, nous avons pu observer que l'effet de W est beaucoup plus important que l'effet de T. Néanmoins, les charbons obtenus ne permettent pas d'arriver à des capacités de stockage supérieures à 6.6% en poids.

- **Effet des conditions d'activation sur la capacité de stockage d'hydrogène des charbons actifs (article 5)**

A partir de la précédente étude d'optimisation, nous avions obtenu les conditions expérimentales pour obtenir un maximum dans le stockage d'hydrogène mais pas vraiment un optimum (cf. Figure 10 précédente). Nous avons donc élargi l'intervalle de variation de W de 1.5 à 7, de T de 700 à 800°C, et la vitesse de chauffe, Hr, de 1 à 5°C/min. Cela nous a permis de constater que le maximum à W = 4 était aussi un optimum. De la même manière nous avons pu observer que la loi de chauffe à des valeurs inférieurs à 5°C/min n'a pas d'effet sur la capacité de stockage d'hydrogène. La Figure 11 montre l'évolution de la capacité de stockage d'hydrogène avec W et Hr.

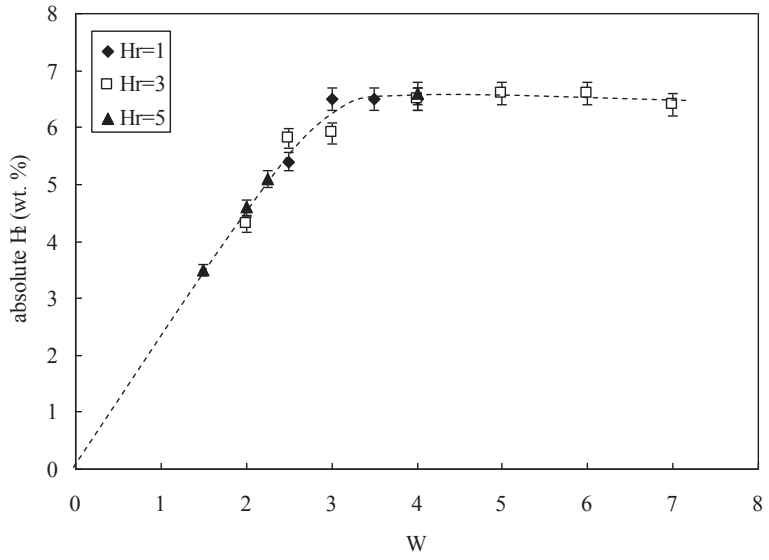

Fig. 11 : Effet de W et Hr sur la capacité de stockage d'hydrogène des charbons activés résultants.

Une fois que nous avons montré que Hr n'avait pas d'effet significatif sur les caractéristiques des charbons actifs, nous avons étudié l'effet de la T à différents valeurs du rapport W. La Figure 12 montre la variation de la capacité de stockage d'hydrogène avec W et T. L'effet de T est plus important aux faibles valeurs de W, mais pour valeurs de W supérieures à 3, l'effet de la T n'est plus significatif.

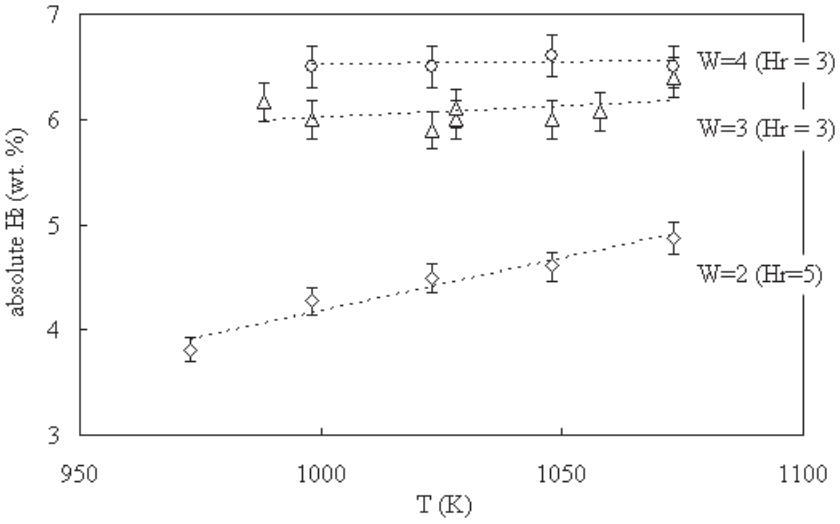

Fig. 12 : Effet de T, aux valeurs de W comprises entre 2 et 4, sur la capacité de stockage d'hydrogène des charbons activés résultants.

Après avoir analysé d'une manière phénoménologique les effets de W, T et Hr sur la capacité de stockage d'hydrogène, nous avons entamé une analyse statistique pour laquelle nous avons utilisé 39 charbons actifs. L'application d'ANOVA a permis de prouver que : (i) Hr et le produit WT n'ont pas d'effet significatif sur la capacité de stockage d'hydrogène ; (ii) W a un effet beaucoup plus important que T. L'expression polynomiale qui permet de corréler les capacités de stockage d'hydrogène à W, T, W^2 et T^2 est la suivante:

$$H_2 \text{ (wt. \%)} = - 206.777 + 2.488\ W + 3.984\ 10^{-1}\ T + 2.531\ 10^{-1}\ W^2 - 1.9\ 10^{-4}\ T^2$$

La Figure 13 montre que cette équation permet de bien prédire les résultats expérimentaux. Les lignes en pointillée sont les limites de confiance à 95%. Tous les résultats obtenus à partir de cette équation sont dans ces limites.

Les charbons obtenus ne permettent pas d'arriver à des capacités de stockage supérieures à 6.6% en poids. Ce fait nous confirme la conclusion obtenue dans nos travaux précédents. Il existe, pour la capacité de stockage d'hydrogène dans un charbon actif, un maximum intrinsèque à la limite physique de l'aire spécifique, qui ne peut excéder 2630 m^2/g. Si nous voulons augmenter la capacité de stockage d'hydrogène sur les charbons actifs, nous devrons utiliser d'autres stratégies comme le dopage avec des nanoparticules métalliques, comme le dopage avec du palladium (article 6) ou le dopage avec des hétéroatomes, comme l'azote (article 7).

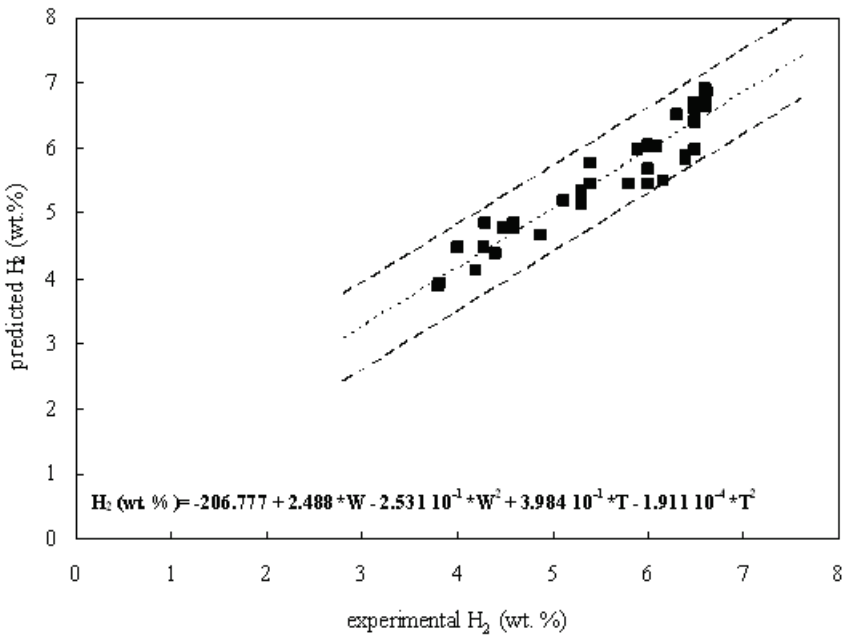

Fig. 13 : Corrélation entre capacités de stockage d'hydrogène expérimentales et calculées (équation incluse dans la figure). Les pointillés matérialisent l'intervalle de confiance à 95%.

- **Charbons activés dopés avec des nanoparticules de palladium pour le stockage d'hydrogène (article 6)**

Afin d'explorer l'effet de la présence de nanoparticules de palladium sur la capacité de stockage d'hydrogène des adsorbants carbonés, nous avons utilisé 3 charbons actifs préparés dans notre laboratoire par activation avec du KOH et présentant des surface spécifiques apparentes comprises entre 2450 et 3200 m^2/g. Ces charbons ont été dopés avec des nanoparticules de palladium et les teneurs finales en palladium oscillent entre 1.3 et 10.0 wt.%.

La Figure 14 montre la variation de S_{BET} avec le pourcentage de palladium introduit. Les symboles pleins correspondent à l'aire spécifique exprimée en m^2 par g de matériau (charbon actif + palladium), tandis que les symboles creux correspondent à l'aire spécifique exprimée en m^2 par g du carbone seul. Cette figure montre que la surface est réduite après dopage, et que cette réduction est indépendante de la quantité de Pd introduit.

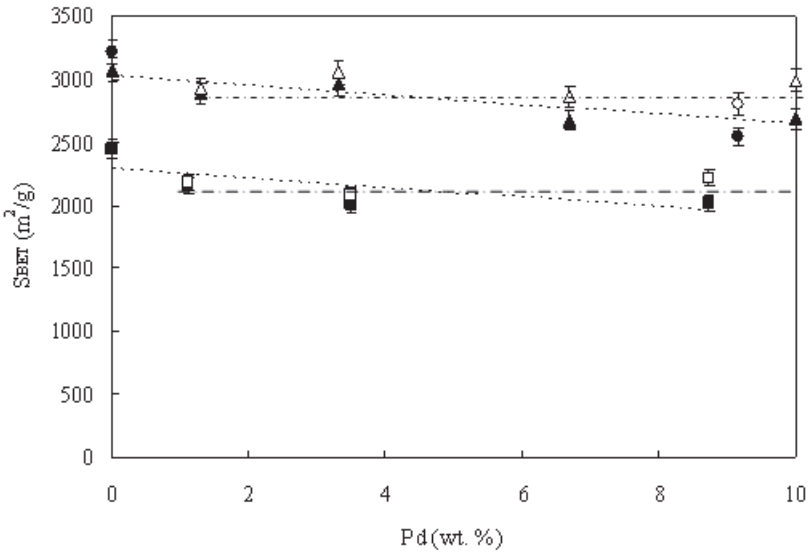

Fig. 14 : Effet du pourcentage de palladium sur la S_{BET} exprimée en m^2 per g de charbon activé dopé (symboles pleins) et de charbon activé (symboles creux) pour les trois séries de charbons activés.

Nous avons mesuré les capacités de stockage d'hydrogène en excès à 77 et à 298 K à des pressions allant jusqu'à 8 MPa. Ces résultats sont représentés en Figure 15 en fonction du pourcentage de palladium introduit.

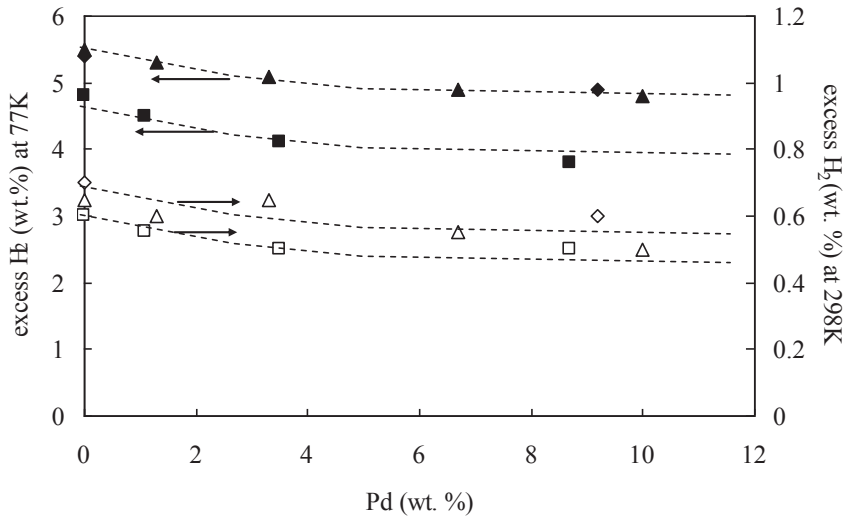

Fig. 15 : Effet du pourcentage de palladium sur les capacités de stockage d'hydrogène à 77K (symboles pleins) et à 298K (symboles creux).

En fait, nous avons pu montrer que la capacité de stockage d'hydrogène, à 77 K comme à 298K, dépend linéairement du volume de micropores, lequel diminue lorsque le pourcentage de palladium introduit augmente. Cette évolution est montrée dans la Figure 16.

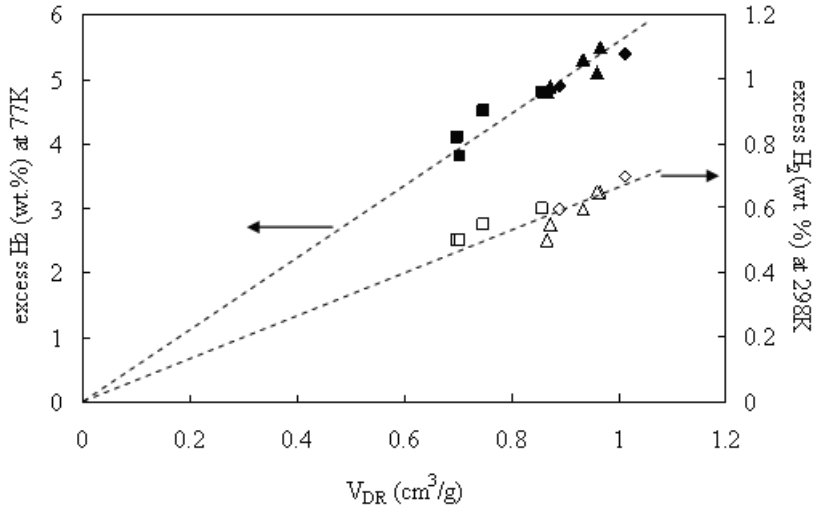

Fig. 16 : Effet du volume de micropores sur les capacités de stockage d'hydrogène à 77K et 4MPa (symboles pleins), et à 298K et 8MPa (symboles creux).

Ainsi, nous avons pu conclure que le stockage de hydrogène à 298K dépend de la teneur en palladium jusqu'à des pressions de 2–3 MPa, en dessous desquelles la quantité d'hydrogène stockée est inférieure à 0.2 wt.%. A des pressions supérieures, le volume de micropores contrôle la capacité de stockage d'hydrogène. A 77 K, le dopage avec des nanoparticules de palladium a un effet négatif sur la capacité de stockage d'hydrogène et cela dans tout l'intervalle de pression considéré. Les études d'adsorption d'azote à 77 K, TPR, XRD, TEM, et chimisorption d'hydrogène nous ont permis de conclure que: (i) les nanoparticules de palladium restent très probablement à la surface externe des grains de charbon actif; (ii) la taille des particules métalliques augmente avec la teneur en palladium; (iii) les charbons actifs de plus haute surface spécifique sont ceux qui présentent la meilleure dispersion et des particules plus petites pour une même teneur en palladium.

Le dopage de charbons actifs avec des nanoparticules de palladium n'a pas d'intérêt pratique puisque la méthode fait que la surface spécifique et le volume de micropores diminuent avec le taux de métal incorporé. Une fois cette voie explorée, nous avons décidé d'étudier l'effet de l'introduction d'azote sur la capacité de stockage de l'hydrogène dans le même type d'adsorbant carboné : des anthracites activés chimiquement.

- **Dopage des charbons activés d'haute surface spécifique avec de l'azote (article 7)**

Pour étudier l'effet de l'introduction de l'hétéroatome azote sur la capacité de stockage d'hydrogène, nous avons utilisé trois charbons actifs de haute surface spécifique apparente, 2527, 2955 and 3434 m^2/g, comme précurseurs de charbons activés enrichis en azote. Ces charbons ont été dopés à l'azote par réaction avec de l'urée à 623K, pour atteindre des teneurs en azote comprises entre 7.8 et 15.1 % en poids. La Figure 17 montre l'effet du pourcentage d'azote introduit sur la S_{BET}. La réaction avec de l'urée est donc très efficace pour le dopage, mais produit une réduction de l'aire spécifique et du volume de micropores. Cette réduction est proportionnelle à la quantité d'azote introduite.

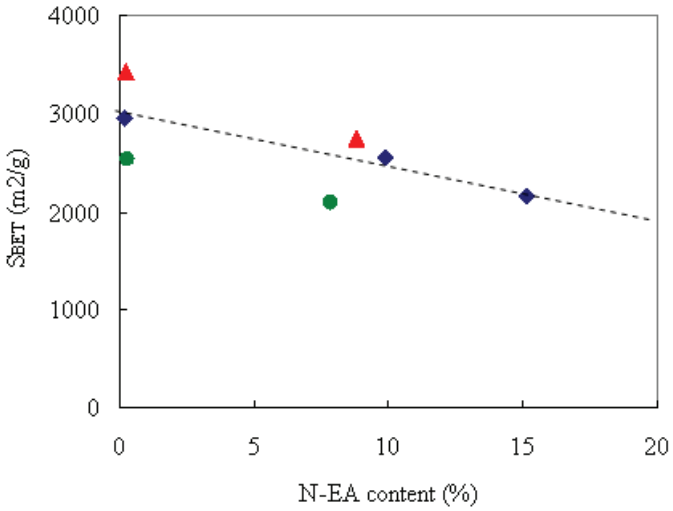

Fig. 17 : Effet du pourcentage d'azote sur la S_{BET}.

La Figure 18 a) montre que la capacité de stockage d'hydrogène augmente linéairement avec la S_{BET}. Etant donné que l'adsorption physique de l'hydrogène à 77K est dominée par les caractéristiques de la structure poreuse de l'adsorbant, la capacité de stockage d'hydrogène diminue aussi avec le pourcentage d'azote introduit comme l'indique la Figure 18 b).

Le taux d'azote incorporé étant lié aux caractéristiques structurales qui gouvernent le stockage d'hydrogène, il n'est pas possible d'analyser les deux effets séparément. La Figure 19 montre les capacités de stockage d'hydrogène à 77K et 2MPa pour les travaux existants dans la littérature. Nous avons y également inclus nos propres résultats.

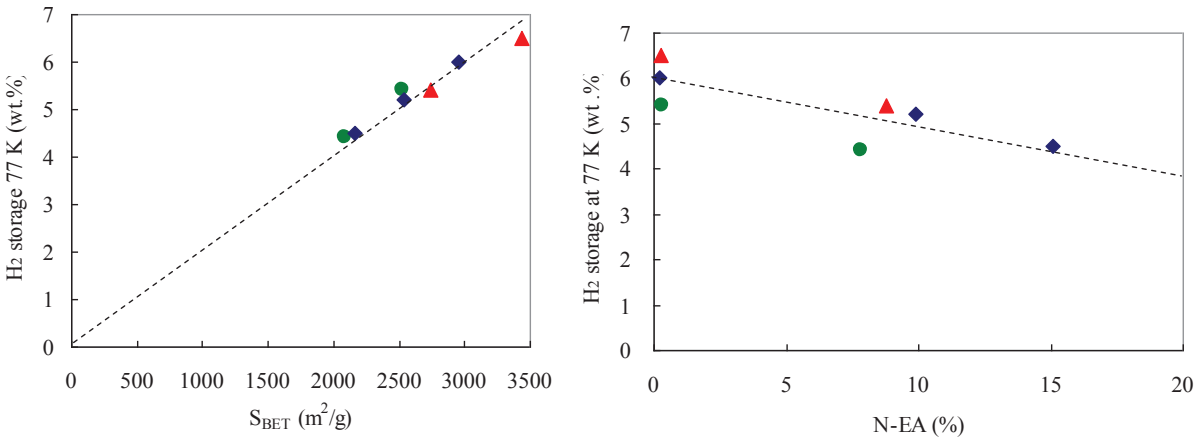

Fig. 18 : Capacité de stockage d'hydrogène en fonction de (a) S_{BET} , et (b) du pourcentage d'azote introduit.

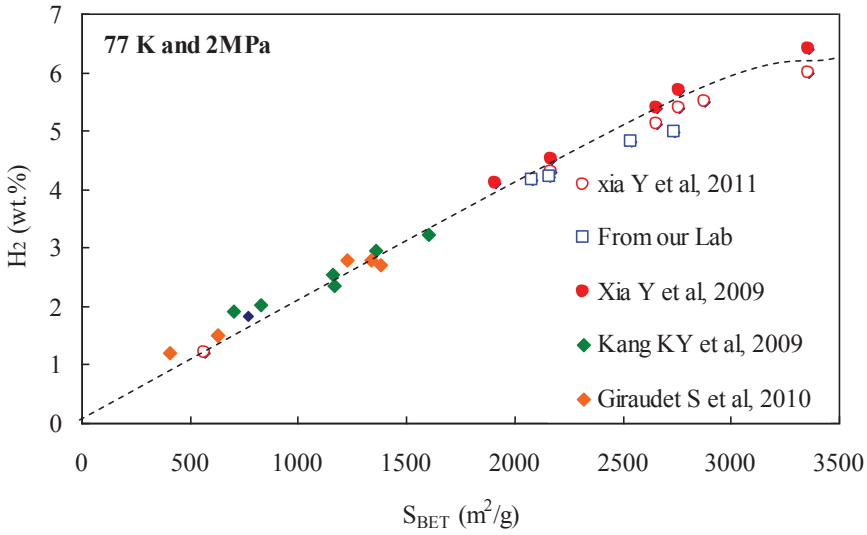

Fig. 19 : Hydrogène stocké à 77Ket 2MPa en fonction de la S_{BET} pour différents travaux existants dans la littérature.

Nous avons considéré que la capacité de stockage d'hydrogène est le résultat de deux contributions : l'aire spécifique (S_{BET}) et la teneur en azote mesurée par analyse élémentaire (N_{EA}), soit H_2 (%) = a × S_{BET} (m^2/g) + b × N_{EA} (%). Ainsi, si nous représentons H_2 (%) / S_{BET} (m^2/g) en fonction de N_{EA} (%) / S_{BET} (m^2/g), nous devrions voir l'effet de l'azote seul sur la capacité de stockage d'hydrogène. La Figure 20 montre cette représentation faite avec les mêmes références bibliographiques que dans la Figure 19. On peut observer donc qu'il y a un effet positif, mais faible, du dopage avec de l'azote des charbons actifs sur leur capacité à adsorber l'hydrogène.

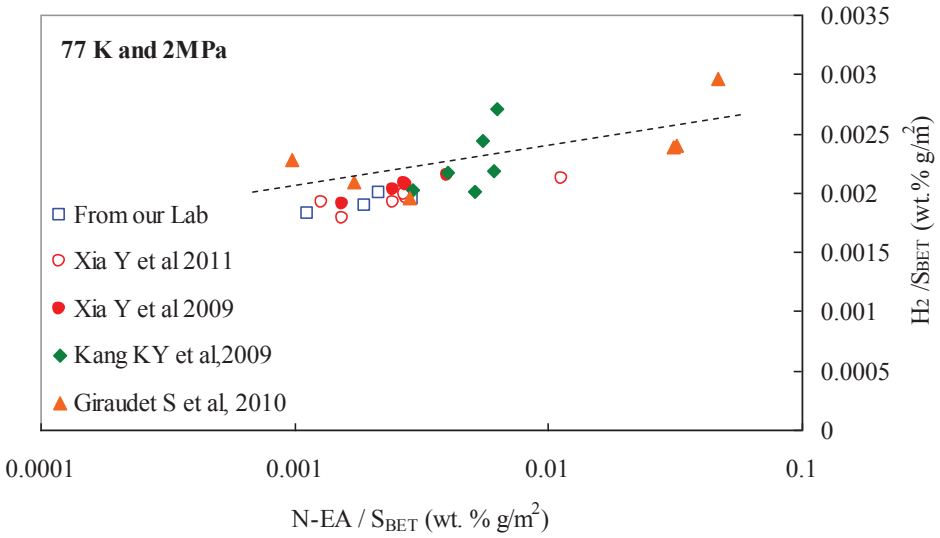

Fig. 20 : H_2 (%) /S_{BET} (m^2/g) en fonction de N-EA (%)/S_{BET} (m^2/g) pour les mêmes matériaux que dans la Figure 19.

En définitive, nous avons pu montrer au cours de cette thèse le potentiel et les limitations des charbons actifs pour le stockage de l'hydrogène. Il semble peu vraisemblable d'obtenir des matériaux carbonés dont la surface spécifique apparente soit supérieure aux valeurs rencontrées ici. Dans ces conditions, 7 % massique à 77K et 4MPa apparaît être une limite haute que peu de matériaux peuvent approcher. Par ailleurs, le poids du réservoir de stockage et du dispositif cryogénique, tous deux nécessaires pour maintenir les conditions de pression et de température dans lesquelles ces résultats ont été obtenus, doivent être pris en compte. La cible définie par l'US DOE est donc d'autant plus difficile à atteindre, celle-ci définissant un pourcentage d'hydrogène stocké par unité de masse du système entier et pas seulement de l'adsorbant.

Pour autant, les valeurs rapportées ici sont parmi les meilleures de la littérature. Si quelques publications ont parfois prétendu des capacités de stockage plus élevées dans es carbones dopés, l'analyse des résultats correspondants ne fait pas état de réversibilité totale comme c'est le cas ici. Il est en effet possible, en particulier dans le cas de charbons actifs dopés avec des nanoparticules de métaux de la 1ère série de transition, qu'une partie de l'hydrogène stocké ait été utilisé pour la réduction de ces métaux au degré d'oxydation zéro. La désorption, non présentée, aurait alors montré

ce phénomène, et le pourcentage d'hydrogène stocké réversiblement aurait été plus réaliste.

Cependant, la piste du dopage reste à privilégier à partir du moment où l'interaction carbone solide – hydrogène gaz est très faible, et que le développement de la porosité et de l'aire spécifique correspondante a atteint ses limites. Elle apparaît être un moyen avantageux, sous réserve du maintien de la structure poreuse, de renforcer les interactions solide – gaz et donc d'améliorer encore la capacité de stockage. Toute la difficulté réside dans le contrôle du dopage, qui réduit la porosité accessible, et dans le choix de l'élément qui permette une meilleure affinité pour l'hydrogène, tout en garantissant la réversibilité du stockage. Une seconde thèse est actuellement en cours sur ce thème.

Chapitre Ⅰ

Stockage de l'Hydrogène dans les Charbons Actifs

In this chapter, the global energy trends and the hydrogen economy will be introduced first. Hydrogen storage is a crucially missing step towards a future "hydrogen economy." Therefore, an overview/analysis of the progresses of hydrogen storage using various methods is presented next. A brief introduction to activated carbons is then given, considering their interest as materials for hydrogen storage. At the end of this chapter, hydrogen storage via spillover in carbons is also briefly reviewed.

1 Global Energy Trends

Population and income growth are the two most powerful driving forces behind energy demand. From 1900, the world population has more than quadrupled. It increased by 1.6 billion people in the last 20 years, and it is foreseen to rise by 1.4 billion for the next 20 years. In contrast, from 1900 again, real income has grown by a factor 25. The world's real income has risen by 87 % over the past 20 years, and it is foreseen to rise by 100 % in the next 20 years. At the global level, more people with more income means that the production and consumption of energy will raise [1].

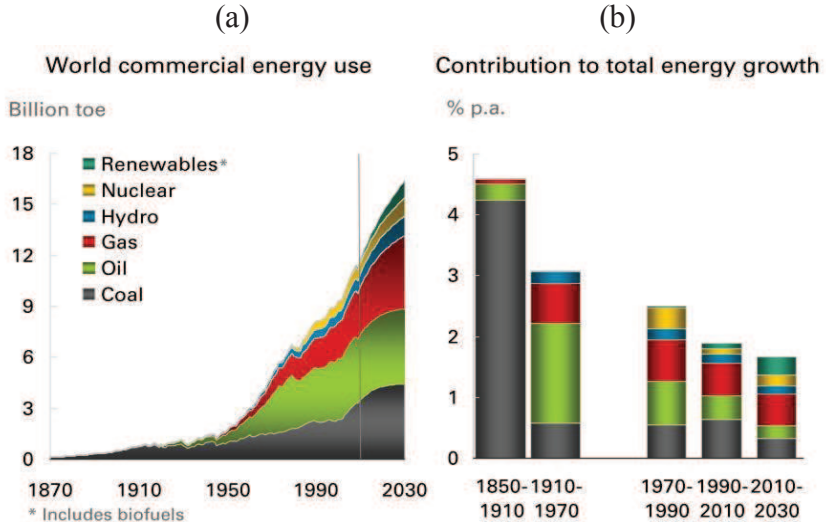

Figure 1 Illustration of the world commercial energy use (a), and the contribution of the energy growth (b) [1]

Figure 1(a) shows that the world primary energy consumption grew by 45 % over the past 20 years, and is likely to grow by 39 % over the next 20 years. Diversification of energy sources increased over the decades. Clean energy is the ultimate goal, being highly desired by an increasing number of people [2]. However, Figure 1(b) shows that the dominant fuels are of fossil nature and represent about 86% of the total: coal, followed by oil and gas. There are two key problems associated with them: the environmental impacts of their use, and the limited nature of these resources.

Burning fossil fuels has an environmental impact due to combustion products, in particular CO_2. CO_2 is a greenhouse gas, able to absorb radiation from the sun and causing the surface temperature of Earth to increase. The greenhouse effect is a natural process, but extensive use of fossil fuels has produced an unwanted further warming effect.

A method should be found to produce energy with a limited detrimental effect on the environment. Total independence from fossil fuels would be ideal, but it is difficult to achieve. Changing national power generation to renewable resources is a key step, but it is also important to consider mobile applications. Another possible method would involve hydrogen as an energy carrier, due to it is totally non-polluting character (only water is exhausted).

2 The Hydrogen Economy

Hydrogen economy is a proposed system of energy delivery based on hydrogen. The term “hydrogen economy” was coined by John Bockris during a talk he gave in 1970 at General Motors Technical Centre. Hydrogen is the most abundant element in the universe, but it does not naturally exist in its elemental form on Earth, and must be prepared from other molecules. This makes hydrogen an energy carrier rather than a primary fuel. As shown in Figure 2, hydrogen economy infrastructure comprises five key elements that are: Production, Delivery, Storage, Conversion, and Applications.

These elements are presently in different stages of technological advancement.

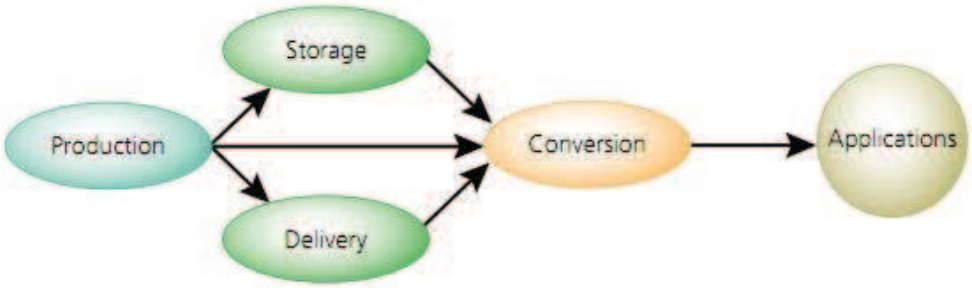

Figure 2 The elements of the hydrogen economy

The hydrogen economy is suggested to solve some of the negative effects of using hydrocarbon fuels, for which the carbon is released to the atmosphere. Compared with other fuels in common use today:

- Hydrogen gas is very powerful: it has the highest energy (286 kJ/mol) per unit of weight among all other chemical fuels;
- Hydrogen is a highly abundant element: it is one of the most common substances on earth;
- Hydrogen is environmentally friendly, totally non-polluting. Only water is exhausted, according to:

  $H_2 + \frac{1}{2}O_2 \rightarrow H_2O + energy$;
- Hydrogen can help to prevent the depletion of fossil fuel reserves.

Despite all the aforementioned advantages, moving to a "Hydrogen Economy" won't happen overnight. There are some technical challenges which should be solved before using hydrogen as an energy carrier [3]. Three critical technology barriers have been pointed out:

a. Reducing the cost of hydrogen: this includes the cost of production, delivery and storage, to be competitive with conventional fuels (on a cost-per-mile basis);
b. Reducing fuel cell cost and improving durability to compete with conventional technologies;

c. Improving hydrogen storage technology: the low volumetric energy density of hydrogen makes storage a real challenge. No current hydrogen storage technology enables to meet the DOE's targets.

3 Obstacles to Hydrogen Storage

Hydrogen has a very high energy content by unit weight (about three times higher than that of gasoline), but it has a very low energy content by unit volume (liquid hydrogen is about four times less dense than gasoline). 4 kg of hydrogen, which are required for a practical driving distance, occupies a volume as large as 49 m^3 at room temperature [4]. This makes hydrogen storage difficult, especially as soon as the size and the weight constraints of a vehicle are considered.

Hydrogen storage for transportation must indeed operate within minimum volume and weight specifications, supply enough hydrogen to enable a 480 km driving range, charge/recharge near room temperature, and provide hydrogen at rates fast enough for fuel cell locomotion of cars, trucks, and buses. The hydrogen storage requirements for transportation applications are thus far more stringent and difficult to achieve than those of stationary applications. Finding onboard hydrogen storage solutions for transportation applications is one of the major challenges in achieving the hydrogen economy. Current hydrogen storage materials or systems are still far not enough for achieving target goals set for either 2010 or 2015. The targets for 2010, suggested by the US Department of Energy (DOE), were revised in 2009 based on real-world experience with hydrogen fuel cell vehicles. Old and new targets are shown in Table 1 [5].

Table 1 DOE's new and old targets for hydrogen storage [5]

Target	2010 (new)	2010 (old)	2015 (new)	2015 (old)	Ultimate Full Fleet
System Gravimetric Density (% wt)	4.5 (1.5 kWh/kg)	6 (2.0 kWh/kg)	5.5 (1.8 kWh/kg)	9 (3 kWh/kg)	7.5 (2.5 kWh/kg)
System Volumetric Density (g/L)	28 (0.9 kWh/L)	45 (1.5 kWh/L)	40 (1.3 kWh/L)	81 (2.7 kWh/L)	70 (2.3 kWh/L)
System Fill Time for 5-kg fill, min (Fueling Rate, kg/min)	4.2 min (1.2 kg/min)	3 min (1.67 kg/min)	3.3 min (1.5 kg/min)	2.5 min (2.0 kg/min)	2.5 min (2.0 kg/min)
Storage System Cost ($/kg H_2): To be determined in conjunction with other Partnership cost target changes	TBD	133 ($4/kWh)	TBD	67 ($2/kWh)	TBD

4 Methods for Hydrogen Storage

Hydrogen can be physically stored either as gas or as liquid in tanks. Storage as gas typically requires high-pressure tanks (350 ~ 700 bar). Storage of hydrogen as liquid requires cryogenic temperatures, because the boiling point of hydrogen at 1 atm is only 20.3 K. Hydrogen can also be stored at the surface of solids (by adsorption) or within solids (by absorption). In adsorption, hydrogen is attached to the surface of a material either as hydrogen molecules or as hydrogen atoms. In absorption, hydrogen is dissociated into H-atoms, then the hydrogen atoms are incorporated into the solid framework.

4.1 Hydrogen Stored by compression

Hydrogen storage by compression is the oldest solution. The energy density of gaseous hydrogen can be increased by storing it at high pressures. High pressures require special materials and designs in order to ensure tank integrity. Cylinders capable of withstanding pressures up to 700 bar and having weights lower than 110 kg are already produced industrially. In these conditions, gravimetric density of 6 % and a volumetric density of 30 kg/m^3 are obtained[4].

The driving range of fuel cell vehicles with compressed hydrogen tanks depends,

of course, on vehicle type, design, and on the amount and pressure of stored hydrogen. By increasing amount and pressure of hydrogen, a greater driving range can be achieved but at the expense of cost and available space within the vehicle. Volumetric capacity, high pressure, and cost are thus key challenges for compressed hydrogen tanks. Refuelling times, compression energy expenses, and heat-management requirements during compression also need to be considered as the mass and pressure of on-board hydrogen are increased.

Carbon fibre-reinforced 350 bar and 700 bar-compressed hydrogen gas tanks are under development by Quantum Technologies (as shown in Figure 3) and others. Such tanks are already used in prototype hydrogen-powered vehicles. The cost of high-pressure compressed gas tanks is essentially dictated by the cost of the carbon fibre that must be used for lightweight structural reinforcement. Thus, lowering cost without compromising weight and volume is a key challenge.

Figure 3 Quantum pressured storage tank [6]

A report from Linde Company estimates that the cost of compressed H_2 is much higher than the cost of liquid hydrogen [7]. It seems, therefore, that this method is not likely to be used in the future. Furthermore, the safety of pressurized cylinders is a major concern especially in densely populated regions.

Other interesting approaches are being pursued to increase gravimetric and volumetric storage capacities of compressed gas tanks above their current levels, like cryo-compressed tanks. This is based on the fact that, at fixed pressure and volume,

gas tank volumetric capacity increases as the tank temperature decreases. Thus, by cooling a tank from room temperature to liquid nitrogen temperature (77 K), its volumetric capacity will increase by a factor four, although system volumetric capacity will be less than this, due to the increased volume required for the cooling system [6].

4.2 Hydrogen Storage by Liquefaction

The energy density of hydrogen can be improved by storing hydrogen in a liquid state. It is denser than gaseous hydrogen and therefore has higher energy content on a per-unit-volume basis. The volumetric capacity of liquid hydrogen is 0.070 kg/L, compared to 0.030 kg/L for 700 bar gas tanks.

To convert gaseous hydrogen into a liquid, it must be cooled to 20 K and be stored in insulated pressure vessels to minimize hydrogen loss through evaporation. There are two challenges to face. One is the efficiency of the liquefaction process. The theoretical work necessary to liquefy hydrogen gas from room temperature is 3.23 kWh/kg, but the technical work is about 15.2 kW h/kg [6]. The other one is the boil-off. The critical temperature of hydrogen is very low (33.2 K), above which liquid state can not exist. Liquid hydrogen can thus only be stored in an open system otherwise the pressure in a closed system can be as high as 1000 MPa at room temperature. Figure 4 shows the illustration of the hydrogen liquefier and the liquid hydrogen tank system from Linde Company [7].

The relatively large amount of energy necessary for liquefaction and the continuous boil-off of liquid limit the utilizations of this storage system.

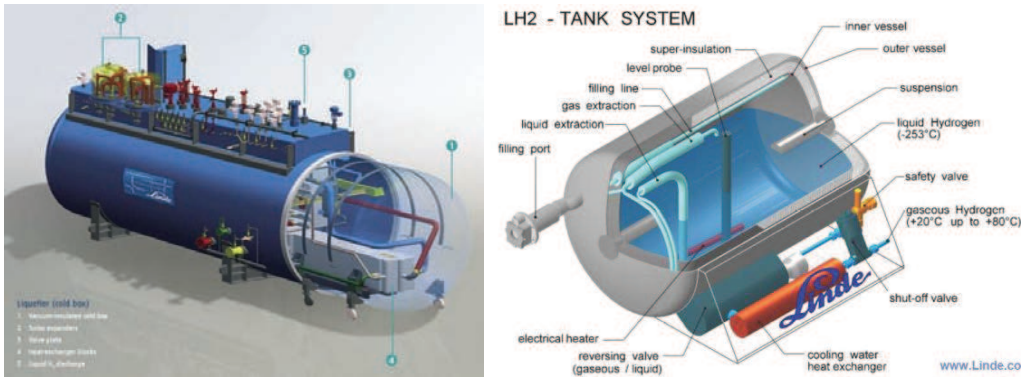

Figure 4 Linde liquefier and liquefied hydrogen storage tank [7]

4.3 Hydrogen Storage Using Materials

Hydrogen can also be stored within solids (by absorption) or at the surface of solids (by adsorption). By absorption, hydrogen is dissociated into H-atoms, and then hydrogen atoms are incorporated into the solid framework (Fig. 5 a). By adsorption, hydrogen is attached to the surface of a material either as hydrogen molecules and/or as hydrogen atoms (Fig. 5 b).

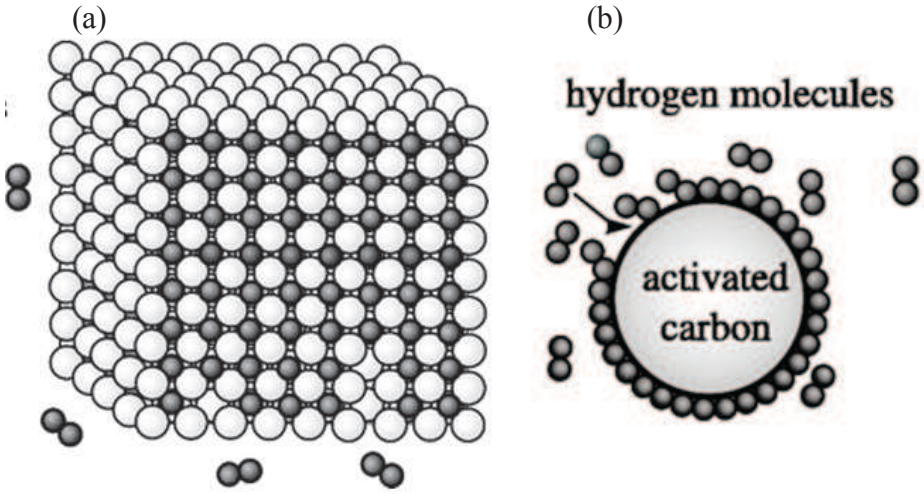

Figure 5 Scheme of hydrogen (a) absorption and (b) adsorption [8]

4.3.1 Hydrogen Storage by absorption (Metal hydrides)

Hydrogen storage within metal hydride materials is a safe and efficient storage method. It has advantages over the gas and liquid storage methods. Metal hydrides

indeed have higher storage density (more than 6.5 H atoms/cm^3 for MgH_2) than gaseous (0.99 H atoms/cm^3 at 200 bar and room temperature) or liquid hydrogen (4.2 H atoms/cm^3 at 20K and room pressure) [9~10]. This can be explained if one considers that one Mg atom absorbs 2 H atoms, resulting in a very dense packing of H-atoms. In the hexagonal close-packed MgH_2, the cell parameters for a and b vectors are 0.37 nm, while they are only 0.47 nm in the pure solid hydrogen phase. Therefore, some metals can store hydrogen in an extremely dense form. However, the weight percent of hydrogen is still low, due to the very low atomic weight of hydrogen compared to that of metal atoms, even for the lightest ones such as Mg. The heavier are the elements used in a metal-hydride system, the lower is the weight percent of gas stored.

Hydrogen is a highly reactive element and has been shown to form hydrides and solid solutions with many metals and alloys. Two possible ways can be used for hydriding a metal: direct dissociative chemisorption and electrochemical splitting of water [9, 11]. These reactions are, respectively:

Ⅰ. $M + \frac{x}{2} H_2 \leftrightarrow MHx$

Ⅱ. $M + \frac{x}{2} H_2 + \frac{x}{2} e^- \leftrightarrow MHx + \frac{x}{2} OH^-$

where M represents the metal.

There are two classes of hydrides: metallic hydrides and complex hydrides. The main difference between them is the transition from metallic to ionic or covalent compounds for the complex hydrides upon absorbing hydrogen.

Hydrogen storage by metal hydrides formation has been the aim of intensive research [4, 9, 12, and 13]. It was shown that hydrogen can be stored reversibly in some materials. Reversibility means that hydrogen can be released from the material by raising its temperature. LaNi and FeTi have high volumetric hydrogen storage densities (higher than the liquid hydrogen density), and require rather low temperatures about 343~373 K for releasing H_2. But the problem is their very low gravimetric storage (1~3 wt %). MgH_2 combines a high H_2 capacity of 7.7 wt% with

the benefit of the low cost of the abundantly available magnesium with good reversibility. The main disadvantages of MgH_2 as a hydrogen storage material is the high temperature of hydrogen discharge (573 K), slow desorption kinetics and a high reactivity towards air and oxygen [9]. Disadvantages for MgH_2 are typical of most metal hydrides due to the fact that their formation is an exothermic reaction. Significant heat is released during hydrogen absorption, and the same amount of heat is required in order to release hydrogen from the hydrides. The more stable is the hydride, the more heat is needed to release hydrogen. As a result, high temperatures around 393 K ~ 573 K are required to release their hydrogen content.

Most complex hydrides contain transition metals (TM). When transition metals are combined with a Group IA or IIA element in the presence of hydrogen, a low valence complex of the TM and multiple H atoms is formed. The number of hydrogen atoms per metal atom is two in many cases. This kind of complexes shows the highest volumetric density, 150 kg/m^3 in Mg_2FeH_6 and $Al(BH_4)_3$, and the highest gravimetric density at room temperature known today in $LiBH_4$ (18 wt%). The low dynamics of the hydrogen releasing process is a major problem. Some researchers thought complex hydrides as the promising solution of the hydrogen storage problem maybe because this group of material has not been well studied with respect to the behaviour as a hydrogen carrier [4].

Metal hydride storage systems have been suggested for mobile applications. However, metallic hydrides based on heavy metals cannot get rid of the constraint of gravimetric density. The relatively high temperature of ab- and desorption and the large amount of energy required for releasing hydrogen remain serious obstacles for using metal hydrides [4].

4.3.2 Hydrogen Storage in Metal Organic Frameworks (MOF)

Metal organic framework (MOF) materials have attracted extensive attention due to their wide potential range of applications [15~26]. MOFs can be classified into two

types: nonporous and porous, depending on whether the networks allow access of guest molecules or not. In nonporous MOFs, the template molecules in final products filling the cavities interact with the framework through strong electrostatic host–guest ions to contribute to the whole lattice energy. Upon removal of the template, the MOF framework looses its integrity. The irremovable molecules in pores prohibit guest molecules from access. In contrast, porous MOFs do not suffer from such disadvantage. The open channels in porous MOFs allow guest molecules to diffuse to some localized sites. In some cases, the blocked channel can be opened by means of thermal or chemical treatment or their combination, in order to remove the solvents inside the channels without any damage to the integrity of the framework [15~16].

MOFs have their own unique structural features that are not encountered in other porous materials. Typical MOF materials suggested for hydrogen storage include MOF-5, -74 and -177, HKUST-1, MIL-100 and -101, etc., which have unique crystallographic structures as shown in Figure 6. They have demonstrated exceptional performances for hydrogen storage and adsorption of other gases [15~16]. MOFs adsorb non-polar hydrogen molecules at their surface mainly through weak London (dispersion) interactions.

Exceptional hydrogen storage of 4.5 wt % at 1 bar and 78 K was reported on MOF-5. This value was later corrected to 1.32 wt% with S_{BET} of 3362 m^2/g [17, 18]. The hydrogen uptake of MOF-5 can reach a saturation value of 5.1 wt% at 77 K and over 80 bar [19~20]. The synthesis methods may affect the hydrogen storage performances. Li et al. [21] synthesized 3 types of MOF-5 samples by different methods. They exhibited rather high, but different, hydrogen-storage capacities: 2.63 wt%, 3.20 wt% and 3.60 wt. %, at 1.74 MPa and 77 K.

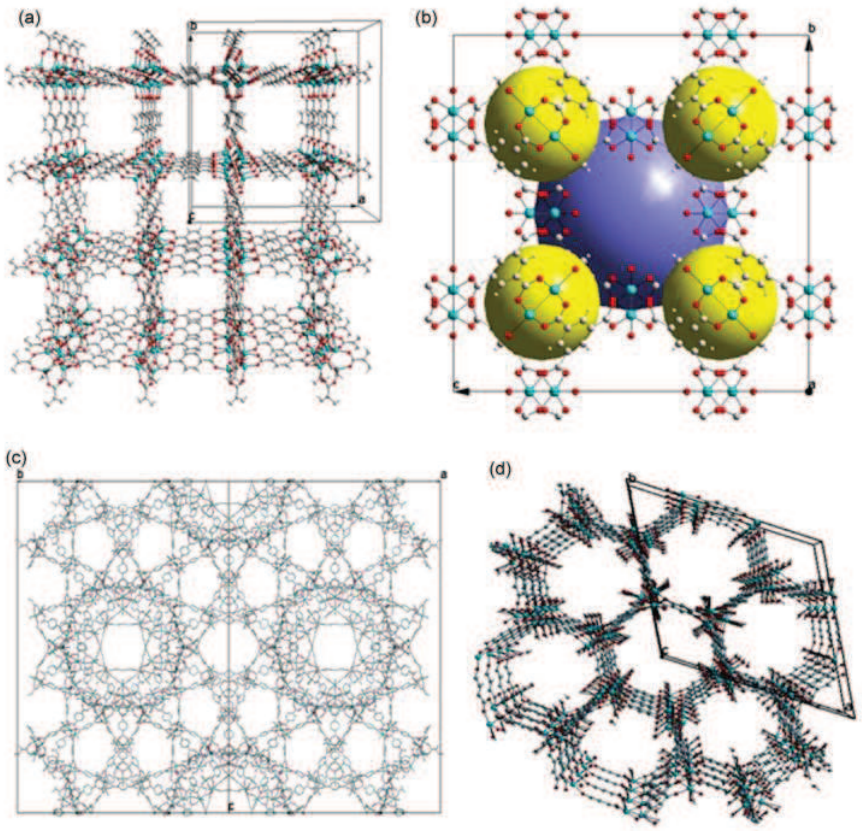

Figure 6 Crystal structure of metal organic frameworks: (a) MOF-5; (b) HKUST-1 (cavities, yellow and blue balls); (c) MIL-101 and (d) MOF-74 or CPO-27-Co (Ni) (metals, cyan; oxygen, red; carbon, grey) [15~16]

The very high surface area and large pore volume are the main attractive features of MOF-177. The Langmuir specific surface area of this adsorbent varies from 4300 m^2/g [25] to 5994 m^2/g [23], and the BET surface area varies from 3275 m^2/g [23] to 4630 m^2/g[24]. The median pore diameters recorded in the microporous region are between 1.1 nm [22] and 1.3 nm [23]. Pore volume as high as 2.65 cm^3/g was reported [23]. The best hydrogen storage capacity for MOF-177 is 7.5 wt % at 77 K and 90 bar [24, 26]. A linear correlation between hydrogen storage capacity and surface area exists and is shown in Figure 7. MOF-177 shows the highest uptake on a gravimetric basis (7.5 wt %), whereas IRMOF-20 shows the highest uptake on a volumetric basis (34 g/L) [26].

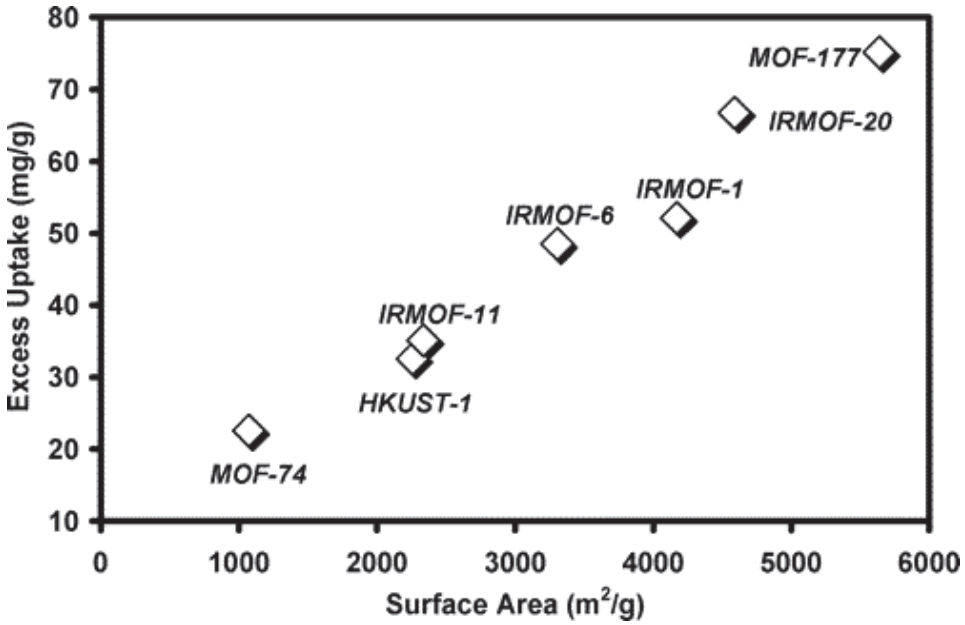

Figure 7 Saturation H_2 uptake at 77 K and 70 bar plotted versus Langmuir surface area [19~20]

To obtain the best performances, a balance between material density and porosity is needed. This is because adsorbents with high surface areas and pore volumes tend to have lower bulk densities, leading to low volumetric capacities. Thus, MOF-177 was reported to store as much as 7.5 wt % H_2 at 77 K and 7 MPa, while its volumetric capacity is 32 g/L. MIL-101 had a gravimetric uptake of 6.1 wt % at 77 K and 8 MPa, and a volumetric capacity of 26 g/L [28]. More work should be done for obtaining higher volumetric capacities, because the new 2015 DOE's target is 40 g/L. Linares-solano et al. [40] reported the capacities of two activated carbons (ACs) and MOF-5 for storing gases. The results showed that, a similar tap density of the three samples, MOF-5 presented, for all gases and conditions studied, lower adsorption capacities in volumetric basis than ACs.

MOFs have very large surface areas, high porosities, uniform and adjustable pore sizes and well-defined hydrogen occupation sites, so they might be used for hydrogen storage in the future. The inconvenient is their low volumetric density.

4.3.3 Hydrogen Storage by adsorption in Carbon-based Adsorbents

Carbon is a non-metallic, tetravalent element. The allotropes of carbon are the different molecular configurations that pure carbon can take. Carbon allotropes are: diamond, graphitic and non-graphitic carbons [29]. Diamond is the hardest material known, has a regular three-dimensional network of σ-bonds. Graphite is a layered structure, graphitic layers being held together by van der Waals forces. Graphite exists in nature, or can also be made artificially, usually by heating petroleum coke or coal pitch at very high temperatures (~ 2773 K). Non-graphitic (or amorphous) carbon materials can be subdivided into carbon blacks, coke, char and activated carbons. New forms of carbon, including fullerenes and nanotubes have been also discovered.

Figure 8 illustrates carbon allotropes [29]. 90% of carbon materials used in the industries are graphitic or graphite-like, consisting of sp^2 carbon in hexagonal planes. Stacking hexagonal planes, with thicknesses ranging from a few to several hundreds of nanometres, is the basis of the structure of graphitic carbons [30].

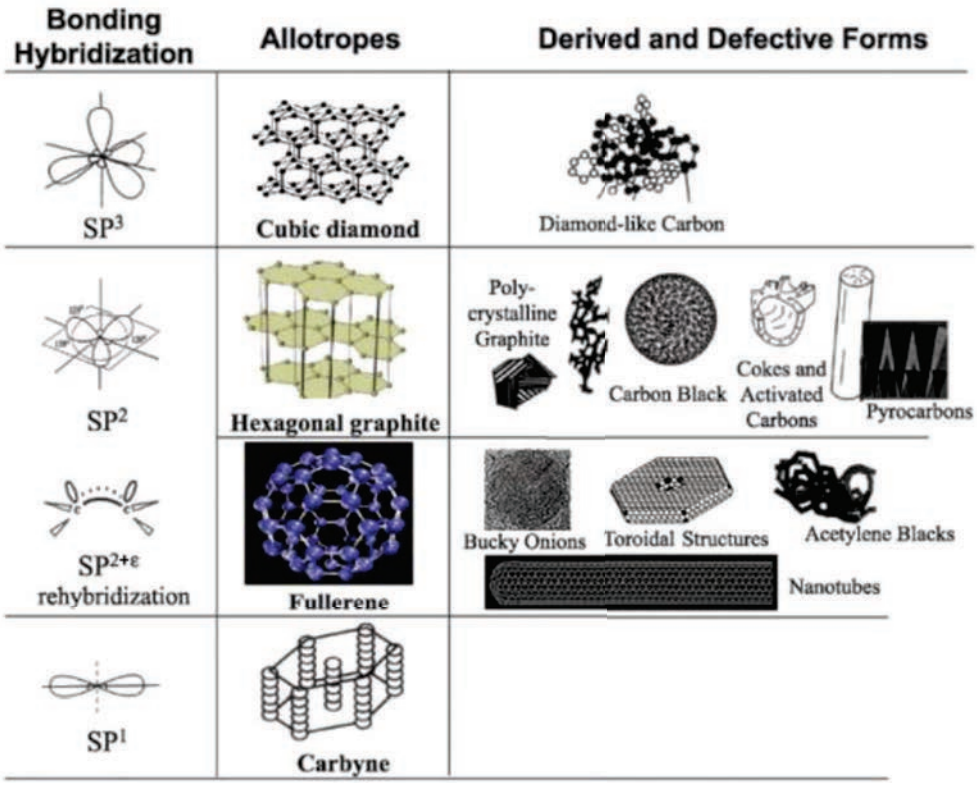

Figure 8 Carbon allotropes, adapted from Bourrat's Figure [29]

Unlike metal hydride hydrogen storage systems, there is no chemical reaction between carbon materials and hydrogen. The hydrogen molecules are bound to the surface of the adsorbing material by weak forces only. The most promising and investigated materials for hydrogen adsorption are porous carbon adsorbents due to their light weight, high surface area and tailorable porous structure. Carbon-based adsorbents suggested for hydrogen storage include carbon nanotubes (CNTs), graphite nanofibers (GNFs), activated carbons (ACs), templated carbons (TCs), etc. Studies have shown that high surface area carbons (above 2000 m^2/g) may store 5~10 wt % of hydrogen [31-35]. However, these storage capacities are only observed at low temperatures (77 ~ 180 K) due to the weak interaction between hydrogen molecules and the material. At room temperature, the storage capacity drops to less than 1 wt% at 4 MPa [35].

4.3.3.1 Carbon Nanotubes (CNTs)

Carbon nanotubes (CNTs, as shown in Figure 9) are allotropes of carbon having a cylindrical nanostructure. Nanotubes have been obtained with length-to-diameter ratios of up to 132 000 000:1, i.e. with aspect ratios that are much higher than for any other materials. Nanotubes are categorized as single-walled nanotubes (SWNTs) or multi-walled nanotubes (MWNTs), and were the new carbon form discovered by Iijima 20 years ago [37].

Hydrogen storage in carbon nanotubes (CNTs) was first reported by Dillon et al. [38] in 1997. The hydrogen storage capacity of both single-walled nanotubes and multi-walled nanotubes has attracted many attentions. Experimental results obtained in the evaluation of hydrogen storage capacity of carbon nanotubes varied significantly from one research team to another. Storage capacities of CNTs ranging from negligible amount to 20 wt % have indeed been reported.

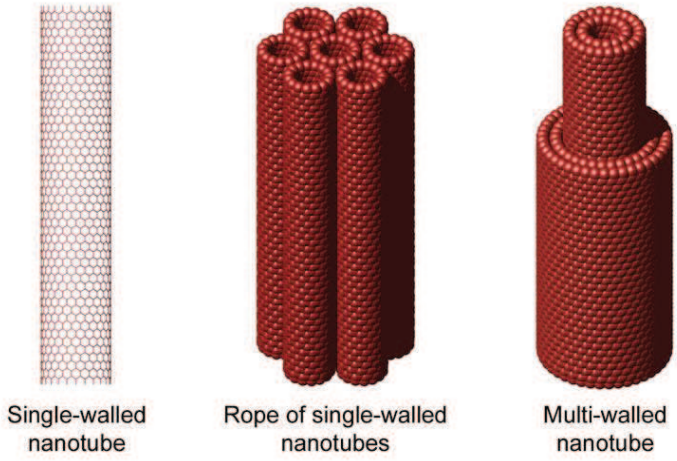

Figure 9: Representation of the carbon nanotube structures [1]

From the early reports, hydrogen storage capacities of CNTs at room temperature as high as 5% and 10% were reported [38, 39]. Later studies showed that the hydrogen storage capacities of pure CNTs are well below 1 wt% [41~43]. Zhou et al. [41] studied the hydrogen adsorption on CNTs at temperatures from 233 to 318 K up to 12 MPa, and the storage capacity was always about 0.25 wt%. In 2001, Tibbetts et al. [42] studied the sorption of hydrogen at pressures up to 11 MPa and temperatures from 193 to 773 K in carbon nanotubes. The largest hydrogen sorption observed was less than 0.1 wt % at room temperature. All these results caused serious doubts on any claim higher than 1 wt% concerning room temperature hydrogen sorption in carbon materials.

The differences and discrepancies in the storage capacities of CNTs might be due to experimental errors. Zlotea et al. [169] found the H_2 adsorption results are scattered not only by the diversity of instrumentation (two gravimetric and two volumetric devices in the corresponding study), but also depend on the originating laboratories (4 different laboratories). Lachawiec et al. [44] measured accuracies of volumetric measurements of hydrogen storage at high pressures. When all errors were minimized or eliminated from the measurements, the hydrogen storage capacities of all carbon nanotubes were below 0.3 wt % at 298 K and 10 MPa.

Hydrogen storage capacity of CNTs is rather low compared to that of activated carbons (see below), so more work should be done in the future for improving their hydrogen storage capacity.

4.3.3.2 Graphite Nanofibres (GNF)

Graphite nanofibre is a type of fibrous carbon consisting of tiny graphite platelets stacked in an arranged conformation, as shown in Figure 10 [45]. From the early reports, the hydrogen storage capacities of GNF at room temperature were very high [45~47]. In 1998, Chambers and co-workers [45] investigating hydrogen adsorption on nanofibres with tubular, platelet and herringbone structures at 298 K and 12 MPa, reported extraordinary high storage capacities of 11.26, 53.68, and 67.55 wt %, respectively.

As it already happened with CNTs, there were several attempts to confirm these high adsorption capacities, but so far none has succeeded. The maximum achieved storage capacity with the same material was 1.52 wt% at room temperature under 13 MPa [48]. Ahn et al. [43] synthesized graphite nanofibres and studied their hydrogen adsorption/desorption properties at 77 and 300 K. The absolute level of hydrogen desorption measured from these materials was typically less than the 0.01 H/C atom. Lueking et al. [50] studied exfoliated graphite nanofibres for hydrogen storage. The hydrogen storage capacity was only 0.34 wt% at 77 K and 20 bar and 0.02 wt% at 300 K and 20 bar.

As shown above, graphite nanofibre seems not suitable for being be used for hydrogen storage, and the results are still controversial.

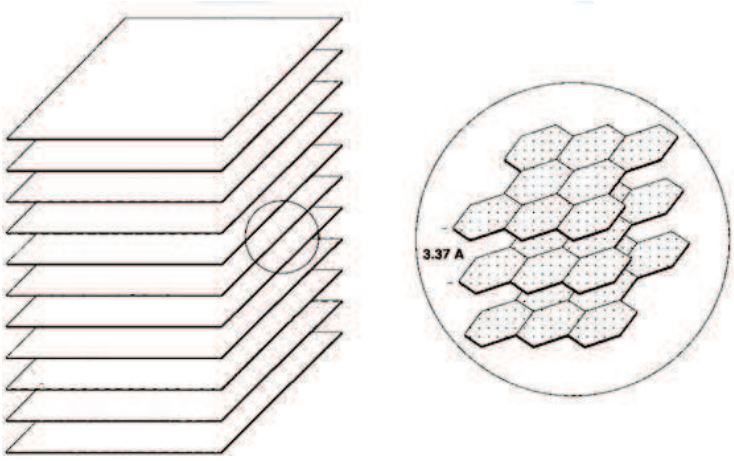

Figure 10: (a) Schematic representation of the arrangement of platelets in a catalytically grown graphite nanofiber; (b) an enlarged section showing the detail of area marked in (a) [45]

4.3.3.3 Graphene and Graphite

Graphene is a single monolayer of carbon atoms arranged in a two-dimensional (2D) honeycomb lattice, and is a basic building block for graphitic materials. It can be wrapped up into 0D fullerenes, rolled into 1D nanotubes or stacked into 3D graphite. The C-C bond length in graphene is about 0.142 nm. Graphene sheets stack to form graphite with an interplanar spacing of 0.335 nm, which means that a stack of three million sheets would be only one millimetre thick. Graphene is the basic structural element of some carbon allotropes including graphite, charcoal, carbon nanotubes and fullerenes. Figure 11 shows graphene and graphite structures.

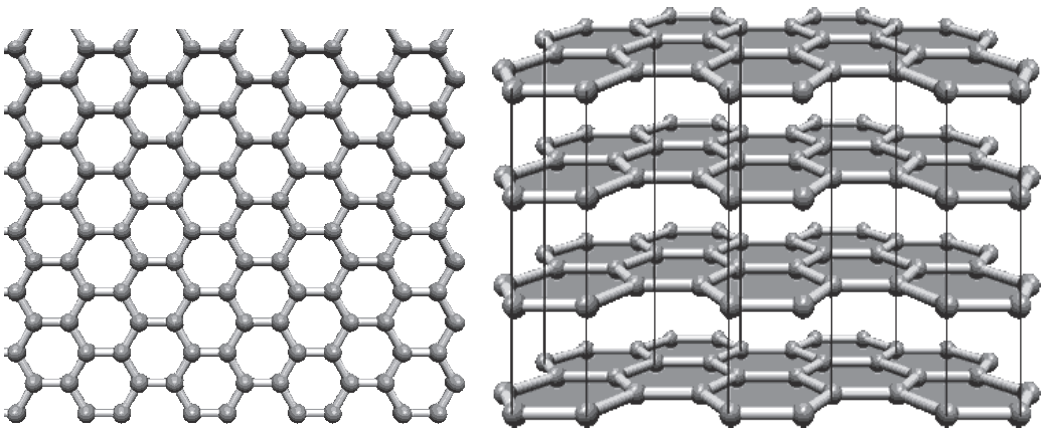

Figure 11 The structure of graphene (left) and graphite (right)

Both theoretical calculations and experimental results showed that graphite and graphene might be suitable for hydrogen storage [51~53]. Zhang et al. [52~53] ball milled graphite under 3 bar hydrogen in a tungsten carbide milling pot. After milling for 10 hours, 5.5 wt% hydrogen was released upon heating under argon to 1263 K. Using graphite doped with 0.5 wt% Fe sample, 9.6 wt% of hydrogen was released under the same conditions, heating under argon to 1263 K.

However, most results are again still controversial. For example, less than 1 wt% of hydrogen uptake was measured at room temperature under 10 MPa on grapheme [54, 55]. Additional studies are still required.

4.3.3.4 Activated Carbons (ACs)

ACs are characterized by high apparent surface areas typically ranging from 300 to 4000 m^2/g, as measured by the BET method. Commercial grades of AC are designated for either gas phase or liquid phase applications. AC might be an interesting option for hydrogen storage due to the very high surface areas and micropore volumes [31~35]. More information about ACs will be given in section 5.

4.4 Comparison of Current Hydrogen Storage Methods

As we have seen, each hydrogen storage alternative has advantages and disadvantages. Table 2 summarizes the main characteristics and provides a comparative summary of hydrogen storage systems.

As we know, hydrogen is not a primary source of energy since it does not exist naturally on Earth. Hydrogen can be found in water and several other chemical compounds from which it has to be separated before it can be used. Hydrogen thus has a high production cost, which made it three times more expensive than petroleum products. Therefore, any method of storage should not further increase too much the cost of hydrogen fuel. Although new materials and methods may improve hydrogen storage and production technology, difficult challenges remain to be solved [4].

Hydrogen storage based on adsorption at 77K on carbons having high surface area and micropore volume seems to be one of the best ways to achieve the DOE's target.

Table 2 Comparison of Current Hydrogen Storage Methods

Methods	Compression	Liquid hydrogen	Metal hydride	MOF	Carbon adsorption
Content	High pressure and ordinary temperature; Up to 70MPa	Atmospheric P; 20.4K; 70.8Kg/ m^3; Insulated vessel (Dewar or tank); Max. 3200m^3	At or above room temperature and pressure; Storage in vessel; This method has been put into practice	Combined use of physical adsorption and compressive packing with low T and moderate P (up to 10 MPa)	Combined use of physical adsorption and compressive packing with low temperature (77K) and moderate pressure (up to 5 MPa)
Merits	Relatively easy handling of gas with low pressure less than 350 bar; Fair densities up to 700 bar	High compressive density; High bulk density; High storage capacity	Greater safety; Discharge by heat	High gravimetric density	High density; Cheap price; Fast kinetics; Total reversibly
Demerits	Rather poor efficiency of storage with low P; Increasing P increases cost and safety risk	Large power requirement and high cost of liquefaction; Boil-off; Flashing; Safety concerns	Large power requirement for discharge; Expensive alloy material	Low bulk density; Coolants requireds	Required liquid N_2 or other coolants

5 Hydrogen Storage in Activated Carbon

5.1 Activated Carbon (AC)

AC is one of the allotropes of disordered carbon having been processed to make it extremely porous, and thus to have a very large surface area available for adsorption or chemical reactions. The term active or activated carbon refers to carbon materials manufactured by high temperature (773 to 1273 K) pyrolysis of various vegetable residues (i.e., wood chips, peat, nutshells, pits, etc.) as well as pitch, coal or polymers, followed by activation to create desirable porous structure of the target materials, as shown in Figure 12 [56]. Activation can be a "physical" or a "chemical" process.

Physical activation consists in partial carbon gasification by reaction with steam, CO_2, or air at temperatures up to 1173 K. Most reactive amorphous components are burned off. Chemical activation consists of heat treatment in the presence of alkali (NaOH, KOH), inorganic acids (H_2SO_4, H_3PO_4), or salts ($ZnCl_2$) in an inert atmosphere at typical temperatures from 873 to 1073 K. The advantage of chemical activation is the more uniform pore structure of the resultant activated carbon materials. Chemical activation is also a 1-step process while physical activation requires a previous pyrolysis.

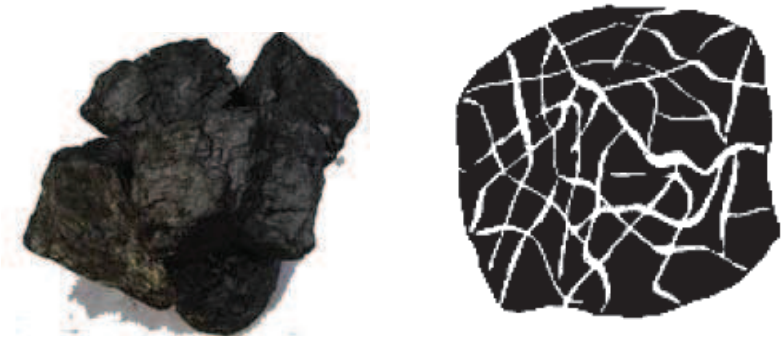

Figure 12 Raw carbon material (anthracite) on the left schematically transforms into the carbon on the right after activation [57]

AC's structure is formed by imperfect stacking of carbon layers which are bonded together to build a 3-dimensional structure, as shown in Figure 13. The basic structural unit of activated carbon may be approximated by that of graphite with, however, a higher interlayer spacing and the possibility of having some carbon layers rotated with respect to each other. Activated carbon may thus be considered as a carbon form allied to graphite, but highly disorganised due to impurities and to the method of preparation (activation process).

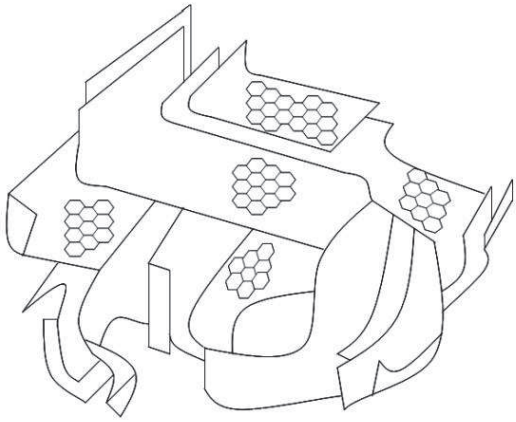

Figure 13 Schematic representation of the structure of AC [58]

ACs can be classified on the basis of their application (e.g. gas vs liquid phase), precursor (e.g. wood, coal, etc.), and final shapes (e.g. powder, grains, pellets, etc.).

5.1.1 Precursors

Any cheap material having high carbon and moderate inorganic contents can be used as raw material for AC production. In general, commercial processes for preparing AC are based on precursors which are either resources derived from degraded or fossil biomass (e.g. peat, lignite and all ranks of coal), or fresh biomass (e.g. wood, coconut shells, etc.). Such resources are either inexpensive or have a high carbon content, or both.

The raw material has a strong influence on the characteristics and on the performances of ACs, each precursor producing an AC having its own surface area, total pore volume and pore size distribution. Lenghaus et al. [59] investigated the carbon structures obtained from different phenolic resin precursors and found that the carbons from para alkyl phenols have wide micropores, whereas the carbons from phenol and 3,5-dimethylphenol have narrow micropores under the same carbonization conditions.

Anthracite is an attractive AC precursor because of its very narrow initial pore structure, which can be utilized for producing microporous carbons both by physical and chemical activation. Gergova et al. [60] prepared activated anthracites by steam

activation having N_2 Langmuir surface areas from 400 to 1400 m^2/g. Lillo-Ródenas [61~62] found that high micropore volume activated carbons (up to 1.45 cm^3/g) with a quite narrow micropore distribution and BET surface area as large as 3200 m^2/g can be prepared from Spanish anthracites by KOH activation.

In our group, we used the anthracite from Taisi mine (Shizuishan city, China) as precursor for preparing ACs. The ash, S and P contents of Taisi are 8.54, 0.3 and less than 1 wt%, respectively. We got ACs having high apparent surface areas up to 3500 m^2/g and narrow micropores, which were shown to be suitable for hydrogen storage [35].

5.1.2 Physical Activation

Physical activation develops porosity by controlled gasification. This method should be performed after a preliminary carbonization, except when using an already mineral carbon, see Fig. 14. Carbonization consists of pyrolysis at temperatures in the range of 873 ~ 1173 K, in inert atmosphere (using gases such as argon or nitrogen). This step produces a char having higher carbon content. Because of blockage of the pores by tars, the surface area of char is rather low [64]. The second step of the physical activation is the controlled gasification at high temperature (1073 ~ 1373 K) using oxidizing agents such as steam (H_2O) or carbon dioxide (CO_2), which produces activated carbon with high porosity. Porosity development is due to the penetration of oxidizing agent into the internal structure of char, and removal of carbon atoms by reaction into gas, which results in opening and widening the porosity [64~65].

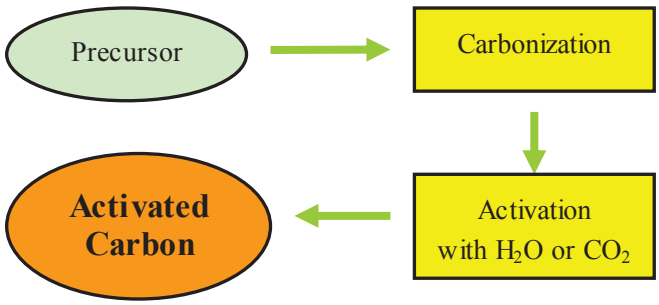

Figure 14 The general flow sheet for physical activation

The reactions mechanisms between steam and solid carbon on one hand, and carbon dioxide and solid carbon on the other, were studied by numerous groups [64].

- The overall steam gasification reaction can be represented by:

Ⅰ. $C+H_2O \rightleftharpoons H_2+CO$ $\Delta H = +118$ kJ/mol

However, the reaction is much more complex and involves several steps. H_2O gasification is more complex than CO_2 gasification because not only H_2O is involved but also H_2, CO_2 and CO due to the equilibrium of the water gas shift reaction. Two further reactions are also possible at high temperatures for steam activation, as shown below:

Ⅱ. $CO+H_2O \rightleftharpoons CO_2+H_2$ $\Delta H = -41$ kJ/mol

Ⅲ. $CO+3H_2 \rightleftharpoons CH_4+H_2O$ $\Delta H = -206$ kJ/mol

- The overall CO_2 gasification reaction can be represented by:

Ⅳ. $C+CO_2 \rightleftharpoons 2CO$ $\Delta H = +162$ kJ/mol

Thus, the overall steam/carbon and carbon dioxide/carbon reaction is endothermic. Therefore, an external heat source, such as a furnace, is necessary. A number of different types of kilns and furnaces can be used for carbonization/activation and include rotary (fired directly or indirectly), vertical multi-hearth furnaces, fluidized bed reactors and vertical single throat retorts. Each manufacturer has its own preference [67].

Physical activation uses gaseous activation agents and does not produce waste water, so it is considered to be “greener”. But it takes long time, because a previous pyrolysis at high T and much energy are required for producing microporous activated carbons. Another inherent drawback of this method is that large amount of carbon is eliminated to obtain well developed pore structure. Therefore, a limited carbon yield is obtained by this route [66].

5.1.3 Chemical Activation

Compared to physical activation, chemical activation consists of heat treatment in the presence of alkali (NaOH, KOH), inorganic acids (H_2SO_4, H_3PO_4), or salts ($ZnCl_2$) in an inert atmosphere from 700 to 1225 K. Advantages of chemical activation are a more uniform pore structure of the resultant activated carbon materials, and higher carbon yield. The general flow sheet for chemical activation is shown in Figure 15.

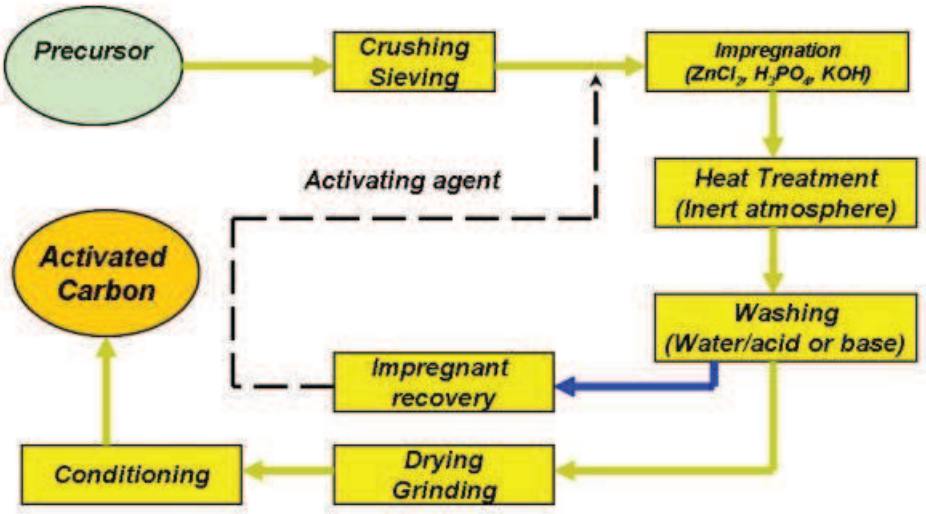

Figure 15 The general flow sheet for chemical activation [67]

Among all chemicals, KOH is one of the most effective activating agent for producing high surface area ACs. The effectiveness of KOH activation relative to either physical activation methods or activation by other chemical agents can be attributed to the ability of K to form easily intercalation compounds with carbon. In addition, K_2O formed in-situ during the process of KOH activation can easily infiltrate the pores. K_2O is reduced to K by carbon, resulting in carbon gasification with a subsequent emission of CO_2 leading to the formation of pores. K atoms that intercalate into the lamellae of the carbon crystallites also widen the space between the adjacent carbon layers (intercalation phenomenon), resulting in an increase in the value of specific surface area [67~69]. KOH reacts with disordered or amorphous carbon

at high temperatures to form K_2CO_3 as well as the decomposition product K_2O along with the evolution of hydrogen [67~70].

In general the mechanism of chemical reaction between KOH and carbon material can be written as follows:

Ⅰ. $4\ KOH + C \rightarrow K_2CO_3 + K_2O + 2\ H_2$

Considering the decomposition of KOH into K_2O as well as the reducing ability of carbon, additional reactions take place during the process of activation as shown below:

Ⅱ. $2\ KOH \rightarrow K_2O + H_2O$

Ⅲ. $C + H_2O\ (steam) \rightarrow H_2 + CO$

Ⅳ. $CO + H_2O \rightarrow H_2 + CO_2$

Ⅴ. $K_2O + CO_2 \rightarrow K_2CO_3$

Ⅵ. $K_2O + H_2 \rightarrow 2\ K + H_2O$

Ⅶ. $K_2O + C \rightarrow 2\ K + CO$

Ⅷ. $K_2CO_3 + 2\ C \rightarrow 2\ K + 3\ CO$

Pores are produced by carbon removal in three different ways: (i) K_2O and H_2O production from KOH at temperature higher than 673 K, then steam activation of carbon leading to $CO + H_2$; (ii) reduction of K_2O by carbon; (iii) reduction of K_2CO_3 by carbon. All the corresponding carbon losses contribute to the creation of porous network in the carbon material. Thus, AC with apparent surface area higher than 3000 m^2/g can be produced by KOH chemical activation.

KOH chemical activation can be used for inducing microporosity in mesoporous carbon materials [71]. Figure 16 shows the formation of micropores in a mesoporous carbon upon activation with KOH at 973 K in N_2 atmosphere.

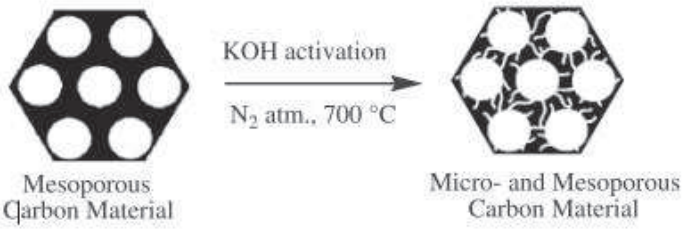

Figure 16 Representation of the formation of micropores in a mesoporous carbon upon activation with KOH at 973 K in N_2 atmosphere [71]

The weight ratio of KOH to precursor, the activation temperature, the N_2 flow rate, the heating rate, and the washing process etc. are the factors determining the characteristics of the activated carbon.

Weight ratio of KOH/precursor (W): The weight ratio has been found to be the most important parameter in chemical KOH activation process. Zengmin et al. [72] evaluated the effect of the amount of activating agent (KOH) on the process of activation. The activation of mesocarbon micro beads (MCMBs) was carried out with different W = 3, 5, 7, 8, 10 and 12 at 1123 K. It was observed that up to W = 8, the apparent surface area value increased up to 3182 m^2/g. Lozano-Castelló et al. [62] prepared activated carbons from Spanish anthracite by KOH chemical activation at 1073 K and showed that higher W produced a great enhancement of N_2 adsorption capacity at 77 K. Surface area and micropore volume both increased continuously with W, reaching a maximum at W = 4. It was also shown that W has an influence not only on micropore volume and surface area, but also on the micropore size distribution.

To sum up, the optimum W changed with the precursors but was always observed. Increasingly high values of W always led to increased S_{BET} and pore volumes, until a maximum is reached before the pore textures parameters start to decrease.

Activation temperature (T): Activation temperature is the other important parameter for preparing activated carbons. Increasing T brings significant changes to the porosity of activated carbon. CNFs were activated by Yoon et al. [74] (KOH, W = 4)

at three different T, which were 1073, 1123 and 1273 K. The apparent surface area of the CNFs upon activation increased from 174 to 439, 587 and 1212 m^2/g, respectively. Kim et al. [75] examined the process of KOH activation of graphitic nanofibres (W = 3.5). Upon activation with KOH at three different temperatures, 1172, 1273 and 1373K, the apparent surface area values increased to 500, 580 and 790 m^2/g, respectively. Cardoso et al. [76] studied the activated carbon made from wastes of the cork industry by KOH activation. It was concluded that at constant W, the surface areas and microporous volumes increased linearly with T from 773 to 1073 K. The same conclusion was obtained by Sudaryanto et al. [77]. Figure 17 shows the relationship between surface area and T of activated carbon from Evans et al. [78]. The highest surface area was around 2500 m^2/g for the sample treated at 1023 K. The Dubinin micropore volumes of these samples followed a similar trend with the highest micropore volume achieved for samples treated at 1023 K.

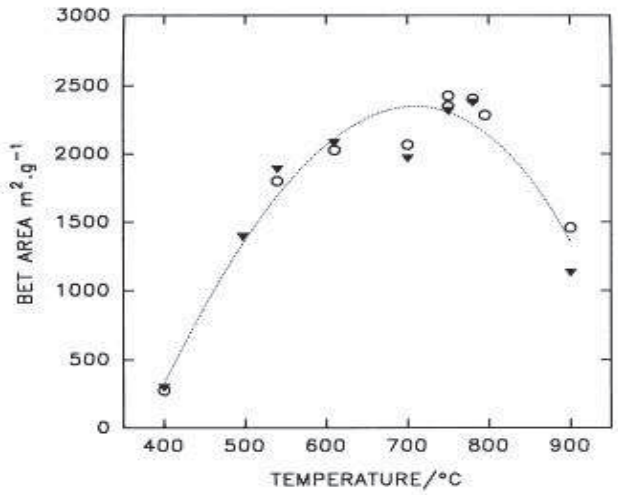

Figure 17 Surface areas after KOH activation of Spanish anthracite at different T and constant W = 4 [78]

During KOH activation, formation of mesopores and pore widening are the two pathways for the development of porosity. In general, the process of pore widening takes place at high W. In addition the pore widening process is accelerated as T is raised from 1073 to 1225 K and this can be attributed to the fact that at higher temperatures of activation, the melt of K_2CO_3 and K_2O as well as the vapour of K

possess higher activity accelerating the pore widening process [72].

As a conclusion, the porosity of the activated carbon increases with both W and T until a maximum is reached, higher values of W and T producing too wide pores and decreasing the surface area.

Flow rate of inert gas: Flow rates of nitrogen from 80 to 800 mL/min were used for the preparation of activated carbons by chemical activation of Spanish anthracite with KOH. The effects on porosity development were then investigated by Lozano-Castelló et al. [62]. It was observed that nitrogen flow rate changed the porous texture of the samples drastically. ACs with much higher adsorption capacities and much higher micropore volumes were obtained using higher nitrogen flow rates. The same conclusion was found by Lillo-Ródenas et al. [80]. At flow rates of 40, 100 and 400 mL/min, the S_{BET} surface area were 1588, 1989 and 2193 m^2/g, respectively. It was also found that steam is a good atmosphere for the activation process, alone or joined with nitrogen, but not as good as pure nitrogen. Fierro et al. [79] found that the flow rate of inert gas has a much lower effect when compared to T and W. High flow rates decreased the efficiency of the activation, giving less micropores and lower surface areas.

Nitrogen is thus the best and most common general inert gas used for activation. The optimal nitrogen flow rate is hardly predicted because it strongly depends on the geometry (especially the diameter) of the reactor. Its impact is also hardly predicted because of two antagonistic effects. The flow of inert gas may evacuate activation by-products (such CO and CO_2), which is favourable, but may also evacuate vapours of reactants (e.g. K and KOH vapours), which is not favourable.

Heating rate (Hr): Lozano-Castelló et al. [62] tested two Hr, 5 and 20 K/min. It was found that the lower the Hr, the higher the micropore volume of the ACs. During the heating process, KOH melts (melting point of KOH is 633 K), so it is reasonable that a lower heating rate allows a better contact between the carbon and the molten

KOH before the reaction temperature is reached. In addition, it is known that some surface oxygen complexes are produced by KOH activation which are responsible for further carbon gasification and release of gaseous products such as CO_2, CO, etc. Then, a lower Hr would produce a slower and more controlled evolution of gaseous products, which could also explain the better microporosity development when a lower heating rate is used.

Activation time (t): The influence of the activation time has been reported by several groups. Lozano-Castelló et al. [81] found that when t increased from 0.5 to 2 h for KOH-activated carbons, both the pore volume and the surface area increased. Other authors found that activation time is one of the variables to which the final properties of ACs characteristics are less sensitive. Evans et al. [81] prepared ACs from sucrose chars by KOH activation. Results showed that increasing t by holding the samples at the maximum temperature for a longer duration time did not have a drastic effect on the product. Longer holding times resulted in slightly lower yields of product with a lower total porosity, determined by nitrogen adsorption, in the microporous region. Sudaryanto et al. [77] also concluded that t has no significant effect on the yield of activated carbon and surface area. Fierro et al. [79] found that t ranging from 0.5 to 2 h is not a significant parameter, and only little improvement of the carbon characteristics can be achieved through their variation. It can be concluded from all these studies that, again, an optimal value of t can be found for both improving the pore texture characteristics and decreasing the production costs.

Particle size: Particle size is a known parameter that has a direct effect on the physical properties of the resultant carbon. It was found that samples with small particle size are superior in terms of surface area and micropore volume. This is due to the higher contact surface of the small particles compared to that of the larger particles [82~84].

5.1.4 Surface chemistry

The amount and the nature of the surface groups affect adsorption properties. Although the surface of ACs is primarily non-polar, some surface oxides exist. It is also well known that ACs are characterized by a certain degree of surface chemical heterogeneity, which is related to the presence of heteroatoms. The kind of heteroatoms is controlled primarily by precursor, activation agent, activation method, and post-treatments. Oxygen, hydrogen, nitrogen, phosphorus, sulphur, and halogens are the main heteroatoms in the activated carbon structure. Hydrogen is bonded to edge atoms of carbon layers but others heteroatoms may be connected to edges and also in-ring within carbon layers [85]. The atomic sizes of boron and nitrogen are similar to that of carbon; hence, it is relatively easy to incorporate them into the carbonaceous network. These surface functional groups play a very important role and as such, influence the performance in the final application.

Oxygen: Oxygen is the most important heteroatom that is covalently bonded to carbon. Surface functional groups containing oxygen have a major role in ACs' properties such as surface reactivity, hydrophobicity, catalytic and adsorptive properties, and may be used for further surface modification [86]. Figueiredo et al. [87] summarized the chemical structures of surface groups on activated carbon and showed that these surface oxygen groups decompose upon heating by releasing CO and CO_2 at different temperatures (see Fig. 18) [86].

The adsorption of organic and inorganic compounds has also been found to be influenced by the presence of carbon-oxygen surface groups. Nevskaia et al. [88] studied the effects of the surface chemistry of carbon materials on the adsorption of phenol–aniline mixtures from water. The phenol adsorption isotherms are affected by the amount of oxygen surface group. Goyal et al. [89] also studied the influence of carbon-oxygen surface groups on the adsorption of several metal cations such as Cr (III), Cr (VI), Co (II), Cu (II), and Ni (II) on several activated carbons having different surface areas and associated with various amounts of carbon-oxygen surface

groups. They found that the adsorption could not be related to surface area alone, but also depended on the amount of the surface oxygen groups.

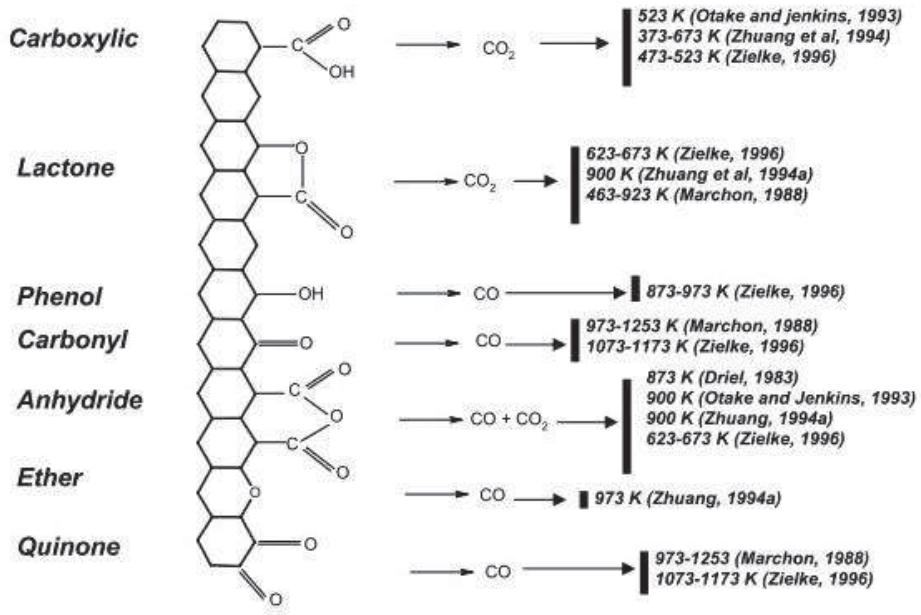

Figure 18 Summary of the chemical structures of surface oxygen groups on AC and their thermal decomposition conditions [87]

Guo et al. [90] studied the effects of surface chemistry (acidity or basicity) on gas-phase adsorption (NO_2 or NH_3) by ACs prepared from oil-palm stones pre-impregnated with various solutions ($ZnCl_2$, H_3PO_4 and KOH). Chemical characterization showed that impregnation affected significantly the surface chemistry, i.e. the nature and the amount of surface functional groups. The samples pre-treated with H_3PO_4 presented acidic groups such as phenols and carboxylic acids, whereas those from KOH impregnation showed basic groups likely to be pyrones (cyclic ketones) and other keto-derivatives of pyran. Adsorption tests of NO_2 and NH_3 showed that the activated carbons pre-treated with KOH could adsorb more NO_2 but less NH_3 than those pre-treated with H_3PO_4, even though they had almost identical apparent surface areas. So the adsorptive capacity of the AC was not only determined by its textural characteristics, but was also related to the surface chemistry. Ania et al. [91] also found that adsorption capacity of different carbon materials do not only

depend on the textural characteristics of the materials but also on their functionalities.

Oxidation may increase or decrease apparent surface area and/or pore volume, depending on the type and the concentration of oxidant, temperature of oxidation, oxidation time, etc. [86].

Boron: Boron and its compounds have often been used for modification of activated carbon. As a substitution element in the carbon structure, B can replace C in the graphitic layers, resulting in changes of electronic structure and providing intrinsic oxidation inhibition [93]. It is a unique element that has been explored for decades as substitution into carbonaceous materials to promote properties such as oxidation resistance [94], Li-ion insertion [95], and electrochemical behaviour [96, 97]. Zha et al. [94] prepared AC from petroleum coke by KOH activation at 1073 K in N_2 atmosphere with W = 2.5. B_4C was used as a boron-doping additive by heat treatment at 1123 K for 5 h to increase its antioxidant ability. Total pore volume, mesopore volume, micropore volume, and BET surface area of porous carbon decreased after boron-doping, but the antioxidant ability of the boron-doped porous carbon at 873 K in air was improved. Wang et al. [95] synthesised and studied the electrochemical property of boron-doped mesoporous carbon in supercapacitor. Low-level boron doping shows catalytic effect on oxygen chemisorption at edge planes and alters electronic structure of doped mesoporous carbon. These characteristics are responsible for substantial improvement of interfacial capacitance, becoming 1.5~1.6 times higher in boron-doped carbon than that in boron-free carbon with alkaline electrolyte (6 M KOH) and/or acid electrolyte (1 M H_2SO_4).

Nitrogen: Nitrogen-containing groups generally provide basic property, which might enhance the interaction between porous carbon and acidic molecules. Nitrogen groups were introduced by amine treatment, nitric acid treatment and some other reactions with nitrogen-containing molecules. The chemical structure of some possible nitrogen surface functionalities can be seen in Figure 19 [98].

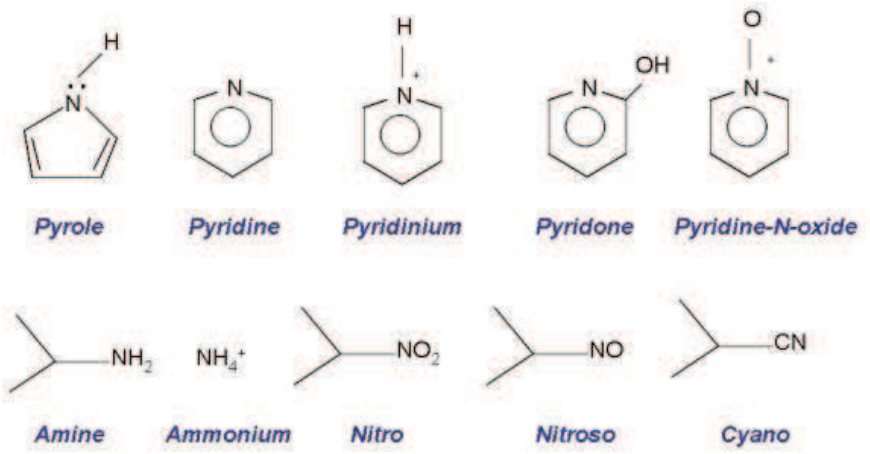

Figure 19 Chemical structures of some nitrogen surface functionalities [98]

Aburub et al. [99] and Pittman et al. [100] stated that, on the surface of ACs, there are two distinct regions which are a basal carbon surface, which is non-polar and hydrophobic, and a region containing diverse functional groups. Both of them influence the adsorption properties. It is also noteworthy that introduction of new functional groups lowers the surface area. Applications of modified ACs thus depend both on textural characteristics and surface chemistry. For this reason, selecting the suitable precursor, activation and modification processes is absolutely necessary.

5.1.5 Porous structure

Pore structure is a key parameter of activated carbon, which includes the specific surface area, the distribution of pore sizes, and the pore volumes.

Specific Surface Area is defined as the area of solid surface per unit mass of material. Gas adsorption measurements can be used for the determination of the surface area and pore size distribution. Nitrogen at 77 K is the recommended adsorbate for this purpose. Not only nitrogen gas can be used, but krypton, argon and carbon dioxide are also very common. The minimum pore size that can be investigated is limited by the size of the probe molecule, about 0.4 nm in the case of nitrogen. The maximum pore size is limited by the practical difficulty of determining

the amount of gas adsorbed at high relative pressure. In the case of nitrogen, the maximum pore size is about 300 nm.

According to the classification of IUPAC [56], six classes of adsorption isotherms exist and are shown in Figure 20.

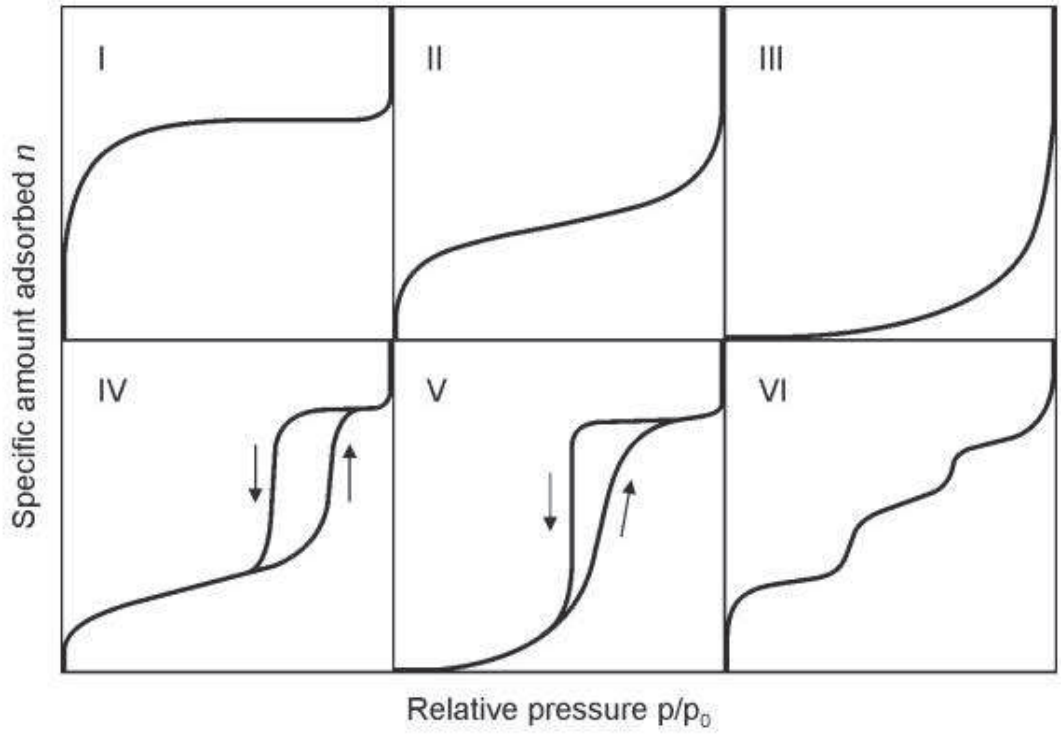

Figure 20 The isotherms classification according to IUPAC [56]

Type I isotherms are observed for microporous solids having relatively small external surfaces (e.g. activated carbons, molecular sieve zeolites, and certain porous oxides). The limiting uptake is governed by the accessible micropore volume rather than by the internal surface area.

Type II isotherm is the normal form obtained with a non-porous or macroporous adsorbent. The type II isotherm represents unrestricted monolayer-multilayer adsorption.

Type III isotherms are convex to the p/p_0 axis over its entire range. This type is not common, but some systems exist (e.g. nitrogen on polyethylene) which exhibit

isotherms with gradual curvature. In such cases, the adsorbate-adsorbate interactions play an important role.

Type IV isotherms exhibit a hysteresis loop, which is associated with capillary condensation taking place in mesopores, and has a limiting uptake over a range of high p/p_0. Type IV isotherms are characteristic of many mesoporous industrial adsorbents.

Type V isotherms are uncommon. They are related to Type III isotherms in that the adsorbent-adsorbate interaction is weak, and they also exhibit hysteresis as in Type IV.

Type VI isotherms exhibit stepwise multilayer adsorption on uniform non-porous surfaces. The sharpness of the steps depends on the system and on the temperature. The step height represents the monolayer capacity and, in the simplest case, remains nearly constant for two or three adsorbed layers. Among the best examples of Type VI isotherms are those obtained with argon or krypton on graphitized carbon blacks at liquid nitrogen temperature.

There are many theoretical models describing the adsorption of gases on porous systems, like Henry model, Langmuir model and Brunauer-Emmett-Teller model. The BET equation is the most commonly used isotherm equation for porous materials and can be used for comparing the surface area of activated carbons. The BET model is used for describing physical adsorption and is based on the following assumptions:

a) Adsorbent consists of a regular array of adsorption sites equal in energy, with a constant enthalpy of adsorption in the monolayer, ΔH_A.

b) Adsorption is localised to these sites.

c) Neighbouring adsorbed molecules do not interact.

d) Multilayer formation is unlimited.

e) Enthalpy of adsorption in second and subsequent multilayers is equal to the enthalpy of liquefaction, ΔH_L.

f) Adsorption or desorption may only occur on or from exposed sites.

The BET equation is conveniently expressed in its linear, following, form:

$$\frac{p/p_0}{n(1-p/p_0)} = \frac{1}{n_m C} + \frac{C-1}{n_m C}(p/p_0)$$

where n is the amount adsorbed at the relative pressure p/p_0, n_m is the monolayer capacity, and C is a constant that is dependent on the isotherm shape.

According to the BET equation, a linear relation is given if $p/\{n(p_0-p)\}$ is plotted against p/p_0 (i.e. the BET plot). In this manner, it is possible to obtain n_m. The second stage in the application of the BET method is the calculation of the surface area, S_{BET}. This requires the knowledge of the average area, a_m (i.e. molecular cross-sectional area), occupied by each adsorbed molecule in the complete monolayer. Thus,

$$S_{BET} = n_m \cdot L \cdot a_m$$

where L is the Avogadro constant. It is usually assumed that the BET nitrogen monolayer is close-packed, giving $a_m(N_2) = 0.162$ nm^2 at 77 K.

Application of the B.E.T equation was shown to be linear only over the range $p/p_0 = 0.05$ to 0.30. The model fails at lower relative pressures and at $p/p_0 > 0.30$ above which neglecting lateral interactions between neighbouring admolecules and capillary condensation process produce deviations in the plot. But for microporous ACs, relative pressure range of 0.01~ 0.05 was recommended by Kaneko et al. instead of the classical 0.05~0.3 range [170]. Doing so, the possibility of getting a negative C value which would have no physical meaning, may be avoided.

Pores comprise two types of surfaces: the internal or microporous surface and the external surface. Internal surface represents the walls of the pores and has a high surface area that may be as high as several thousands m^2 per gram in many activated carbons. External surface comprises the walls of the meso- and macropores as well as

the edges of the outward facing aromatic sheets, and is comparatively much smaller and may vary between 10 and 200 m^2/g for many activated carbons [1]. As shown in Figure 21, probing a micropore with a small molecule slightly underestimates the inner surface and at the same time overestimates the outer surface. For larger molecules the error in the determination of the specific surface area is higher. For the extreme case of molecules that cannot enter the pore, the inner surface is completely disregarded. The accessible surface area thus depends on the diameter of the probe molecule [2].

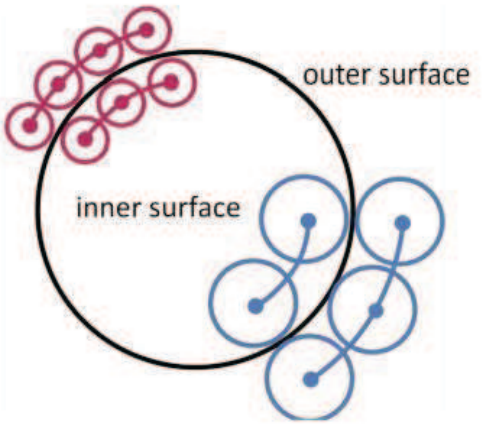

Figure 21 Illustration of inner surface and outer surface for the AC [2]

Hence, the specific surface area has no definite meaning in the case of microporous carbons, because the size of the probe molecule has a profound influence on the measured surface area. Thus, if a carbon is to be used for a particular application, its surface area should be determined with a molecular probe having suitable size and shape.

Pore Volume: The specific pore volume is also most of times determined by nitrogen adsorption at 77 K. As said before, BET surface area is determined typically at a relative pressure below 0.30, below which monolayer adsorption should be completed, or below 0.05 for microporous materials. The total pore volume $V_{0.99}$ is determined at a relative pressure of 0.99 at which the pores of the material are

completely filled. The difference in the uptake between the relative pressure used for S_{BET} and $V_{0.99}$ corresponds to the amount of gas adsorbed as multilayers.

Pore Size: Different types of pores exist in ACs. As shown in Figure 22, region (a) consists of closed pores, i.e. which are inaccessible to an external fluid and are totally isolated from their neighbours. Closed pores influence macroscopic properties such as bulk density, elasticity, mechanical strength, and thermal conductivity, but they are inactive in processes such as fluid flow and adsorption of gases. On the other hand, regions (b, c, d, e and f) correspond to open pores. Open pores are further classified into "through pores" and "blind pores." Through pores have an open channel that begins at one location of the surface, extends into the particle, and re-emerges on the surface at a different location (like the pore channels c-e-c and c-e-d). Blind pores (also called dead-end) are open to the surface only at one end (like b and f). In region (g), the small surface irregularities are technically blind pores. However, it is often more useful and convenient to consider them separately as surface roughness [101]. A simple convention often used is to assume that surface irregularities are counted as pores only if they are deeper than they are wide.

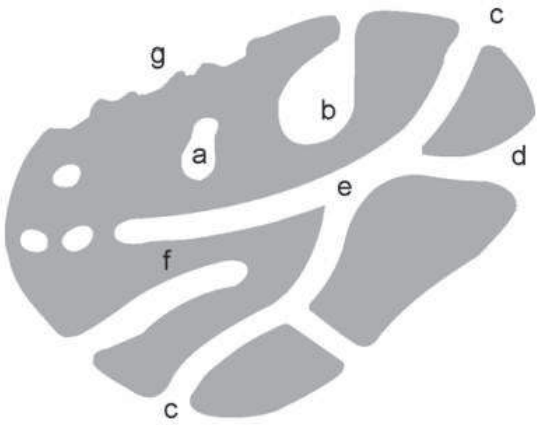

Figure 22 Schematic cross section of a porous solid (from [101])

Pores may be classified further according to their shapes [103] as slit pores, conical pores, interstice pores, spherical (ink-bottle pores) and cylindrical pores, as shown in Figure 23. The pore shape can also influence the adsorption isotherms. But it is difficult to obtain accurate information about the shape of the pores.

Figure 23 Different pore shapes in activated carbon [103]

As we know, ACs comprise pores having widths from less than one nanometre to several thousands nanometres. According to the classification that was proposed by the International Union of Pure and Applied Chemistry (IUPAC), there are three groups of pores: micropores, mesopores and macropores. They are classified by their width, i.e. the distance between the walls of a slit-shaped pore or the radius of a cylindrical pore [101].

Micropores have pores narrower than 2 nm. The adsorption in these pores occurs through volume filling, and no capillary condensation takes place. The adsorption energy in these pores is much higher compared to that of wider mesopores or nonporous surface because of the overlapping of adsorption forces from the opposite walls of the micropores, as shown in Figure 24.

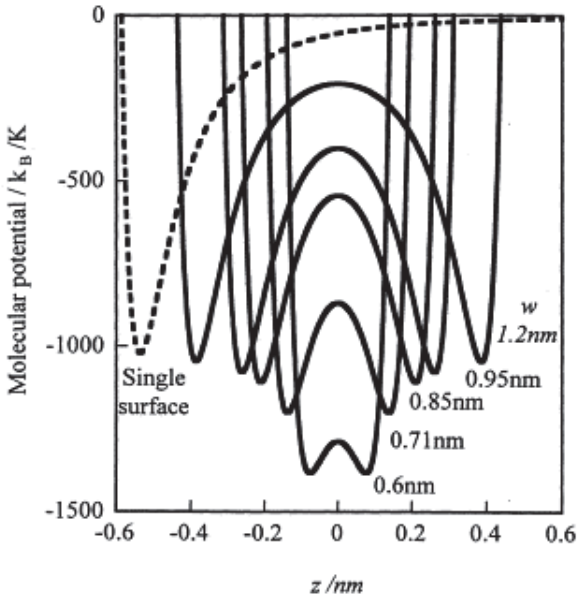

Figure 24 Overlapping of adsorption forces from the opposite walls of the micropores (from [176]).

Mesopores, also called transitional pores, have effective dimensions in the 2 to 50 nm range.

Macropores are wider than 50 nm and frequently in the 500 to 2000 nm range. They are not of considerable importance to the process of adsorption because their contribution to the surface area is very small. They act as transport channels for the adsorbate into micro- and mesopores. Macropores are not filled by capillary condensation and can be characterized by mercury porosimetry [101].

5.1.6 Applications of Activated Carbon

ACs' applications can be classified into two categories: gas phase and liquid phase. ACs are excellent and versatile adsorbents because of their developed porosity which provides high, non specific, adsorption capacity per unit volume, highly microporous structure, a high degree of surface reactivity and their flexible surface chemistry, which make them suitable for different applications. Activated carbons can be used for solvent recovery, gas storage, and catalysis.

Gas-phase applications: Around 20 % of the total production of ACs in industrialized countries is used in gas-phase adsorption processes. The ACs used for gas-phase applications is usually in the granulated form that can be used as such or after impregnation with one or more organic or inorganic compounds. With the granulated form, the process involved is generally only physical adsorption, but with impregnated carbons both adsorption and a chemical reaction can take place.

Liquid-phase applications: Nearly 80 % of the total activated carbon is consumed for liquid-phase applications, where both the granulated and powdered forms of active carbon are used. Activated carbons can be used for water treatment, decolorizing in sugar industry, gold recovery, decolorizing of oils and fats, purification of electrolytic baths, refining of liquid fuels, food processing, preparation of alcoholic beverages, etc.

5.2 Hydrogen Adsorption on activated carbon

The basics of AC have been discussed above. In this section, we will systematically discuss the mechanisms of hydrogen adsorption on AC, and the factors which can influence hydrogen storage in AC.

5.2.1 Mechanisms of hydrogen storage in activated carbon

S*orption* is the non-specific term that describes both adsorption and absorption. It is most often used when it is difficult or impossible to separate adsorption and absorption or when both processes occur simultaneously. *Desorption* is the reverse process of sorption. *Adsorption* is the enrichment or depletion of one or more components in an interfacial layer. These processes are pictured in Fig. 25.

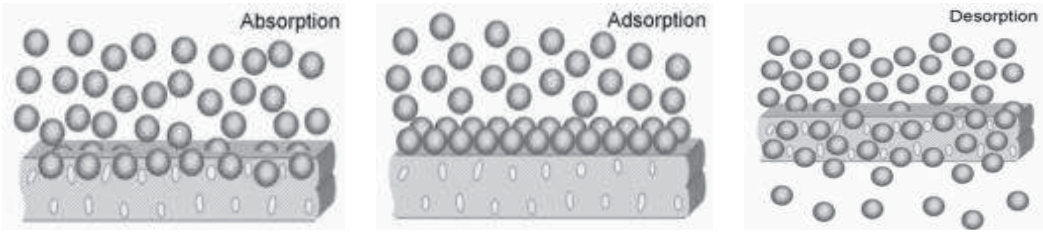

Figure 25 The illustration of absorption, adsorption and desorption (Sources: IFA)

Adsorption involves two types of forces: physical forces that may be polarization forces, dispersive forces, or short-range repulsive interactions, and chemical forces that are valence forces arising out of the redistribution of electrons between the solid surface and the adsorbed atoms. Depending on the nature of the forces involved, the adsorption is of two types: physical adsorption and chemisorption. In the case of physical adsorption, the adsorbate is bound to the surface by relatively weak Van der Waals forces, which are similar to those involved in the condensation of vapours into liquids. Chemisorption, on the other hand, involves exchange or sharing of electrons between the adsorbate molecules and the surface of the adsorbent, resulting in a true chemical reaction. The bond formed between the adsorbate and the adsorbent is essentially a chemical bond and is thus much stronger than in physisorption.

There are two important differences between physisorption and chemisorption. The most important difference is the magnitude of the enthalpy of adsorption. In physical adsorption, the enthalpy is of the same order as the heat of liquefaction and does not usually exceed 10 to 20 kJ per mol, whereas in chemisorption the enthalpy change is generally of the order of 40 to 400 kJ per mol. Another important point of difference between physisorption and chemisorption is the thickness of the adsorbed phase. Whereas it can be multimolecular in physisorption, the thickness is only unimolecular in chemisorption.

Hydrogen can be stored at the surface and in the bulk of chemisorption media. For superficial chemisorption, hydrogen is chemically bound to the medium's surface. For bulk chemisorption, hydrogen dissociates at the surface and transfers into the bulk via atomic diffusion through interstitial sites, where it is ultimately incorporated into the solid phase of the medium [105].

Storage via physisorption is primarily limited to porous and nano-structured media, wherein high surface area-to-volume ratios allow significant uptakes like in high surface area-activated carbons. In contrast to chemisorption, physisorption does not involve a significant change in electronic orbital patterns and is generally more reversible [105]. In the adsorption process, no chemical bonds are formed, therefore the heat of adsorption is low, e.g. for hydrogen it is typically around 1~10 kJ/mol. At temperatures higher than the critical temperature, gases are adsorbed as low-density monolayers on the surface. The heat of adsorption for the second and higher layers would be smaller than for the first layer. Consequently, multilayers only start to form when the temperature is decreasing to close or below the critical temperature of the adsorbate. For hydrogen, the boiling temperature (20.4 K) and critical temperature (33.0 K) are very low, as is the heat of condensation, only 0.9 kJ/mol. Thus, even at 77 K, hydrogen is adsorbed as a monolayer, and no multilayer adsorption takes place in contrast to adsorption at 20 K.

Physisorption is a dynamic equilibrium because the number of molecules sticking to the surface is equal to the number of molecules rebounding from the surface. The amount of hydrogen adsorbed at equilibrium for a given adsorbate-adsorbent system depends on the pressure of the gas and on the temperature of adsorption :

$x/m = f(P, T)$

where x/m is the amount adsorbed per unit mass of the adsorbent at the equilibrium pressure P, and T is the temperature of adsorption.

Physisorption of hydrogen on activated carbon leads to type I isotherms. At low pressure the amount adsorbed increases linearly with pressure which is the so called Henry's law region. When the pressure further increases, the monolayer is getting saturated and therefore a strong deviation from linearity of the gas uptake is observed. If the temperature of the system is close or below the critical temperature of the adsorbate, the completion of the monolayer is followed by multilayer adsorption. Therefore, at higher pressure, the adsorbed amount increases slightly with pressure. For materials with very small pores, almost no multilayer adsorption is observed and therefore the plateau of the isotherm is almost horizontal. At pressure close to the pressure of liquefaction (P/P_0 close to 1), the gas in the pores and the surroundings is getting liquefied and therefore a strong increase of the adsorbed amount is observed.

As shown in Figure 26, there are three different definitions for the hydrogen adsorption capacity, which are excess, absolute and total adsorption. The excess hydrogen storage first increases with pressure, but finally decreases. The absolute storage capacity increases with pressure until a horizontal plateau is reached at higher pressure, and the curve is above that of the excess adsorption capacity. The largest is the total hydrogen capacity, which exhibits a continuous rise of the hydrogen uptake at high pressure.

According to the gas density profile in a pore shown in Figure 27, the adsorbed gas close to the pore walls has a high density, close to that of the liquid. The density decreases with increasing distance from the surface till a minimum is reached, which

is the density of the free gas which depends on the applied pressure. The excess hydrogen uptake n_{exe} is the amount of gas which is adsorbed additionally to the gas that would be present in the pore if there was no adsorption, and is represented by the areas A. The areas B and C represent the molecules present in the free gas phase owing to the applied pressure. The areas B and C increase with pressure, unlike area A, which decreases. Therefore, the excess adsorption isotherm presents a maximum. Absolute adsorption n_{ads} is the amount of gas which is adsorbed on the surface (areas A and B).

If adsorption is used for storage purposes, the amount of interest is the total amount of gas present in the system, which is called total adsorption n_{total}. The total adsorption is given by the excess adsorption (area A) plus the amount of gas in areas B and C.

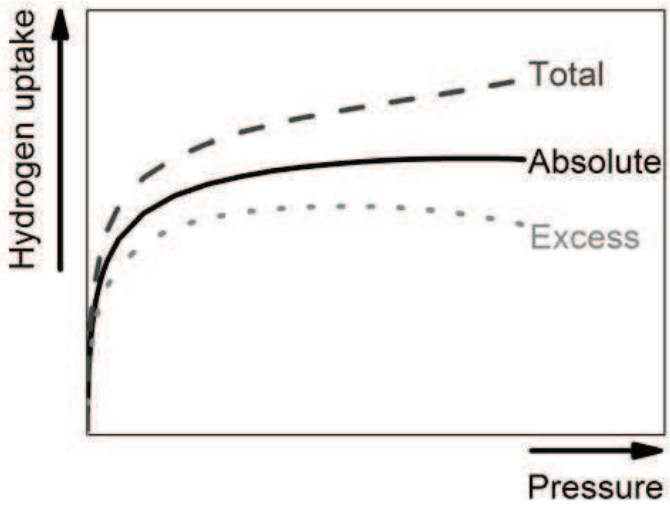

Figure 26 Typical isotherms for excess, absolute and total hydrogen uptake [102]

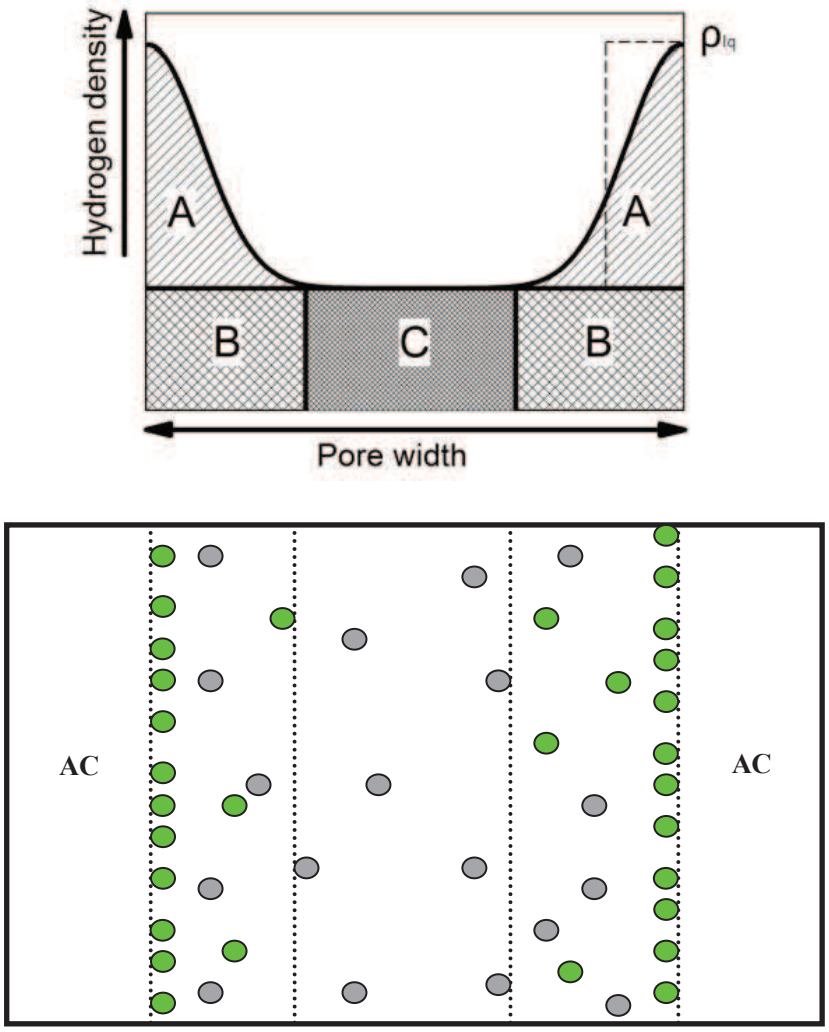

Figure 27 Hydrogen density profile in a pore. A denotes the excess, A+B the absolute, A+B+C the total adsorption

5.2.2 Effect of Surface Area and Pore Volume

There are two very important factors for hydrogen storage, which are the specific surface area and the pore volume, especially the micropore volume. Most authors believe that the hydrogen storage capacity is proportional to the specific surface area [107~108]. Xu et al. studied the hydrogen storage capacity of various carbon materials, including ACs, SWCNTs, MWCNTs, and GNFs. Among these carbons, Maxsorb had the highest surface area of 3300 m^2/g and hence the highest storage capacities of 0.67 wt % at 303 K and 10 MPa, and 5.7 wt % at 77 K and 3 MPa [109]. The storage

capacities of the carbons were found to be proportional to their specific surface area and micropore volume.

Texier-Mandoki et al. [110] found that the hydrogen adsorption capacity of ACs increased with both the total surface area and the micropore volume. No straightforward correlation was observed between the hydrogen adsorption capacity and the total surface area or the micropore volume determined by N_2 adsorption at 77 K. On the contrary, a linear relationship was found between the H_2 adsorption capacity at 10 bar and the micropore volume measured with CO_2 [111~112].

Fierro et al. [113] found that, whatever the materials prepared from the same anthracite activated with alkaline hydroxides, a linear relationship is observed between maximum hydrogen uptake at 77 K and S_{BET} only if the latter is not higher than 2630 m^2/g. Above such a value, which is the theoretical maximum for graphitic materials, a plateau was reached due to a saturation of H_2 storage capacity at 2630 m^2/g, and a slight decrease was found for the highest surface areas probably due to the broadening of the pores (as shown in Figure 28). The same tendency was found by Israel Cabasso [114].

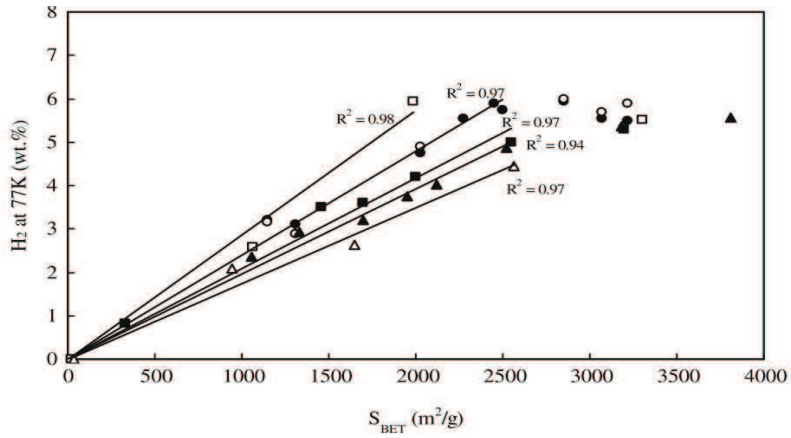

Figure 28 Correlation between S_{BET} and H_2 uptake at 77 K [113]

Hydrogen storage thus requires both high surface area and suitable pore size. Hence, as previously mentioned, the best hydrogen storage performances result from a balance between material density and porosity. Adsorbents with high surface areas

and pore volumes indeed tend to have lower bulk densities, leading to low volumetric capacities.

5.2.3 Effect of Pore Sizes Distribution

The total amount of adsorbed hydrogen strongly depends on the pore size, and on the specific surface area and pore volume. Several authors suggested the following optimum pore diameters for H_2 storage: 0.5~0.7 nm [115], 0.68 nm [116], 0.7 nm [111] or 0.71 nm [117]. Cabria et al. [118] theoretically predicted that, in order to reach the hydrogen storage target of the US Department of Energy for 2010, the pores widths should be equal or larger than 0.56 nm for applications at 77 K and any pressure, and about 0.6 nm for applications at 300 K and at least 10 MPa. Rzepka et al. [111] investigated the storage capability of microporous carbon materials for gaseous hydrogen both theoretically and experimentally. At room temperature, the optimum pore geometry is a slit pore consisting of two graphite platelets separated by a distance that corresponds approximately to two times the diameter of a hydrogen molecule. Gogotsi et al. [119] experimentally demonstrated that ACs with an average pore diameter of 0.6~0.7 nm provide the largest H_2 uptake per unit of specific surface area at elevated pressures and 77 K. Texier-Mandoki et al. [110] found that the hydrogen adsorption capacity of an activated carbon is directly related to its CO_2 micropore volume and showed the importance of the presence of an homogeneous narrow microporosity (0.7 nm) for hydrogen adsorption.

For a given surface area, small pores (1 nm or below) are more efficient for hydrogen sorption. But on the other hand, micropores with diameter wider than 1 nm were also suggested to contribute to the storage capacity. Gadiou et al. [112] investigated hydrogen adsorption on mesoporous carbon and AC with a variety of pore sizes and found that super-micropores with diameters between 1 and 2 nm also contributed significantly to the storage capacity. Panella et al. [120] studied the correlation between the hydrogen storage capacity at 77 K and the pore volume for pores narrower than 1.3 nm. The linear relationship between the pore volume and the

storage capacity demonstrated that ideal carbon materials for hydrogen storage should possess a high microporosity with a small pore dimension.

5.2.4 Effect of Oxygen

In the gas phase, it has been found that the adsorption capacity of AC for non-polar molecules increases with the amount of surface acidic groups [62]. Given that hydrogen is also a non-polar molecule, this conclusion should apply to its adsorption.

As mentioned above, oxygen functional groups at the surface of ACs can be obtained by air, ozone, anodic, acid, plasma oxidations, etc. The influence of the oxidized groups on the hydrogen storage capacity was studied by several authors. Agarwal et al. [121] studied hydrogen adsorption on oxidized carbons and showed that the hydrogen uptake at 78 K increased with the oxygen content in activated carbons modified by gas-phase oxidation. Zhou [122] investigated the influence of the chemical treatment of ACs from coconut shells and found that increasing the amount of acidic functional groups was favourable for the adsorption of hydrogen, but the surface area was still a dominant factor for hydrogen storage.

However, negative impact of oxidation treatment on H_2 storage was also reported by several other authors. The main reason is that acidic group blocked the pores in AC, so that S_{BET} and microporosity decreased. Takagi et al. [123] found that hydrogen uptakes of ACF samples at both 77 and 303 K were remarkably decreased by oxidation and could be attributed to changes in the pore structure. Kim et al. [124] showed that the hydrogen storage of the AC sample after ozone treatment decreased because of the decrease of S_{BET}. Huang et al. [125] studied the effect of surface oxides on the H_2 storage of ACs, and noticed that an excess of acidic functional group on ACs surface were detrimental for H_2 storage. The H_2 uptake decreased when the surface area of the oxidized AC was less than 2358 m^2/g or when the amount of the surface acidic group was higher than 0.8 mmol/g.

As we know, any treatment used for modifying the surface chemistry of AC not only leads to different functional groups, but may also change textural characteristics such as surface area, pore volume, pore size distribution, etc. Because hydrogen storage is sensitive to surface area and pore size, the hydrogen storage is not only influenced by the oxygen groups introduced by different ways, but also by the changes of surface area and pore size distribution after treatment.

5.2.5 Effect of Nitrogen and Boron Doping

Heteroatom doping (e.g. boron, sulphur, phosphorus, and nitrogen) of carbon affects various physicochemical properties of sp^2 carbon materials. Because of their small sizes, B and N atoms can dope carbon materials or replace carbon atoms without significantly altering the structure. But such doping has significantly impact on the interactions between carbon and hydrogen. Recently, attention to N and B doping has been given for hydrogen storage purposes.

Both theoretical and experimental works show that N- and B- substitution in carbon material can significantly increase the interactions between hydrogen (both H and H_2) and carbon, thereby increasing hydrogen storage capacities [126-139]. Zhou et al. [126, 127] investigated the doping effects of B and N on hydrogen storage by using density functional theory calculations. It was found that both B and N doping of carbon materials can increase the heat of adsorption, indicating that the hydrogen storage capacity is improved. Wang [128] found that the N-doped microporous carbon had a storage capacity 18% higher than that of pure carbon with a similar surface area. Significantly higher heats of adsorption were obtained on N-doped microporous carbon samples than that on non-doped carbons for H_2 adsorption. Zhu [129] found that boron substitution destabilizes the graphene structure, increases the electronic density around the substituted atoms, and lowers the electrostatic potential, thus improving the hydrogen adsorption energy of doped carbon. However, this improvement is only 10 ~ 20%.

Just like for modification of carbonaceous materials by oxygen atoms, optimization of both porous structure and N-/B- contents are needed for significantly enhancing hydrogen storage of carbon. Xia et al. [139] found that, for N-doped carbons in which the nitrogen content was kept within a narrow range from 4.7 to 7.7 wt. %, the hydrogen uptake was only related to the induced changes of surface area and micropore volume. By considering the isosteric heat of hydrogen adsorption and excess hydrogen uptake on N-free or N-doped carbons, it was shown that N-doping can be beneficial at lower coverage (low hydrogen uptake) but is detrimental at higher coverage (higher hydrogen uptake). Anyway, a balance should be considered between the porous structure and the N-/B- contents.

6 Hydrogen Storage in Carbon-based Adsorbents via Spillover

In the case of catalytic or adsorbent systems in which a metal species is dispersed on a support (or carrier) material (often quasi-inert oxides, such as alumina or silica), the presence of the metal serves as a lower-energy pathway for gaseous species to first adsorb onto the metal particle and then diffuse to the support surface. This phenomenon is called “spillover”. The spillover effect is possible because the adsorbed species attains a lower energy state once adsorbed onto the metal, thus lowering the activation barrier between the gas phase species and the support-adsorbed species.

Hydrogen storage by spillover is a rather new field, although the phenomenon of ‘‘hydrogen spillover’’ has been known for a long time. Evidence of atomic hydrogen spillover was first observed indirectly in the framework of studies of ethylene hydrogenation by heterogeneous catalysis [143]. Afterwards, hydrogen spillover has been extensively studied particularly in the field of catalysis during the last four decades. Hydrogen spillover is the most common example of an adsorptive spillover. Hydrogen adsorption is most often accompanied with dissociation of molecular

hydrogen (H_2) to atomic hydrogen (H), followed by diffusion of hydrogen atoms [140~142].

6.1 Mechanisms of Hydrogen Spillover

Hydrogen spillover onto carbon-based materials represents a novel technique to store hydrogen in a variety of materials that are readily available. By using hydrogen spillover for hydrogen storage, several research groups worldwide reported significant enhancements in hydrogen storage on carbon nanotubes, carbon fibers, graphite, activated carbons, and templated carbons, MOFs, COFs, polymer, silica and metal oxides [144~148, 150~156]. But using hydrogen spillover for hydrogen storage is still disputed. The first attempt to use the spillover phenomenon for hydrogen storage appeared in a patent entitled, "Metal assisted carbon cold storage of hydrogen," by Schwarz [149]. Schwarz investigated hydrogen adsorption on an activated carbon mixed with transition metal from room temperature to 77 K, and observed that spillover effect was the strongest at 77 K and nearly absent at room temperature. The results also showed that the spillover was fairly fast at 77 K, and was nearly completed in 5 minutes.

More recent results showed that this observation was not correct [150~166]. Yang et al. [150~156] investigated the spillover effect on several carbon materials and they found that the spillover is only significant at room temperature. The mechanisms are shown in Figure 29 and the hydrogen spillover processes can be explained according to three steps:

1. Molecular H_2 dissociation on the metal catalyst particles (this process is energetically favourable)
2. Atomic H migration to the carbon support (may involve both chemisorption and physisorption processes)
3. Diffusion of atomic H across the carbon surface

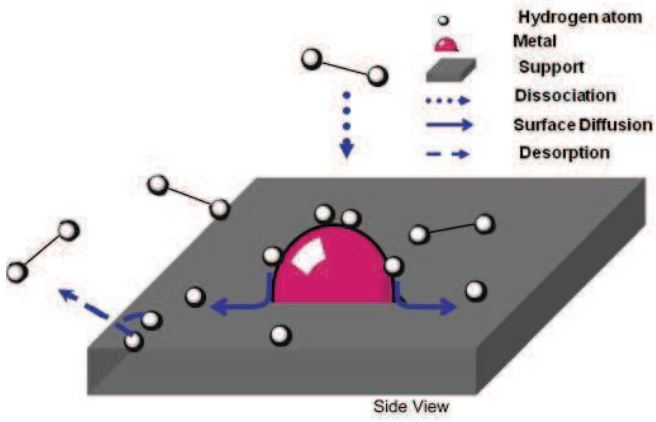

Figure 29 Hydrogen spillover processes [150~156]

6.2 Influencing Factors for Storage via Spillover

Enhanced hydrogen storage capacity by spillover is affected by hydrogen dissociation source, spillover hydrogen receptor, and contact between metal and carbon.

6.2.1 Hydrogen Dissociation Source

The first crucial factor is the hydrogen dissociation source, which is the metal used. Metal nanoparticles must be well dispersed. Increase in metal loading provides more hydrogen dissociation sites, but the entire adsorbent weight will also increase and the porosity might be blocked. High dispersion is needed for getting the smallest nanoparticles contributing to an increased metal surface area for dissociation of hydrogen and contact with carbon receptor. Hydrogen storage capacities of Ru / templated carbon (TC) samples with different Ru loadings (3, 6, and 8 wt %) were compared by Wang and Yang [141]. Hydrogen storage capacities followed the following order of metal loadings: 6 wt % > 8 wt % > 3 wt %. Saha et al [162] dispersed transition metals such as palladium, platinum, nickel, and ruthenium onto ordered mesoporous carbons. Although the S_{BET} was reduced significantly, hydrogen adsorption was increased by a factor 2.7 ~ 5.4 at 1 bar and 1.38 ~ 3.69 at 300 bar due to the spillover effect. Wang and Yang [141] doped two different high surface area

carbon materials, one templated carbon (TC) and one super activated carbon (AX-21), with three different metals (Ru, Pt, and Ni). The results revealed that Ru was more efficient than Pt and Ni, both on TC and AX-21. Reyhani et al. [163] concluded that hydrogen storage capacity can be improved in MWCNTs decorated by Co, Fe, Ni, and Pd metals. In this study, Pd was the most efficient metal. The same conclusion was obtained when comparing multi-walled carbon nanotubes doped with Pd or V [164].

6.2.2 Spillover Hydrogen Receptor

The second crucial factor is the hydrogen receptor, in our case, the AC used. Two essential parameters must be considered, the porosity and the surface chemistry. On one hand, a higher surface area would provide more hydrogen adsorption sites. This is easily understood because at 77 K and high pressure, the hydrogen storage in an adsorbent depends on the surface area, whereas spillover depends on the interaction of hydrogen atoms with the surface sites of the adsorbent. Therefore, the surface area of the adsorbent should be an important factor in hydrogen adsorption by spillover. An adsorbent with high surface area would provide more adsorption sites for hydrogen adsorption via spillover. On the other hand, recent experimental studies have shown that a further enhancement of the storage capacity of metal-doped activated carbons can be achieved by chemically modifying the carbon substrate through the introduction of oxygen functionalities. Modification of carbon materials by oxygen groups will decrease its hydrophobicity and thus make the carbon surface more accessible to the metal precursor during the impregnation step, oxygen groups increasing the interactions between the metal and the carbon substrate. These two effects help to facilitate spillover on the doped sample [16].

The effect of surface oxygen groups in AX-21 on hydrogen storage was investigated [165], and the results showed that Pd supported on oxygen-modified AX-21 (Pd/AX-21-O) had a higher hydrogen storage capacity than Pd supported on unmodified AX-21 (Pd/AX-21). Li et al. [133] pointed out that increased surface

density of oxygen groups leads to a significant enhancement of hydrogen spillover at pressures <100 mbar. Wang et al. [167] modified the carbon surface by O_2 plasma, and found that the H_2 storage capacity at 298 K and 10 MPa was increased from 1.17 wt % (without O_2 treatment) to 1.74 wt. % on Pt-doped carbon pre-treated with O_2 plasma. The hydrogen spillover mechanism on B-doped graphene was explicitly investigated with first-principles calculations by Wu et al [168]. By the incorporation of boron into graphene, the theoretical investigation shows that B doping can substantially enhance the adsorption strength for both H atoms and the metal cluster on the substrate. The firmly bound catalytic metal on B-doped graphene can effectively dissociate H_2 molecules into H atoms, and the H atom is more likely to migrate from the bridge site of the H-saturated metal to the supporting graphene sheet. Yang's group [133] studied hydrogen storage via spillover on Ru-supported B-doped microporous carbon, and obtained a 2.2-fold enhanced hydrogen uptake of 1.2 wt. % at 298 K and 10 MPa.

All these works suggest the favourable effect of chemical modification of the carbon support.

6.2.3 Contact between Metal and Carbon

The third factor is the contact between source and receptor. Because of the existence of physical and energy barriers for transfer of hydrogen atoms from one material to another, intimate contacts should facilitate the spillover and thereby enhance the hydrogen storage capacity. Enhanced storage capacity has been achieved by several methods such as bridge building (see below), plasma-assisted doping and ultrasound-assisted building. However, the contact impact on spillover is still poorly understood.

Bridge building techniques have been developed to enhance spillover through improved contacts between the source and the receptor [152~154]. The bridge building technique involves mixing the catalyst (a small amount) and the sorbent with a small

amount of carbon precursor such as glucose, followed by a temperature programmed heating protocol to carbonize the precursor. By using this simple technique, carbon ‘‘nanobridges’’ can be built between a spillover source particle and a secondary receptor particle. Yang et al. [156] found that the adsorbed hydrogen amounts were increased by a factor of 2.9 on the AX-21 receptor and 1.6 on the SWNT receptor at 298 K and 100 bar.

A direct high-temperature thermal reduction method was applied to increase the contacts between Ru and the carbon support by Wang and Yang [141]. The resulting ruthenium-doped templated carbon sample showed a further increased hydrogen storage capacity of 1.56 wt % at 298 K and 10 MPa.

Recently, a new plasma-assisted reduction method has received much attention for the preparation of nano-sized metal-doped materials. Li and Yang [151] concluded that the doping of carbon by metal can be significantly improved by plasma treatment in two ways: increased dispersion and stronger interactions between metal particles and the substrate, both directly leading to enhanced hydrogen spillover and, thereby, to increased hydrogen storage.

Chapitre II

Détails expérimentaux

1 Precursors and sample preparation procedures

The precursor of the activated carbons (AC) investigated here was the anthracite from China named Taisi. Figure 30 shows the illustration of the process for preparing the AC.

The anthracite was first ground and sieved in order to collect the grains whose average size was in the range 100 ~ 200 μm. The anthracite powder was then physically mixed with potassium hydroxide lentils, according to various mass ratios KOH/anthracite (W). The resultant mixture was introduced into a nickel crucible, and finally heat-treated in a horizontal furnace under a stream of nitrogen at different constant heating rates (Hr) up to different final activation temperatures (T) which were maintained for 2 h. The crucible was then allowed to cool down to room temperature under nitrogen flow.

During the experiments, both alkali metal (produced by the reduction of KOH by carbon at high temperature) and alkali hydroxide were partly transported in the vapour phase, and could be observed at the outlet of the reactor. Alkali metal mixed with alkali carbonate was also found to be present inside the crucible. Therefore, the latter was submitted to atmospheric humidity for one day, during which the alkaline metal slowly oxidised. Finally, the activated anthracite was washed with extreme care, first with 1M HCl, and finally with hot distilled water until the pH of the rinse remained constant and close to 6. After drying in an oven during 24 h, a very pure activated carbon (AC) material was obtained.

The AC was sieved again for recovering particles within the range 100~200 μm, and was submitted to pore texture characterisation, hydrogen adsorption experiments and doping with heteroelements.

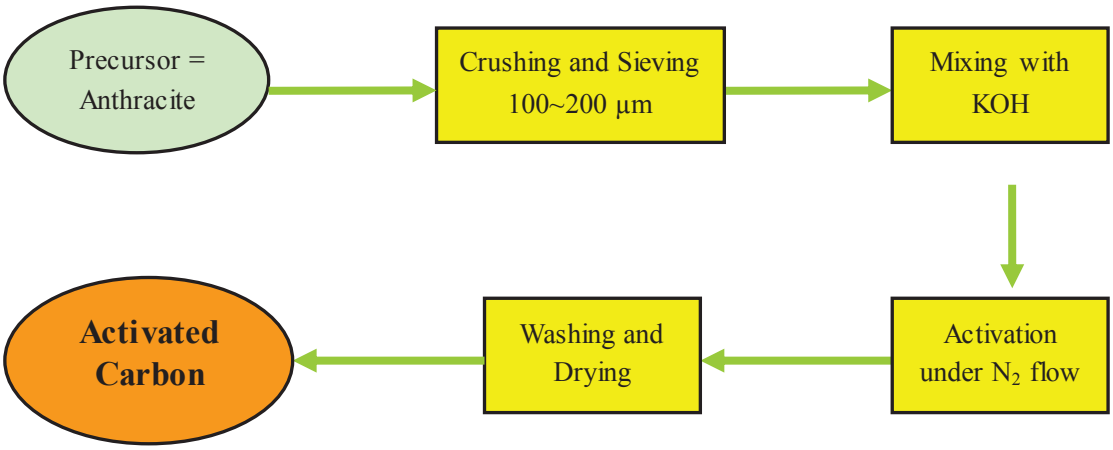

Figure 30 The process for preparing the activated carbon

2 Characterization methods

2.1 Carbon yield

The carbon yield is defined as the ratio of the weight of the carbon residue after carbonization to the weight of the material prior to carbonization [171]. The carbon yield strongly depends on all experimental factors, especially W, Hr, T, and composition of the atmosphere.

2.2 Density

The density of a material is defined as its mass per unit volume. However, such definition may apply either to the solid from which the (porous) material is made, or to the whole material itself, possibly as powder form. Therefore, the two following quantities are introduced.

2.2.1 True density

The true density of powders often differs from that of the bulk material because the process of grinding may change the crystal structure near the surface of each particle. In addition, voids at the surface of a particle, into which liquids can not necessarily penetrate, can generate apparent volume which may cause serious errors when density is measured by liquid displacement.

The true density, ρ_s, sometimes called skeletal density, is the density of the solid from which the investigated material is made. In our case, the true density was measured by helium pycnometry with an Accupyc II 1340 device (Micromeritics, see Figure 31), which was specifically designed to measure the true volume of solid materials by employing Archimedes' principle of fluid (gas) displacement and the technique of gas expansion. True densities are measured using helium gas since helium penetrates every surface flaw down to about one 0.1 nm, thereby enabling the measurement of powder volumes with great accuracy. The high molecular mobility and the very small size of He also allows it to penetrate any kind of open porosity, making it an ideal gas for density determination of porous solids.

Figure 31 The illustration of Accupyc II 1340 Helium pycnometer

Before the experiments, the samples were dried at 443 K in vacuum overnight, in order to avoid the distorting effect of adsorbed water on the volume measurement. Samples were then introduced inside a calibrated volume (1 cm^3), and the induced change of helium pressure was accurately measured. Each determination included 10 helium flushes prior to analysis, in order to clean the volume chamber, and 50 analytical runs.

2.2.2 Tap density

The density of a powder is the density measured when the volume receptacle is tapped or vibrated under specified conditions while being loaded. Typically, the powder density is 50 % less than the true density if the particles are spherical. Handling or vibration of powdered material makes the smaller particles come into the

spaces between the larger particles. The geometric space occupied by the powder thus decreases, so its density increases. The addition of pressure allows reaching the best particle packing. Under controlled conditions of tap rate, tap force (fall) and cylinder diameter, the condition of maximum packing efficiency is highly reproducible.

The GeoPyc 1360, see Fig. 32, measures envelope density using a non-destructive volume displacement technique. It can also measure a density comparable to what is usually termed as tap density. The latter can be defined as the mass of a material that, upon packing in a precisely specified manner, fills a container to a specified volume, divided by the container volume. Traditional methods of determining tap density involve repeatedly lifting and dropping a container of sample to tap down the volume and pack the particles.

Figure 32 The illustration of GeoPyc 1360 envelope density analyser

Using GeoPyc 1360, the volume determination of an empty sample chamber is first made, and the data are stored for repeated use during subsequent sample analysis. Next, a weighed quantity of sample is placed in the sample chamber and a plunger is inserted partially into the chamber. The chamber/plunger assembly is mounted on the instrument. The desired consolidation force (force with which the sample is compressed), sample weight and other parameters are entered, and analysis begins. The plunger exerts the consolidation force in stages. The plunger retracts a short distance, the sample is agitated, and then the plunger moves forward again until the desired force is reached and a measurement of the sample volume is made. Then the plunger retracts slightly. This is called the consolidation cycle. The force required to

move the plunger into the sample chamber is detected by a force transducer, which ensures that the plunger exerts a consistent force upon the sample. After the consolidation cycles are completed, the instrument uses the stored data to calculate the results [172].

2.3 Surface area and porosity from N_2 and CO_2 adsorption

Surface area and porosity are two important physical properties that determine the characteristics and applications of many materials. Differences in the surface area and porosity of a material can greatly influence its performances. The fully automated ASAP 2020 (Accelerated Surface Area and Porosimetry) system was used in the present work for obtaining nitrogen (at 77 K) and carbon dioxide (at 273 K) adsorption isotherms (see Figure 33). The AC samples were degassed for 24 h under vacuum at 523 K prior to any adsorption experiment.

Figure 33 The illustration of ASAP 2020 automatic adsorption apparatus

In order to obtain the so-called ‘‘high resolution’’ adsorption isotherms, adsorbed volumes of nitrogen were measured at relative pressures P/P_0 as low as 10^{-7}. Adsorption isotherms were determined by dosing N_2 volumes of 25 STP cm^3 g^{-1} up to $P/P_0 = 10^{-6}$, whereas a table of relative pressures was used to build the isotherms up to a final P/P_0 of 0.99. Equilibrium time of 20 s was used.

Surface areas, S_{BET}, were determined by the BET calculation method applied to the adsorption branch of the N_2 isotherms, as discussed in chapter 1. The micropore

volume, $V_{DR;N2}$, was determined according to the Dubinin–Radushkevich (DR) method [174] using correlation coefficients equal to or higher than 0.999. The total pore volume, sometimes referred to as the so-called Gurvitch volume, $V_{0.99}$, was defined as the volume of liquid nitrogen corresponding to the amount adsorbed at a relative pressure $P/P_0 = 0.99$ [175]. The average pore diameter, L_0, was calculated from the following expression [106]:

$$L_0 = 10.8 \text{ (nm KJ mol}^{-1}) / [E_0 - 11.4 \text{ (KJ mol}^{-1})]$$

where E_0 is the characteristic adsorption energy of nitrogen and was derived from the corresponding adsorption isotherms at 77 K, applying the Dubinin–Radushkevich method.

Adsorption isotherms of carbon dioxide were determined by dosing CO_2 volumes of 0.2 STP cm^3 g^{-1} up to $P/P_0 = 10^{-4}$, and a table of relative pressures was used to build the CO_2 adsorption isotherm up to a final P/P_0 of 0.025. Equilibrium time of 50 s was used. The CO_2 data were interpreted on the basis of the DR model, with correlation coefficients equal to or higher than 0.999. Micropore volume determined by CO_2 adsorption, $V_{DR;CO_2}$, gives information about micropores narrower than 0.7 nm, provided that the suitable interval of P/P_0 is chosen for its determination.

Finally, the pore size distributions (PSD) were calculated by application of the DFT model [92] supplied by Micromeritics software, considering slit-shaped pores.

2.4 Structural characterizations

Structural characterizations were performed by X-ray diffraction (XRD) using a Brüker D8 Advance instrument (Cu-K_α, Bragg-Brentano geometry). Microstructural observations were performed by Transmission Electron Microscopy (TEM-Tecnai F20 with a Field Emission Gun 200 KV, punctual resolution 0.24 nm and Energy Filtering GIF)

2.4.1 X-ray diffraction (XRD) analysis

Diffraction occurs as waves interact with a regular structure whose repeat distance is about the same as the wavelength. The phenomenon is common in the natural world, and occurs across a broad range of scales. For example, light can be diffracted by a grating having scribed lines spaced on the order of a few thousand angstroms, about the wavelength of light. When certain geometric requirements are met, X-rays scattered from a crystalline solid can constructively interfere, producing a diffracted beam. In 1912, W.L. Bragg recognized a predictable relationship (as shown in Figure 34):

$2 d \sin \theta = n \lambda$

wherein λ is the wavelength of the X-ray, θ the scattering angle, d the lattice spacing, and n an integer representing the order of the diffraction peak.

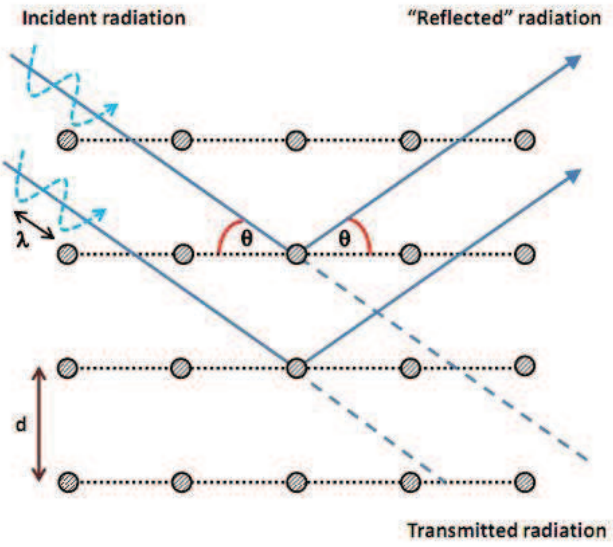

Figure 34 The illustration of Bragg's Law

Powder XRD is perhaps the most widely used X-ray diffraction technique for characterizing materials. It is a rapid analytical technique primarily used for phase identification of a crystalline material and can provide information on unit cell dimensions. The analyzed material is finely ground, homogenized, and average bulk composition is determined. X-ray diffractometers consist of three basic elements: an X-ray tube, a sample holder, and an X-ray detector, as shown in Figure 35. X-rays are

generated by a cathode ray tube, filtered to produce monochromatic radiation, collimated to concentrate, and directed toward the sample. The interaction of the incident rays with the sample produces constructive interference (and a diffracted ray) when conditions satisfy Bragg's Law. These diffracted X-rays are then detected, processed and counted. By scanning the sample through a range of 2θ angles, all possible diffraction directions of the lattice should be attained due to the random orientation of the powdered material. Conversion of the diffraction peaks to d-spacings allows identification of the mineral because each mineral has a set of unique d-spacings. Typically, this is achieved by comparison of d-spacings with standard reference patterns.

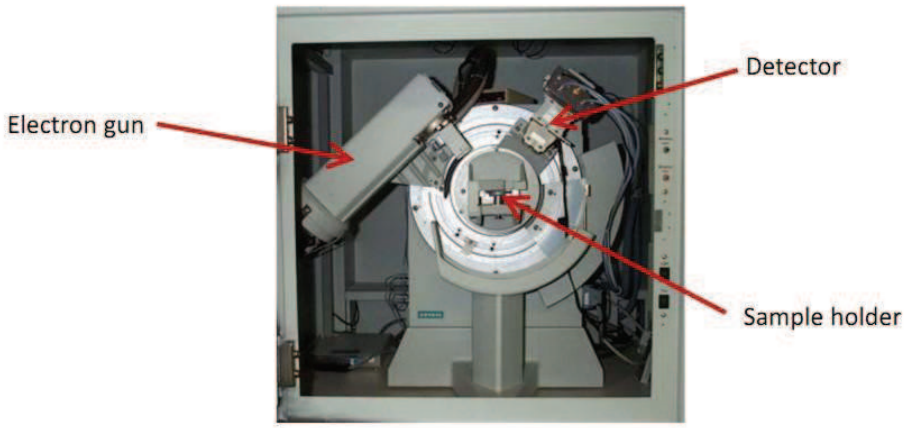

Figure 35 The illustration of basic elements of an X-ray diffractometer

2.4.2 Transmission Electron Microscopy (TEM) analysis

Transmission electron microscopy (TEM) is a microscopy technique whereby a beam of electrons is transmitted through an ultra thin specimen, interacting with the specimen as it passes through. The transmission electron microscope (TEM) operates on the same basic principles as the light microscope but uses electrons instead of light. Using electrons as "light source" makes it possible to get a resolution a thousand times better than with a light microscope, due to their much lower wavelength than that of photons.

The elements of a TEM are shown in Figure 36. A "light source" at the top of the microscope emits the electrons that travel through vacuum in the column of the microscope. Instead of glass lenses focusing the light in a light microscope, the TEM uses electromagnetic lenses to focus the electrons into a very thin beam. The electron beam then travels through the specimen to be studied. Depending on the density of the material present, some of the electrons are scattered and disappear from the beam. At the bottom of the microscope, the unscattered electrons hit a fluorescent screen, which gives rise to a "shadow image" of the specimen with its different parts displayed in varied darkness according to their density. The image can be studied directly by the operator or photographed with a camera [63].

Figure 37 presents the example of the AC modified by iron (our work). As it can be seen, observing objects of the order of a few nanometres (nm) is possible with TEM.

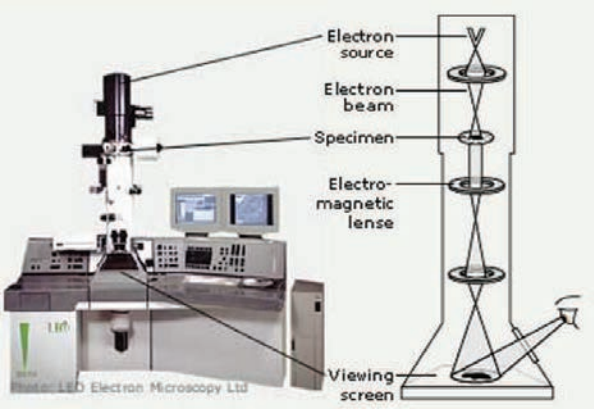

Figure 36 The illustration of the elements of a TEM [63]

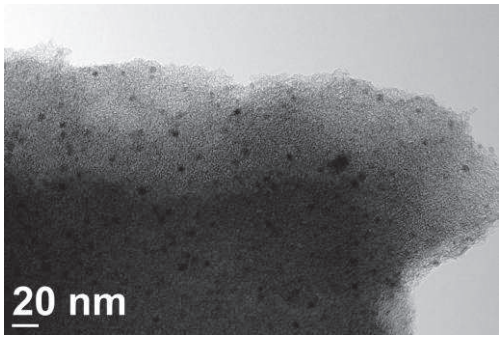

Figure 37 The TEM image of AC modified by iron

2.5 Inductively coupled plasma - optical emission spectrometer

The inductively coupled plasma - optical emission spectrometer (ICP-OES, see Figure 38) is used to determine the concentrations of a wide range of elements in solution. It can analyze 73 elements in the periodic table, including all metal-elements and many non-metal elements, such as As, Se, P, Si, Te, etc. Its detection limit is ~1 ppb with a relative precision of 1~2 %. It allows two analytical operation modes: multi-element mode and single-element mode, in which the latter provides a better precision. With the relatively high precision, fast measuring process, low cost and low detection linit, ICP-OES can be used in a wide range of application fields in academic research, industries and environmental monitoring [27].

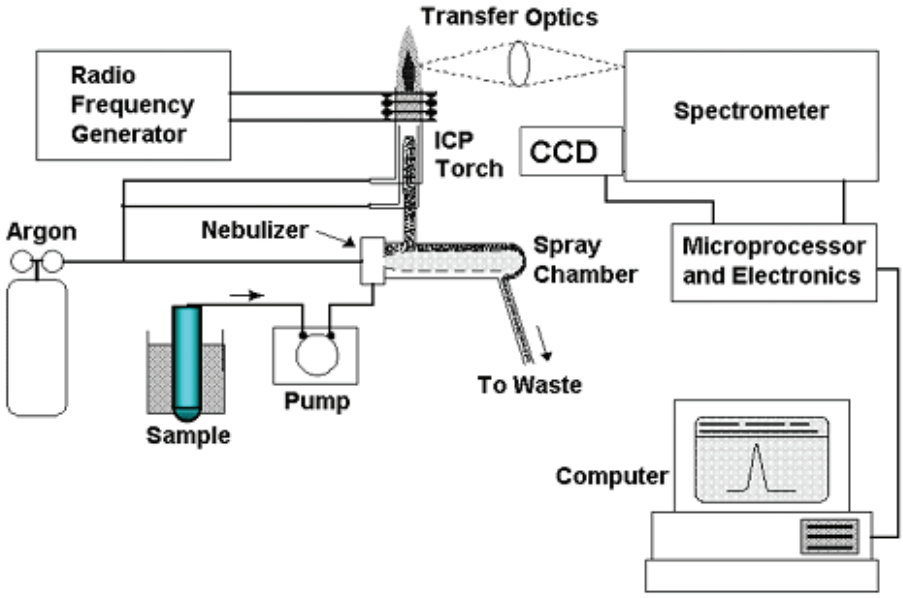

Figure 38 The illustration of ICP-OES (Varian Vista Axial ICP-OES) device

The ICP-OES is composed of two parts: the ICP and the optical spectrometer. The ICP torch consists of 3 concentric quartzglass tubes. The output or "work" coil of the radio frequency (RF) generator surrounds part of this quartz torch. Argon gas is typically used to create the plasma. When plasma energy is given to an analysis sample from outside, the component elements (atoms) are excited. When the excited atoms return to low energy position, emission rays (spectrum rays) are released and

the emission rays that correspond to the photon wavelength are measured. The element type is determined based on the position of the photon rays, and the content of each element is determined based on the rays' intensity. ICP can be used for quantitative analyses of elemental contents in all types of samples, which must be dissolved in acidic solution first.

2.6 H_2 Chemisorption and Temperature-Programmed Reduction (TPR)

The chemisorption of H_2 was carried out in Micromeritics AutoChem II 2920 (see Figure 39). The AutoChem II 2920 is a fully automated chemisorption analyzer that can provide the ability to conduct a comprehensive array of highly precise studies of chemical adsorption and temperature-programmed reactions (TPR). Valuable information about the physical properties of catalyst, catalyst support, or other materials like ACs can be obtained with such instrument. It can determine the properties of doped ACs such as percent of metal dispersion, active metal surface area, and acid strength, and surface acidity, distribution of strength of active sites, BET surface area, and more.

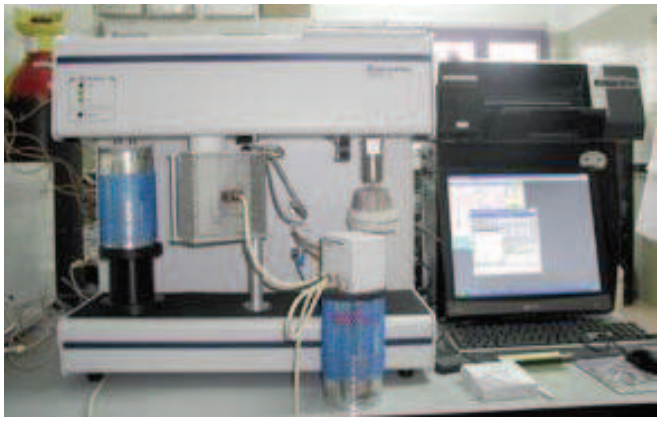

Figure 39 The illustration of AutoChem II 2920 chemisorption device

For our ACs doped with metal, the active surface area (ASA), metal dispersion and particle size were estimated from the chemisorption of H_2. H_2 chemisorption was carried out as follows: a raw sample was loaded in the sample tube and dried in a flow of He at 373K for 30 min. The sample was then cooled in Ar to 303 K. Temperature

was increased up to 573 K with a heating rate of 10 K/min in a flow of 10% H_2 in Ar, and the final temperature was held for 1 h. This pre-treatment was carried out to remove any oxygen adsorbed during handling, in order to have clean Pd particle surfaces exposed to chemisorption. The sample was cooled in Ar up to 363 K and maintained at this temperature during chemisorption experiment. Pulses of 10% H_2 in Ar were injected at certain time intervals until saturation was reached. The amount of H_2 chemisorbed was determined from cumulative integrated areas. Dissociative adsorption hypothesis was applied and metal/H_2 stoichiometry was chosen as 1 for calculations. Spherical geometry of the metal crystallites was assumed for calculating average particle diameters [73].

Temperature-Programmed Reduction (TPR) was carried out in the same apparatus as for chemisorption. TPR determines the number of reducible species present on the AC surface and reveals the temperature at which the reduction of each species occurs. An important aspect of TPR analyses is that the sample does not need to have any special characteristics except than containing reducible metals. The TPR analysis begins by flowing an analysis gas (typically hydrogen in an inert carrier such as nitrogen or argon) through the sample, usually at room temperature. While the gas is flowing, the temperature of the sample is increased linearly with time and the consumption of hydrogen by adsorption/reaction is monitored. Changes in the concentration of the gas mixture downstream from the reaction cell are determined. This information yields the volume of hydrogen uptake.

The reducibility of the doped ACs was determined by TPR experiments. During the experiments, the accuracy in the measurements of the TPR peak was ±1 K. The amounts of H_2 consumed or evolved were monitored continuously. Prior to the TPR experiment, the sample was flushed with Ar during 1 h. After this pre-treatment, samples were heated at 10 K/min from room temperature to 573 K in a mixture 10% H_2 / 90% Ar flowing at 20 mL/min.

Once the amount of gas chemisorbed on (or desorbed by) a monolayer has been determined (n_{ads}), the metal surface area A_{sam} was derived from the following equation [14]:

$$A_{sam} = L\, n_{ads}\, F_s\, a_{met}\, 10^{-23}$$

wherein L is the Avogadro number (6.023 10^{23} / mol), n_{ads} is the amount of gas adsorbed in pulse chemisorption, F_s = 2 mol metal/mol gas is a stoichiometric factor, and a_{met} is thecross-section of a metal atom.

The metal dispersion D_{met} (adsorbing metal atoms/total metal atoms) is defined as the number of adsorbing metal atoms (or moles) referred to the total number of metal atoms (or moles) that are contained in the ACs [14]:

$$D_{met} = (N_{ads}\, F_s\, 10\, M_{met})/X_{met}$$

wherein M_{met} is the metal atomic weight, and X_{met} is the metal percentage.

The calculation of the average metal aggregate size d_{met} is based on the assumption that the aggregate has a spherical shape laying on the support surface [14]:

$$d_{met} = S_f\, 10^3 /(A_{met}\, \rho_{met})$$

wherein S_f = 6 is the shape factor, $A_{met} = A_{sam}\,(1/X_{met}) \times 10^2$ is the metal surface area, and ρ_{met} the metal density.

3 Measurement of hydrogen storage capacities

There are a number of measurement methods that can be used to investigate hydrogen storage materials and systems. Gravimetric and volumetric methods are the most reliable methods for investigating hydrogen storage. Temperature-programmed desorption and differential scanning calorimetry may be additional useful techniques.

The volumetric method of hydrogen storage measurement, also known as the manometric method, or as Sievert's method in honour of the German chemist of the same name, uses temperature-pressure-volume correlations to determine hydrogen concentration and the storage properties of a material. A generalized volumetric system with typical components is shown in Figure 40. The system volumes are

carefully pre-calibrated. To test a sample using the volumetric method, the gas reservoir is filled with H_2 to a pressure P and then allowed to react with the specimen reactor by opening the top valve. An equilibrium pressure P' is reached between the gas reservoir and the specimen reactor that can be used to precisely determine the amount of hydrogen sorbed by the material [166].

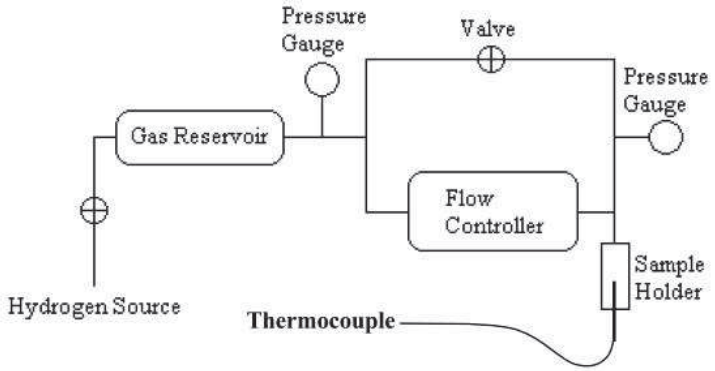

Figure 40 Scheme of multipurpose gas sorption/desorption system for hydrogen storage testing [166]

The gravimetric method uses weight measured with a balance to determine the storage properties of a material. A scheme of a simple gravimetric system is presented in Figure 41. Before the test, the weight of the non hydrogenated sample is measured and the sample is placed at one end of a symmetric microbalance in a sample holder. In more advanced systems, an inert tare with the same weight and comparable density as that the non hydrogenated sample is placed on the other end of the microbalance. After the chamber containing the sample is evacuated, hydrogen from an external source is allowed to enter, generally using incremental pressure steps as it is sorbed by the sample in the sample holder. The microbalance is typically equipped with an electronic circuit that measures the strain on the balance that is directly related to the change in weight of the sample. This information combined with pressure and temperature readings can be used to derive hydrogen storage properties of the sample [166].

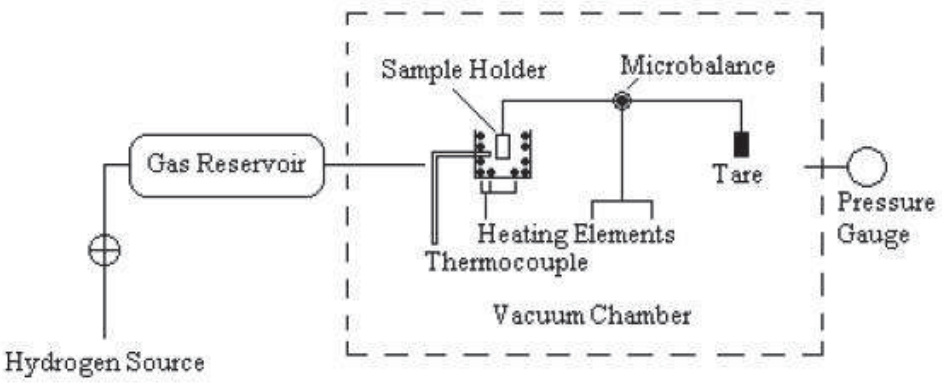

Figure 41 Scheme of a gravimetric system for hydrogen storage testing [166]

In our case, determination of H_2 storage capacities at 77 and 298 K was carried out in parallel with a volumetric device at ICMPE (Thiais, France) on one hand, and with a gravimetric device at ICB (Zaragoza, Spain) on the other hand.

3.1 Volumetric analysis

Determination of hydrogen storage at 77 and 298 K and up to 10 MPa was carried out at Institut de Chimie et des Matériaux Paris-Est (ICMPE, Thiais, France), UMR CNRS 7182. Pressure–Composition–Isotherm (PCI) curves have been recorded using a volumetric device equipped (see Figure 42) with calibrated and thermalised volumes and pressure gauges (Sievert's method [49, 166]). The sample was enclosed in a stainless steel sample holder closed with a metal seal. Before any sorption measurements, the sample was degassed under primary vacuum at 493 K for 12 h. The sample holder was immersed in a liquid N_2 Dewar at 77 K or in a thermalised water bath maintained at 298 K, and high purity hydrogen (6 N) was introduced step by step up to 10 MPa. The pressure variations due to both gas cooling and hydrogen adsorption were measured after reaching thermodynamic equilibrium, usually in the range of minutes. Real equation of state for hydrogen gas was used from the program GASPAK V3.32 (Cryodata, Inc.). The PCI curves were measured twice (i.e. corresponding to two full adsorption–desorption cycles) in order to check the hysteresis effect and the measurement repeatability. All capacities reported here refer to the sample dry mass

(i.e. degassed mass). Sample volume correction was derived from density measurement obtained with a helium AccuPyc 1330 Micromeritics pycnometer using around 100 mg of sample.

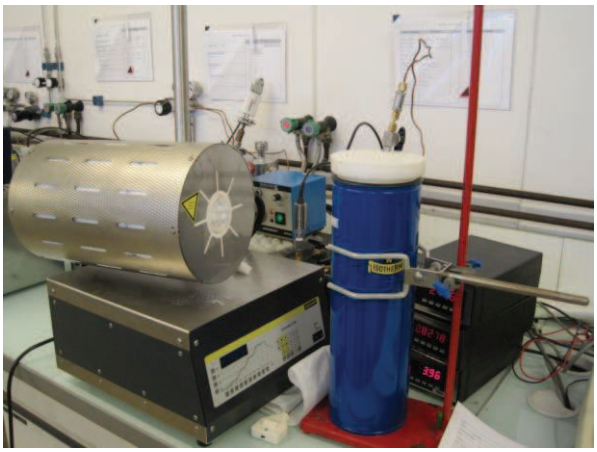

Figure 42 Determination of H_2 storage properties carried out with a volumetric device at ICMPE (Thiais, France)

3.2 Gravimetric analysis

Determination of hydrogen storage at 77 K and up to 10 MPa was carried at Instituto de Carboquímica ICB-CSIC (Zaragoza, Spain). The apparatus used for hydrogen adsorption studies was a gravimetric analyser from VTI Corporation (Miami, USA). The instrument (see Figure 43) allows adsorption and desorption isotherms at each pressure step to be determined. The system consists of a fully computer-controlled microbalance, which automatically measures the weight of the carbon sample as a function of time, with the same hydrogen pressure and sample temperature under control. Hydrogen isotherms were obtained by setting pressure steps within the range 0~10 MPa at 77 K. For each run, approximately 500 mg of activated carbon sample were placed into a bucket made from stainless steel mesh. Hydrogen pressure was gradually increased to prevent disruption of the microbalance, until the desired value was reached. A pressure transducer (accuracy 0.05% of the full pressure range up to 10 MPa) was used to monitor hydrogen pressure in the system. Pressure was maintained constant during relaxation with the help of inlet/outlet

control valves with high-resolution stepper motors. After the equilibrium was reached, the hydrogen pressure was increased to the next set pressure value, and the subsequent uptake was measured until equilibrium was re-established. The sample temperature was constantly monitored all through the duration of the experiments, and the variation was found to be not higher than 0.5 K. The reverse procedure was used for studying the desorption process.

Figure 43 Determination of H_2 storage carried out with a gravimetric device at ICB (Zaragoza, Spain)

The compensation for buoyancy was obtained experimentally. A first approach was considered by introducing an equivalent volume of a non-adsorbent material into the microbalance. Previously, the true density of the carbons was obtained using a helium pycnometer AccuPyc II 1340 from Micromeritics. A second approach was based on the visual inspection of the isotherm. High pressure points of the isotherm exhibit no hydrogen adsorption and thus the measured variation of weight is only attributable to buoyancy. From these high-pressure data points, a straight line is obtained and a slope can be calculated with regression coefficients near 1. This slope can be used to correct the weight of all points of the isotherm. This second approach can avoid the problems of helium entrapment observed in the determinations of true density. The latter problems might be minimised, but only through a very long

procedure. Both ways of determination of buoyancy were compared for some samples, giving accurate, identical, recalculated isotherms. Therefore, the faster method using the slope was finally chosen.

Chapitre III

Publications scientifiques

Article n°1

Adsorption and compression contributions to hydrogen storage in activated anthracites

V. Fierro, W. Zhao, M.T. Izquierdo, E. Aylon, A. Celzard

International Journal of Hydrogen Energy 35 (2010) 9038-9045

Dans ce travail, nous avons préparé des charbons actifs (CAs) à partir d'anthracites, présentant des surfaces spécifiques (S_{BET}) jusqu'à 2772 m^2 g^{-1}. Les anthracites activés avec KOH ont montré de plus hautes capacités d'adsorption d'hydrogène, avec un maximum de 5.3 % en poids à 77 K et 4 MPa, que ceux activés avec NaOH. Nous avons observé une linéarité entre la capacité de stockage d'hydrogène à 77K et S_{BET} tant que la valeur de cette dernière n'excède pas 2630 m^2 g^{-1}, qui est précisément la limite théorique pour l'aire spécifique d'un charbon actif.

Nous avons séparé les contributions à la capacité de stockage totale de l'adsorption d'une part, et de la compression du gaz dans la porosité et les interstices du charbon d'autre part, et cela nous a permis de conclure que le stockage d'hydrogène par adsorption n'est réellement avantageux qu'à des pressions modérées : autour de 3 MPa et de 0.15 MPa à 298 et 77 K, respectivement.

Le stockage d'hydrogène par adsorption sur les charbons actifs à haute pression n'a même pas d'intérêt à des pressions supérieures à 30 MPa à 298 K, ou supérieures à 8 MPa à 77 K, puisqu'on peut stocker davantage d'hydrogène par simple compression dans le même volume de réservoir.

INTERNATIONAL JOURNAL OF HYDROGEN ENERGY 35 (2010) 9038–9045

Available at www.sciencedirect.com

ScienceDirect

journal homepage: www.elsevier.com/locate/he

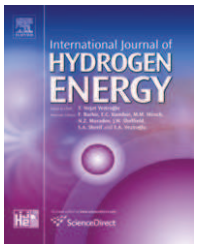

Adsorption and compression contributions to hydrogen storage in activated anthracites

V. Fierro [a,*], W. Zhao [a], M.T. Izquierdo [b], E. Aylon [b], A. Celzard [a]

[a] Institut Jean Lamour, Département 2: Chimie et Physique des Solides et des Surfaces, UMR 7198, CNRS – Nancy-Université – UPV-Metz, ENSTIB, 27 rue du Merle Blanc, BP 1041, 88051 Epinal cedex 9, France

[b] Instituto de Carboquímica (CSIC), Miguel Luesma Castán, 4. 50018 Zaragoza, Spain

* Corresponding author. Fax: +33 329 29 61 38.
E-mail address: vanessa.fierro@lcsm.uhp-nancy.fr (V. Fierro).

0360-3199/$ – see front matter
doi:10.1016/j.ijhydene.2010.06.004

Article n°2

Activated carbons with appropriate micropore size distribution for hydrogen adsorption

W. Zhao, V. Fierro, C. Zlotea, E. Aylon, M. T. Izquierdo, M. Latroche, A. Celzard

International Journal of Hydrogen Energy 36 (2011) 5431-5434

Nous avons mesuré les capacités de stockage d'hydrogène de cinq charbons actifs commerciaux bien connus, et nous avons comparé leurs capacités pour le stockage d'hydrogène avec celles des charbons actifs que nous avions préparé par activation d'anthracite avec KOH. Ainsi, nous avons pu constater que les capacités de stockage d'hydrogène des charbons préparés dans notre laboratoire sont supérieures pour des aires spécifiques très comparables à celles des autres adsorbants commerciaux. Notre meilleur charbon activé a une capacité de stockage d'hydrogène en excès de 6% en poids à 77K et 4 MPa.

Nous avons calculé la contribution à la capacité de stockage d'hydrogène en excès de différents volume poreux, en les divisant en 4 intervalles de diamètres : < 0.5 nm, 0.5 – 0.7 nm, 0.7 – 2 nm, et > 2 nm). Pour cela, nous avons utilisé 15 charbons activés : 9 préparés dans notre laboratoire et 6 commerciaux.

Nous avons démontré que la supériorité de nos charbons actifs est due à leur distribution de tailles de pore. Ainsi, pour la même aire spécifique, il y a plus de petits pores dans les charbons du laboratoire. Par ailleurs, pour avoir des capacités de stockage supérieures à 3%, les pores de diamètre supérieur à 0.7 nm sont absolument nécessaires.

INTERNATIONAL JOURNAL OF HYDROGEN ENERGY 36 (2011) 5431–5434

Available at www.sciencedirect.com

ScienceDirect

journal homepage: www.elsevier.com/locate/he

Technical Communication

Activated carbons with appropriate micropore size distribution for hydrogen adsorption

W. Zhao [a], V. Fierro [a,*], C. Zlotea [b], E. Aylon [c], M.T. Izquierdo [c], M. Latroche [b], A. Celzard [a]

[a] Institut Jean Lamour, Département 2: Chimie et Physique des Solides et des Surfaces, UMR 7198, CNRS, Nancy-Université, UPV-Metz, ENSTIB, 27 rue du Merle Blanc, BP 1041, 88051 Epinal cedex 9, France

[b] Chimie Métallurgique des Terres Rares, Institut de Chimie et des Matériaux de Paris Est, UMR 7182, CNRS, 2-8 rue Henri Dunant, 94320 Thiais Cedex, France

[c] Instituto de Carboquímica (CSIC), Miguel Luesma Castán, 4. 50018 Zaragoza, Spain

* Corresponding author. Fax: +33 329 29 61 38.
E-mail address: Vanessa.Fierro@lcsm.uhp-nancy.fr (V. Fierro).

doi:10.1016/j.ijhydene.2010.12.137

Article n°3

High-performances carbonaceous adsorbents for hydrogen storage

W. Zhao, V. Fierro, E. Aylon, M. T. Izquierdo, A. Celzard

IOP Conference Series (2012) sous presse

Nous avons préparé des charbons activés à porosité contrôlée, et leurs capacités de stockage d'hydrogène ont été mesurées par gravimétrie. Ces adsorbants sont des anthracites chinois activés avec les hydroxydes alcalins NaOH ou KOH.

Nous avons obtenu, pour quelques-uns de ces matériaux à 4MPa et 77 K, des capacités totales de stockage d'hydrogène de 6.6 % en poids, correspondant à des capacités en excès de 6.2 % en poids. Ces valeurs sont parmi les meilleures qui ont été publiées, et sont supérieures à celles du charbon commercial Maxsorb-3, souvent considéré comme l'adsorbant de référence pour le stockage d'hydrogène.

Ces excellentes capacités d'adsorption sont dues à la plus grande quantité de micropores (< 2nm).

High-performances carbonaceous adsorbents for hydrogen storage

Weigang Zhao[1], Vanessa Fierro[1], E. Aylon[2], M. T. Izquierdo[2], Alain Celzard[1]

[1] Institut Jean Lamour – UMR UHP - CNRS 7198, ENSTIB, 27 rue Philippe Séguin, F-88051 Epinal cedex 9

[2]Instituto de Carboquímica (CSIC), Miguel Luesma Castán, 4. 50018 Zaragoza, Spain

E-mail: Vanessa.Fierro@lcsm.uhp-nancy.fr

Article n°4

Optimization of hydrogen storage capacity onto activated carbons

W. Zhao, V. Fierro, C. Zlotea, E. Aylon, M.T. Izquierdo, M. Latroche, A. Celzard

International Journal of Hydrogen Energy 36 (2011) 11746-11751

Nous avons optimisé la préparation de charbons actifs pour le stockage d'hydrogène par adsorption, par activation chimique d'anthracite avec KOH. Pour cela, nous avons appliqué un plan d'expériences et la méthodologie de surface de réponse. Nous avons ainsi étudié l'effet du rapport massique KOH/anthracite (W) et de la température d'activation (T) sur la capacité de stockage de l'hydrogène.

Nous avons obtenu une expression polynomiale qui permet de corréler W et T à la capacité de stockage d'hydrogène mesurée à 77K et 4MPa. L'analyse de la variance a montré que W est le seul paramètre significatif dans l'intervalle des conditions expérimentales testées.

Le charbon activé préparé dans les conditions optimales a une capacité bien supérieure à celle du charbon commercial MAXSORB-3 utilisé comme référence pour le stockage d'hydrogène.

INTERNATIONAL JOURNAL OF HYDROGEN ENERGY 36 (2011) 11746–11751

Available at www.sciencedirect.com

ScienceDirect

journal homepage: www.elsevier.com/locate/he

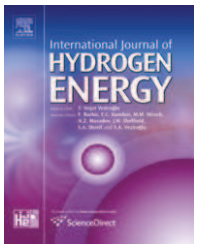

Optimization of activated carbons for hydrogen storage

W. Zhao [a], V. Fierro [a,*], C. Zlotea [b], E. Aylon [c], M.T. Izquierdo [c], M. Latroche [b], A. Celzard [a,1]

[a] Institut Jean Lamour, Département 2: Chimie et Physique des Solides et des Surfaces, UMR 7198, CNRS - Nancy-Université – UPV-Metz, ENSTIB, 27 rue Philippe Séguin, BP 1041, 88051 Epinal cedex 9, France

[b] Chimie Métallurgique des Terres Rares, Institut de Chimie et des Matériaux de Paris Est, UMR 7182, CNRS, 2-8 rue Henri Dunant, 94320 Thiais Cedex, France

[c] Instituto de Carboquímica (CSIC), Miguel Luesma Castán 4, 50018 Zaragoza, Spain

* Corresponding author. Fax: +33 329 29 61 38.
E-mail address: Vanessa.Fierro@lcsm.uhp-nancy.fr (V. Fierro).

[1] Member of the Institut Universitaire de France.

doi:10.1016/j.ijhydene.2011.05.181

Article n°5

Impact of synthesis conditions of KOH activated carbons on their hydrogen storage capacities

W. Zhao, V. Fierro, N. Fernández-Huerta, M. T. Izquierdo, A. Celzard

International Journal of Hydrogen Energy 37 (2012) 14278-14284

Nous avons préparé 39 charbons actifs par activation d'anthracite Taisi avec KOH, en utilisant des rapports massiques KOH/anthracite (W) variant de 1.5 à 7, des températures d'activation (T) entre 973 et 1073 K, et des vitesses de chauffe (Hr) de 1 à 5 K min^{-1}. Ce faisant, nous avons produit des matériaux présentant des surfaces spécifiques apparentes très élevées (jusqu'à 3400 m^2 g^{-1}), des volumes de micropores très importants (> 1 cm^3 g^{-1}) et de hautes capacités de stockage d'hydrogène (jusqu'à 6.6 % en poids).

Nous avons mené à bien une étude statistique pour vérifier l'effet des conditions expérimentales d'activation sur le stockage d'hydrogène des charbons activés ainsi produits. L'analyse de variance (ANOVA) montre que W et T ont un effet significatif sur la capacité de stockage d'hydrogène tandis que Hr n'en a pas.

Nous avons corrélé les capacités de stockage d'hydrogène à une expression polynomiale basée sur W^2, W, T^2 et T. Cette expression polynomiale a permis d'évaluer les effets des conditions d'activation des charbons activés sur leurs capacités de stockage d'hydrogène.

INTERNATIONAL JOURNAL OF HYDROGEN ENERGY 37 (2012) 14278–14284

Available online at www.sciencedirect.com

SciVerse ScienceDirect

journal homepage: www.elsevier.com/locate/he

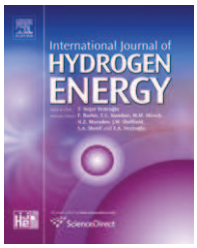

Impact of synthesis conditions of KOH activated carbons on their hydrogen storage capacities

W. Zhao [a], V. Fierro [a,*], N. Fernández-Huerta [b], M.T. Izquierdo [b], A. Celzard [a,1]

[a] Institut Jean Lamour, Département 2: Chimie et Physique des Solides et des Surfaces, UMR 7198, CNRS – Université de Lorraine, ENSTIB, 27 rue Philippe Séguin, BP 1041, 88051 Epinal Cedex 9, France

[b] Instituto de Carboquímica (ICB-CSIC), Miguel Luesma Castán 4, 50018 Zaragoza, Spain

* Corresponding author. Fax: +33 329 29 61 38.
E-mail address: Vanessa.Fierro@lcsm.uhp-nancy.fr (V. Fierro).

[1] Member of the Institut Universitaire de France.

http://dx.doi.org/10.1016/j.ijhydene.2012.06.110

Article n°6

Activated carbons doped with Pd nanoparticles for hydrogen storage

W. Zhao, V. Fierro, C. Zlotea, M.T. Izquierdo, C. Chevalier-César, M. Latroche, A. Celzard

International Journal of Hydrogen Energy 37 (2012) 5072-5080

Nous avons utilisé 3 adsorbants carbonés microporeux préparés dans notre laboratoire par activation d'anthracite avec KOH et présentant des surface spécifiques apparentes entre 2450 et 3200 m^2/g. Ces charbons actifs ont été dopés avec des nanoparticules de palladium à des teneurs variant entre 1.3 et 10.0 % en masse. Nous avons mesuré les capacités de stockage d'hydrogène en excès à 77 et à 298 K, et à des pressions allant jusqu'à 8 MPa.

Nous avons montré que la capacité de stockage d'hydrogène à 298K dépend de la teneur en palladium jusqu'à des pressions de 2–3 MPa, en dessous desquelles la quantité d'hydrogène stockée est inférieure à 0.2 % massiques. A des pressions supérieures, c'est le volume de micropores qui contrôle la capacité de stockage d'hydrogène. A 77 K, le dopage avec des nanoparticules de palladium a un effet négatif sur la capacité de stockage d'hydrogène, et cela dans tout l'intervalle de pression considéré.

Les études d'adsorption d'azote à 77K, de TPR, XRD, TEM, et chimisorption d'hydrogène nous ont permis de conclure que: (i) les nanoparticules de palladium restent très probablement à la surface externe des grains de charbon actif; (ii) la taille moyenne des particules métalliques augmente avec la teneur en palladium; (iii) les charbons activés avec une plus haute surface spécifique ont une meilleure dispersion et des particules plus petites pour une même teneur en palladium.

INTERNATIONAL JOURNAL OF HYDROGEN ENERGY 37 (2012) 5072–5080

Available online at www.sciencedirect.com

SciVerse ScienceDirect

journal homepage: www.elsevier.com/locate/he

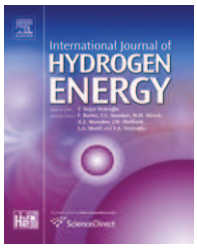

Activated carbons doped with Pd nanoparticles for hydrogen storage

W. Zhao [a], V. Fierro [a,*], C. Zlotea [b], M.T. Izquierdo [c], C. Chevalier-César [b], M. Latroche [b], A. Celzard [a,1]

[a] Institut Jean Lamour, Département 2, Chimie et Physique des Solides et des Surfaces, UMR 7198, CNRS – Nancy-Université – UPV-Metz, ENSTIB, 27 rue Philippe Séguin, BP 1041, 88051 Epinal Cedex 9, France

[b] Chimie Métallurgique des Terres Rares, Institut de Chimie et des Matériaux de Paris Est, UMR 7182, CNRS, 2-8 rue Henri Dunant, 94320 Thiais Cedex, France

[c] Instituto de Carboquímica, ICB-CSIC, Miguel Luesma Castán, 4, 50018 Zaragoza, Spain

* Corresponding author. Fax: +33 329 29 61 38.
E-mail address: Vanessa.Fierro@lcsm.uhp-nancy.fr (V. Fierro).

[1] Member of the Institut Universitaire de France.

doi:10.1016/j.ijhydene.2011.12.058

Article n°7

Hydrogen storage onto N-doped high surface area activated carbons

W. Zhao, V. Fierro, E. Aylon, M.T. Izquierdo, A. Celzard

International Journal of Hydrogen Energy (2012) soumis

Nous avons utilisé trois charbons activés de haute surface spécifique apparente : 2527, 2955 et 3434 m^2/g, comme précurseurs d'adsorbants carbonés enrichis en azote. Ces matériaux ont été dopés à l'azote par réaction avec de l'urée à 623K, ce qui a permis d'obtenir des teneurs en azote comprises entre 7.8 et 15.1 % en poids.

La réaction avec l'urée s'est donc montrée très efficace pour le dopage à l'azote, mais a toutefois produit une baisse de la surface spécifique et du volume de micropores proportionnelle à la quantité d'azote introduite.

L'adsorption physique de l'hydrogène à 77K est dominée par les caractéristiques de la structure poreuse de l'adsorbant. Nous avons pu néanmoins démontrer qu'il y a un effet positif du dopage avec de l'azote en représentant la capacité de stockage d'hydrogène normalisée par la surface spécifique, H_2 (%) / S_{BET}, en fonction du taux d'azote lui aussi normalisé par la surface BET, N (%) / S_{BET}. On a pu aussi constater cet effet positif du dopage en représentant de la même manière les résultats d'autres travaux publiés dans la littérature.

Hydrogen storage on N-doped high surface area-activated carbons

W. Zhao[1,2], V. Fierro[*1], N. Fernández-Huerta[3],
M.T. Izquierdo[3], A. Celzard[**1,2]

[1] *Institut Jean Lamour, UMR CNRS 7198. ENSTIB, 27 rue Philippe Séguin, BP 1041, 88051 Epinal cedex 9, France*

[2] *Université de Lorraine. ENSTIB, 27 rue Philippe Séguin, BP 1041, 88051 Epinal cedex 9, France*

[3] *Instituto de Carboquímica (ICB-CSIC), Miguel Luesma Castán, 4. 50018 Zaragoza, Spain*

[*] Corresponding author
Fax: +33 329 29 61 38; e-mail: Vanessa.Fierro@lcsm.uhp-nancy.fr
[**] Member of the Institut Universitaire de France

Références bibliographiques

1. The BP Energy Outlook 2030, London, 2011.

2. T. Jamasb, M.G. Pollitt, W. Nuttal. Future Technologies for a Sustainable Electricity System. Cambridge University Press: Cambridge. 2006. ISBN-10:0521860490.

3. http://www.hydrogen.energy.gov/

4. L. Zhou. Progress and problems in hydrogen storage methods. Renewable and Sustainable Energy Reviews, 9 (2005):395–408.

5. Targets for Onboard Hydrogen Storage Systems for Light-Duty Vehicles, US department of Energy Office of Energy Efficiency and Renewable Energy and The freedom CAR and fuel partnership, 2009.

6. http://www1.eere.energy.gov/hydrogenandfuelcells/storage/hydrogen_storage.html

7. http://www.linde-kryotechnik.ch/

8. P.P. Edwards, V.L. Kuznetsov, W.I.F. David. Hydrogen energy. Philosophical Transactions of the Royal Society A, 365(2007): 1043-1056.

9. B. Sakintuna, F. Lamaridarkrim, M. Hirscher. Metal hydride materials for solid hydrogen storage: A review. International Journal of Hydrogen Energy, 32 (2007):1121-1140.

10. R.C. Weast, M.J. Astle, W.H. Beyer. CRC handbook of chemistry and physics, (64th ed.), CRC Press, Boca Raton, FL, 1983.

11. G. Sandrock. A panoramic overview of hydrogen storage alloys from a gas reaction point of view. Journal of alloys and compounds, 293-295(1999):877-888.

12. L. Zhou, Y. Zhou, Y. Sun. Studies on the mechanism and capacity of hydrogen uptake by physisorption-based materials. International Journal of Hydrogen Energy, 31(2006):259–264.

13. U. Eberle, G. Arnold, RV. Helmholt. Hydrogen storage in metal—hydrogen systems and their derivatives. Journal of Power Source, 154(2006):456–460.

14. Temperature-programmed Desorption/Reduction/Oxidation (TPD/TPR/TPO) and Pulse-Sorption/Chemisorption. http://www.zeta-pa.de/pics/ZetA-tpd-info_e.pdf

15. S. Ma, H. Zhou. Gas storage in porous metal–organic frameworks for clean energy applications. Chemical Communication, 46(2010):44–53.

16. L. Wang, R.T. Yang. Hydrogen Storage on Carbon-Based Adsorbents and Storage at Ambient Temperature by Hydrogen Spillover. Catalysis Reviews: Science and Engineering, 52(2010):411–461.

17. N.L. Rosi, J. Eckert, M. Eddaoudi, et al. Hydrogen storage in microporous metal-organic frameworks. Science, 300(2003):1127–1129.

18. J.L.C. Rowsell, A.R. Millward, K.S. Park, et al. Hydrogen sorption in functionalized metal-organic frameworks. Journal of the American Chemical Society, 126(2004):5666–5667.

19. B. Panella, M. Hirscher. Hydrogen physisorption in metal–organic porous crystals. Advance Material, 175(2005):538–541.

20. B. Panella, M. Hirscher, H. Putter, et al. Hydrogen adsorption in metal–organic frameworks: Cu-MOFs and Zn-MOFs compared. Advanced Functional Materials, 164(2006):520–524.

21. J. Li, S. Cheng, Q. Zhao, et al. Synthesis and hydrogen-storage behavior of metal–organic framework MOF-5. International Journal of Hydrogen Energy, 34(2009):1377-1382.

22. HK. Chae, DY. Siberio-Perez, J. Kim, et al. A route to high surface area, porosity and inclusion of large molecules in crystals. Nature, 427(2004):523–527.

23. D. Saha, Z. Wei, S. Deng. Equilibrium, kinetics and enthalpy of hydrogen adsorption in MOF-177. International Journal of Hydrogen Energy, 33(2008):7479–7488.

24. H. Furukawa, M.A. Miller, M. Yaghi. Independent verification of the saturation hydrogen uptake in MOF-177 and establishment of a benchmark for hydrogen adsorption in metal-organic frameworks. J. Mater. Chem., 17(2007):3197–3204.

25. Y. Li, R.T. Yang. Gas adsorption and storage in metal-organic framework MOF-177. Langmuir, 23(2007):12937–12944.

26. A.G. Wong-Foy, A.J. Matzger, O.M. Yaghi. Exceptional H_2 saturation uptake in microporous metal-organic frameworks. Journal of American Chemical Society, 128(2006):3494–3495.

27. J. Nolte. ICP Emission Spectrometry: A Practical Guide. ISBN-10: 3527306722.

28. M.P. Suh, H.J. Park, T.K. Prasad, et al. Hydrogen Storage in Metal–Organic Frameworks. Chemical Reviews, 112(2012):782–835.

29. H. Marsh, R. Menendez. Introduction to Carbon Science, (3rd edn.), Butterworths, London, 1989.

30. I. Mochida, S.H. Yoon, W. Qiao. Catalysts in syntheses of carbon and carbon precursors. Journal of the Brazilian Chemical Society, 17(2006):1059-1073.

31. V. Fierro, W. Zhao, M.T. Izquierdo, et al. Adsorption and compression contributions to hydrogen storage in activated anthracites. International Journal of Hydrogen Energy, 35(2010):9038-9045.

32. W. Zhao, V. Fierro, C. Zlotea, et al. Activated carbon with appropriate micropore size distribution for hydrogen adsorption. International Journal of Hydrogen Energy, 36(2011):1-4.

33. W. Zhao, V. Fierro, C. Zlotea, et al. Optimization of activated carbons for hydrogen storage. International Journal of Hydrogen Energy, 36(2011):11746-11751.

34. W. Zhao, V. Fierro, E. Aylon, et al. High-performances carbonaceous adsorbents for hydrogen storage. IOP conference series, sous presse.

35. W. Zhao, V. Fierro, E. Aylon, et al. Effect of KOH activation conditions on hydrogen storage onto activated carbons. International Journal of Hydrogen Energy, soumis.

36. http://en.wikipedia.org/wiki/Carbon_nanotube.

37. S. Iijima. Helical microtubules of graphitic carbon. Nature, 354 (1991):56-58.

38. A.C. Dillon, K.M. Johns, T. A. Bekkedahl, et al. Storage of hydrogen in single-walled carbon nanotubes. Nature, 386(1997):377-379.

39. A.C. Dillon. Hydrogen storage in carbon single-wall nanotubes. Proceedings of the 2002 U.S. DOE Hydrogen Program Review NREL/CP-610-32405.

40. J.P. Marco-Lozar, J. Juan-Juan, F. Suárez-García, et al. MOF-5 and activated carbons as adsorbents for gas storage. International Journal of Hydrogen Energy, 37 (2011):2370–2381.

41. L. Zhou, Y. Zhou, Y. Sun. A Comparative Study of Hydrogen Adsorption on Superactivated Carbon versus Carbon Nanotubes. International Journal of Hydrogen Energy, 29(2004):475–479.

42. G.G. Tibbetts, G.P. Meisner, C.H. Olk. Hydrogen storage capacity of carbon nanotubes, filaments, and vapor-grown fibers. Carbon, 39(2001):2291-2301.

43. C.C. Ahn, Y. Ye, B.V. Ratnakumar, et al. Hydrogen desorption and adsorption measurements on graphite nanofibers. Applied Physical Letters, 73(1998):3378-3380.

44. A.J. Lachawiec, T.R. DiRamondo, R.T. Yang. A Robust Volumetric Apparatus and Method for Measuring High Pressure Hydrogen Storage Properties of Nanostructured Materials. Review of Science Instruments, 79(2008):063906–063917.

45. A. Chambers, C. Park, R.T.K. Baker, et al. Hydrogen Storage in Graphite Nanofibers. Journal of Physical Chemistry B, 102(1998):4253–4256.

46. B.K. Gupta, O.N. Srivastava. Synthesis and hydrogenation behaviour of graphitic nanofibres. International Journal of Hydrogen Energy, 25(2000):825–830.

47. D.J. Browning, M.L. Gerrard, J.B. Lakeman, et al. Studies into the Storage of Hydrogen in Carbon Nanofibers: Proposal of a Possible Reaction Mechanism. Nano Letters, 2(2002):201–205.

48. A. Dillon, M. Heben. Hydrogen-storage materials for mobile applications. Applied Physicals A, 72 (2001):133–142.

49. A. Sieverts. Zur Kenntnis der Okklusion und diffusion von gases durch Metalle. Z Phys Chem, 60(1907):129–201.

50. A.D. Lueking, L. Pan, D.L. Narayanan, et al. Effect of Expanded Graphite Lattice in Exfoliated Graphite Nanofibers on Hydrogen Storage. Journal of Physical Chemistry B, 109(2005):12710-12717.

51. T. Heine, L. Zhechkov, G. Seifert. Hydrogen storage by physisorption on nanostructured graphite platelets. Physical Chemistry Chemical Physics, 6(2004):980-984.

52. Y. Zhang, V. Mann, D. Reed, et al. Hydrogen storage properties of nanostructured graphite-based materials. Sustainable Power Generation and Supply, International Conference, (2009):1–4. DOI: 10.1109/SUPERGEN.2009.5348032

53. Y. Zhang, D. Book. Hydrogen storage properties of ball-milled graphite with 0.5 wt% Fe. International Journal of Energy Research, (2011). DOI: 10.1002/er.1903.

54. L.P. Ma, Z.S. Wu, J. Li, et al. Hydrogen Adsorption Behavior of Graphene Above Critical Temperature. International Journal of Hydrogen Energy, 349(2009):2329–2332.

55. G. Srinivas, Y. Zhu, R. Piner, et al. Synthesis of Graphene-Like Nanosheets and their Hydrogen Adsorption Capacity. Carbon, 48(2010):630–635.

56. Philippe Serp, José Luis Figueiredo. Carbon Materials for Catalysis. ISBN: 978-0-470-17885-0, 2009.

57. http://web.deu.edu.tr/atiksu/ana07/arit4.html

58. H.F. Stoeckli. Microporous carbons and their characterization: the present state of the art. Carbon, 28(1990):1–6.

59. K. Lenghaus, G.G. Qiao, D.H. Solomon, et al. Controlling Carbon Microporosity: The Structure of Carbons Obtained From Different Phenolic Resin Precursors. Carbon, 40(2002):743-749.

60. K. Gergova, S. Eser, H.H. Schobert. Preparation and characterization of activated carbons from anthracite. Energy Fuels, 7(1993):661–668.

61. M.A. Lillo-Ródenas, D. Lozano-Castelló, D. Cazorla-Amorós, et al. Preparation of activated carbons from Spanish anthracite: II. Activation by NaOH. Carbon, 39(2001):751-759.

62. D. Lozano-Castelló, M.A. Lillo-Ródenas, D. Cazorla-Amorós, et al. Preparation of activated carbons from Spanish anthracite: I. Activation by KOH. Carbon, 39(2001):741-749.

63. http://www.nobelprize.org/educational/physics/microscopes/tem/index.html

64. Harry Marsh, Francisco Rodríguez-Reinoso. Activated Carbon. 2005. ISBN: 978-0-08-044463-5

65. F. Rodríguez-Reinoso. Characterization of Porous Solids. Proceedings of the 6th International Symposium on the Characterization of Porous Solids (COPS-VI), Allicante, Spain, May 8-11, 2002.

66. B. Viswanathan, P. Indra Neel, T.K. Varadarajan. Methods of Activation and Specific Applications of Carbon Materials. NCCR internal Bulletin. http://nccr.iitm.ac.in/e%20book-Carbon%20Materials%20final.pdf.

67. R. Azargohar. Production of Activated Carbon and Its Catalytic Application for Oxidation of Hydrogen Sulphide. PhD thesis, University of Saskatchewan, 2009.

68. B. Viswanathan, P. Indra Neel, T.K. Varadarajan. Methods of Activation and Specific applications of Carbon Materials, National Centre for Catalysis Research, 2009.

69. F. Rodríguez-Reinoso. Handbook of Porous Solids, 3(2002):1766-1827.

70. Y. Guo, S. Yang, K. Yu, et al. The preparation and mechanism studies of rice husk based porous carbon. Materials Chemistry and Physics, 74(2002):320-323.

71. J. Gorka, A. Zawislak, J. Choma, et al. KOH activation of mesoporous carbons obtained by soft-templating. Carbon, 46(2008):1159-1161.

72. Z. Shen, R. Xue. Preparation of activated mesocarbon microbeads with high mesopore content. Fuel Processing Technology, 84(2003):95-103.

73. W. Zhao, V. Fierro, C. Zlotea, et al. Activated carbons doped with Pd nanoparticles for hydrogen storage. International Journal of Hydrogen Energy, 37 (2012) 5072-5080.

74. S. Yoon, S. Lim, Y. Song, et al. KOH activation of carbon nanofibers. Carbon, 42(2004):1723-1729.

75. B.J. Kim, Y.S. Lee, S.J. Park. A study on pore-opening behaviors of graphite nanofibers by a chemical activation process. Journal of Colloid and Interface Science, 306(2007):454-458.

76. B. Cardoso, A.S. Mestre, A.P. Carvalho, et al. Activated Carbon Derived from Cork Powder Waste by KOH Activation: Preparation, Characterization, and VOCs Adsorption. Industrial & Engineering Chemistry Research, 47(2008):5841–5846.

77. Y. Sudaryanto, S.B. Hartono, W. Irawaty, et al. High surface area activated carbon prepared from cassava peel by chemical activation. Bioresource Technology, 97(2006):734-739.

78. M. Evans. The production of chemically-activated carbon. Carbon, 37(1999):269–274.

79. V. Fierro, V. Torné-Fernández, A. Celzard. Methodical study of the chemical activation of Kraft lignin with KOH and NaOH. Microporous and Mesoporous Materials, 101(2007):419–431.

80. M.A. Lillo-Ródenas, D. Cazorla-Amorós, A. Linares-Solano. Understanding chemical reactions between carbons and NaOH and KOH: An insight into the chemical activation mechanism. Carbon, 41(2003):267-275.

81. M.J.B. Evans, E. Halliop, J.A.F. MacDonald. The production of chemically-activated carbon. Carbon, 37(1999):269-274.

82. A. Ahmadpour, D.D. Do. The Preparation of Active Carbons from Coal by Chemical and Physical Activation. Carbon, 34(1996):471-479.

83. A. Ahmadpour, D.D. Do. The Preparation of Activated Carbon from Macadamia Nutshell by Chemical Activation. Carbon, 35(1997):1723-1732.

84. C. John Kirubakaran, K. Krishnaiah, S.K. Seshadri. Experimental study of the production of activated carbon from coconut shells in a fluidized bed reactor. Industrial & Engineering Chemistry Research, 30(1991):2411-2416.

85. Y. El-Sayed, TJ. Bandosz. Adsorption of valeric acid from aqueous solution onto activated carbons: role of surface basic Sites. Journal of Colloid and Interface Science, 273(2004):64-72.

86. W.M.A.W. Daud, A.H. Houshamnd. Textural characteristics, surface chemistry and oxidation of activated carbon. Journal of Natural Gas Chemistry, 19(2010):267-279.

87. J.L. Figueiredo, M.F.R. Pereira, M.M.A. Freitas, et al. Modification of the surface chemistry of activated carbon. Caron, 37(1999):1379-1389.

88. D.M. Nevskaia, E. Castillejos-Lopez, A. Guerrero-Ruiz, et al. Effects of the surface chemistry of carbon materials on the adsorption of phenol-aniline mixtures from water. Carbon, 42(2004): 653–665.

89. M. Goyal, V.K. Rattan, D. Aggarwal, et al. Removal of copper from aqueous solutions by adsorption on activated carbons, Colloids Surf. A: Physicochemical and Engineering Aspects, 190(2001):229- 238.

90. J. Guo, A.C. Lua. Effect of surface chemistry on gas-phase adsorption by activated carbon prepared from oil-palm stone with pre-impregnation. Separation and Purification Technology, the Netherlands, 18(2000):47-55.

91. C.O. Ania. Removal of naphthalene from aqueous solution on chemically modified activated carbons. Water research, 41(2007):333–340.

92. P. Tarazona. Solid–fluid transition and interfaces with density functional approaches. Surface Science. 331-333(1995):989–94.

93. Y.J. Lee, Y. Uchiyama, L.R. Radovic. Effects of boron doping in low- and high-surface-area carbon powders. Carbon, 42(2004):2233-2244.

94. Q. Zha, X. Hu, Y. Guo, et al. Improved antioxidative ability of porous carbons by boron-doping. New Carbon Materials, 23(2008):356–360.

95. D. Wang, F. Li, Z. Chen, et al. Synthesis and Electrochemical Property of Boron-Doped Mesoporous Carbon in Supercapacitor. Chemistry of Materials, 20(2008):7195–7200.

96. M. Chen, G. Wu, G. Zhu, et al. Characterization and electrochemical investigation of boron-doped mesocarbon microbead anode materials for lithium ion batteries. Journal of Solid State Electrochemistry, DOI:10.1007/s100080100244, 420-427.

97. P. Aksoy, C.B. Clifford. Preparation and characterization of boron containing carbons derived from coal tar pitch. The Pennsylvania State University.

98. R. Azargohar. Production of Activated Carbon and Its Catalytic Application for Oxidation of Hydrogen Sulphide. PhD thesis, University of Saskatchewan, 2009.

99. A. Aburub, DE. Wurster. Phenobarbital Interations with Derivatized Activated Carbon Surfaces. Journal of Colloid and Interface Science, 296(2006):79-85.

100. J.C.U. Pittman, G.R. He, B. Wu, et al. Chemical modification of carbon fiber surfaces by nitric acid oxidation followed by reaction with tetraethylenepentamine. Carbon, 35(1997):317-331.

101. R.C. Bansal, M. Goyal. Activated carbon adsorption. 2005. ISBN: 9780824753443 0824753445.

102. B. Streppel. Hydrogen Adsorption on Metal-Organic Frameworks. PhD thesis, 2011.

103. F. Rouquerol, J. Rouquerol, K.S.W. Sing. Adsorption by powers and porous solids, Academic press, 1-25, 1999.

104. M.M. Dubinin, E.D. Zaverina. Extended Abstracts 21st Biennal Conference on Carbon. 65 (1949) 295.

105. K.R. Carrington. Fabrication and optimization of nano-structured composites for energy storage. University of California, Berkeley. PhD thesis, 2009.

106. F. Stoeckli, A. Slasli, D. Hugi-Cleary, et al. The characterization of microporosity in carbons with molecular sieve effects. Microporous and Mesoporous Materials, 51(2002):197–202.

107. H. Wang, Q. Gao, J. Hu. High Hydrogen Storage Capacity of Porous Carbons Prepared by Using Activated Carbon. Journal of the American Chemical Society, 131(2009):7016–7022.

108. B. Panella, M. Hirscher, S. Roth. Hydrogen adsorption in different carbon nanostructures. Carbon, 43(2005):2209–2214.

109. W. Xu, K. Takahashia, Y. Matsuoa, et al. Hydrogen Storage Capacity of various Carbon Materials. Int. J. Hydrogen Energy, 32(2007)2504–2512.

110. N. Texier-Mandoki, J. Dentzer, T. Piquero, et al. Hydrogen storage in activated carbon materials: Role of the nanoporous texture Carbon, 42(2004):2744-2747.

111. M. Rzepka, P. Lamp, M.A. de la Casa-Lillo. Physisorption of hydrogen on microporous carbon and carbon nanotubes. Journal of Physical Chemistry B, 102(1998):10894-10898.

112. R. Gadiou, S.E. Saadallah, T. Piquero, et al. The Influence of Textural Properties on the Adsorption of Hydrogen on Ordered Nanostructured Carbons. Micropor. Mesopor. Mater, 79(2005):121–128.

113. V. Fierro, A. Szczurek, C. Zlotea, et al. Experimental evidence of an upper limit for hydrogen storage at 77 K on activated carbons. Carbon, 48(2010):1902-1911.

114. http://www.hydrogen.energy.gov/pdfs/review05/stp_46_cabasso.pdf

115. A. Celzard, V. Fierro, JF. Mareche, et al. Advanced preparative strategies for activated carbons designed for the adsorptive storage of hydrogen. Adsorpt Sci Technol, 25(2007):129-142.

116. S. Patchkovskii, JS. Tse, SN. Yurchenko, et al. Graphene nanostructures as tunable storage media for molecular hydrogen. Proceeding of the National Academy of Sciences, 102(2005):10439-10444.

117. P.A. Georgiev, D.K. Ross, P. Albers, et al. The rotational and translational dynamics of molecular hydrogen physisorbed in activated carbon: a direct probe of microporosity and hydrogen storage performance. Carbon, 44(2006):2724-2738.

118. I. Cabria, MJ. Lopez, JA. Alonso. The optimum average nanopore size for hydrogen storage in carbon nanoporous materials. Carbon, 45(2007):2649-2658.

119. Y. Gogotsi, C. Portet, S. Osswald, et al. Importance of pore size in high-pressure hydrogen storage by porous carbons. International Journal of Hydrogen Energy, 34(2009):6314-6319.

120. B. Panella, M. Hirscher, S. Roth. Hydrogen adsorption in different carbon nanostructures. Carbon, 43(2005):2209–2214.

121. RK. Agarwal, JS. Noh, A. Schwarz, et al. Effect of surface acidity of activated carbon on hydrogen storage. Carbon, 25(1987):219–226.

122. W. Su, Y. Zhou, L Wei, et al. Effect of microstructure and surface modification on the hydrogen adsorption capacity of active carbons. New Carbon Materials, 22(2007):135-140.

123. H. Takagi, H. Hatori, Y. Yamada, et al. Hydrogen adsorption properties of activated carbons with modified surfaces. Journal of Alloys and Compounds, 385(2004):257–263.

124. B.J. Kim, S.J. Park. Influence of surface treatments on micropore structure and hydrogen adsorption behavior of nanoporous carbons. Journal of Colloid and Interface Science, 311(2007):619-621.

125. C. Huang, H. Chen, C. Chen, et al. Effect of surface oxides on hydrogen storage of activated carbonin. Separation and Purification Technology, 70(2010):291-295.

126. Y.G. Zhou, X.T. Zu, F. Gao, et al. Adsorption of hydrogen on boron-doped graphene: A first-principles prediction. Journal of Applied Physicals, 105(2009):014309-014312.

127. Z. Zhou, X. Gao, J. Yan, et al. Doping effects of B and N on hydrogen adsorption in single-walled carbon nanotubes through density functional calculations. Carbon, 44(2006):939-947.

128. L. Wang, R.T. Yang. Hydrogen Storage Properties of N-Doped Microporous Carbon. Journal of Physical Chemistry C, 113(2009):21883–21888.

129. Z.H. Zhu, G.Q. Lu, H. Hatori. New Insights into the Interaction of Hydrogen Atoms with Boron-Substituted Carbon. Journal of Physical Chemistry B, 110(2006):1249–1255.

130. M. Sankaran, B. Viswanathan. The role of heteroatoms in carbon nanotubes for hydrogen storage. Carbon, 44(2006):2816-2821.

131. T.C.M. Chung, Y. Jeong, Q. Che, et al. Synthesis of Microporous Boron-Substituted Carbon (B/C) Materials Using Polymeric Precursors for Hydrogen Physisorption. J. Am. Chem. Soc, 130(2008):6668-6669.

132. B. Viswanathan, M. Sankaran. Hydrogen storage in boron substituted carbon nanotubes. Carbon, 45(2007):1628-1635.

133. L. Wang, F.H. Yang, R.T. Yang. Hydrogen storage properties of B- and N-doped microporous carbon. AIChE Journal, 55(2009):1823-1833.

134. A. Badzian, T. Badzian, E. Breval, et al. Nanostructured, nitrogen-doped carbon materials for hydrogen storage. Thin Solid Films, 398−399(2001):170-174.

135. K.Y. Kang, B.I. Lee, J.S. Lee. Hydrogen adsorption on nitrogen-doped carbon xerogels. Carbon, 47(2009):1171-1180.

136. Z. Yang, Y. Xia, X. Sun, et al. Preparation and Hydrogen Storage Properties of Zeolite-Templated Carbon Materials Nanocast via Chemical Vapor Deposition: Effect of the Zeolite Template and Nitrogen Doping. Journal of Physical Chemistry B, 110(2006):18424-18431.

137. Z.H. Zhu, H. Hatori, S.B. Wang, et al. Insights into hydrogen atom adsorption on and the electrochemical properties of nitrogen-substituted carbon materials. Journal of Physical Chemistry B, 109(2005):16744-16749.

138. Z. Zhang, K. Cho. Ab initio study of hydrogen interaction with pure and nitrogen-doped carbon nanotubes. Physical Review B, 75(2007):075420-075426.

139. X. Yongde, S. Gavin, DM. Walker, et al. Hydrogen Storage in High Surface Area Carbons: Experimental Demonstration of the Effects of Nitrogen Doping. Journal of the American Chemical Society, 131(2009):16493–16499.

140. A.J. Robell, E.V. Ballou, M. Boudart. Surface Diffusion of Hydrogen on Carbon. Journal of Physical Chemistry B, 68(1964):2748–2753.

141. L. Wang, R.T. Yang. Hydrogen Storage Properties of Carbons Doped with Ruthenium, Platinum, and Nickel Nanoparticles. Journal of Physical Chemistry C, 112(2008):12486–12494.

142. G.M. Pajonk. Contribution of Spillover Effects to Heterogeneous Catalysis, Applied Catalysis A, 202(2000):157-169.

143. J.H. Sinfelt, P.J. Lucchesi. Kinetic Evidence for the Migration of Reactive Intermediates in Surface Catalysis. Journal of the American Chemical Society, 85(1963):3365–3367.

144. D. Lupu, AR. Biris, I. Misan, et al. Hydrogen uptake by carbon nanofibers catalyzed by palladium. International Journal of Hydrogen Energy, 29(2004):97-102.

145. R. Zacharia, K.Y. Kim, A.K.M. Fazle Kibria, et al. Enhancement of hydrogen storage capacity of carbon nanotubes via spill-over from vanadium and palladium nanoparticles. Chemical Physics Letters, 412(2005):369-375.

146. M. Zielinski, R. Wojcieszak, S. Monteverdi, et al. Hydrogen storage on nickel catalysts supported on amorphous activated carbon. Commun, 6(2005):777-783.

147. C. Back, G. Sandi, J. Prakash, et al. Hydrogen Sorption on Palladium-Doped Sepiolite-Derived Carbon Nanofibers. Journal of Physical Chemistry B, 110(2006):16225–16231.

148. A. Anson, E. Lafuente, E. Urriolabeitia, et al. Hydrogen Capacity of Palladium-Loaded Carbon Materials. Journal of Physical Chemistry B, 110(2006):6643–6648.

149. J.A. Schwarz. Metal Assisted Carbon Cold Storage of Hydrogen. U.S. Patent 4 716 736, January 5, 1988.

150. W. Zhao, R.T. Yang. Enhanced Hydrogen Storage on Pt-Doped Carbon by Plasma Reduction. Journal of Physical Chemistry C, 114(2010):5956–5963.

151. Y. Li, R.T. Yang. Hydrogen Storage on Carbon Doped with Platinum Nanoparticles Using Plasma Reduction. Industrial & Engineering Chemistry Research, 46(2007):8277–8281.

152. Y.W. Li, R.T. Yang. Significantly Enhanced Hydrogen Storage in Metal–Organic Frameworks via Spillover. Journal of the American Chemical Society, 128(2006):726–727.

153. Y.W. Li, R.T. Yang. Hydrogen Storage in Metal–Organic Frameworks by Bridged Hydrogen Spillover Journal of the American Chemical Society, 128(2006):8136–8137.

154. A.J.Jr. Lachawiec, G. Qi, R.T. Yang. Hydrogen Storage in Nanostructured Carbons by Spillover: Bridge-Building Enhancement. Langmuir, 21(2005):11418–11424.

155. A.D. Lueking, R.T. Yang. Hydrogen Spillover from a Metal Oxide Catalyst onto Carbon Nanotubes—Implications for Hydrogen Storage. Journal of Catalysis, 206(2002):165-168.

156. L. Wang, N.R. Stuckert, H. Chen, et al. Effects of Pt Particle Size on Hydrogen Storage on Pt-Doped Metal–Organic Framework IRMOF-8. Journal of Physical Chemistry C, 115(2011):4793–4799.

157. C. Tsao, Y. Liu, M. Li, et al. Neutron Scattering Methodology for Absolute Measurement of Room-Temperature Hydrogen Storage Capacity and Evidence for Spillover Effect in a Pt-Doped Activated Carbon. The Journal of Physical Chemistry Letters, 1(2010):1569–1573.

158. C.Tsao, Y. Liu, H. Chuang, et al. Hydrogen Spillover Effect of Pt-Doped Activated Carbon Studied by Inelastic Neutron Scattering. The Journal of Physical Chemistry Letters, 2(2011):2322–2325.

159. A.P. Pamitar, J.T.Jr. Yates. Spectroscopic Detection of Hydrogen Atom Spillover from Au Nanoparticles Supported on TiO2: Use of Conduction Band Electrons. Journal of Physical Chemistry C, 111(2007):2959–2964.

160. L. Chen, A.C. Cooper, G.P. Pez, et al. Mechanistic Study on Hydrogen Spillover onto Graphitic Carbon Materials. Journal of Physical Chemistry C, 111(2007):18995–19000.

161. G.M. Psofogiannakis, G.E. Froudakis. DFT Study of the Hydrogen Spillover Mechanism on Pt-Doped Graphite. Journal of Physical Chemistry C, 113(2009):14908–14915.

162. D. Saha, S. Deng. Hydrogen Adsorption on Ordered Mesoporous Carbons Doped with Pd, Pt, Ni, and Ru. Langmuir, 25(2009):12550–12560.

163. A. Reyhani, S.Z. Mortazavi, S. Mirershadi, et al. Hydrogen Storage in Decorated Multiwalled Carbon Nanotubes by Ca, Co, Fe, Ni, and Pd Nanoparticles under Ambient Conditions. Journal of Physical Chemistry C, 115(2011):6994–7001.

164. Y. Suttisawat, P. Rangsunvigit, B. Kitiyanan, et al. Investigation of hydrogen storage capacity of multi-walled carbon nanotubes deposited with Pd or V. International Journal of Hydrogen Energy, 34(2009):6669-6675.

165. L. Wang, F.H. Yang, R.T. Yang. Effect of Surface Oxygen Groups in Carbons on Hydrogen Storage by Spillover. Industrial of Engineering Chemistry Research, 48(2009):2920–2926.

166. K.J. Gross, R. Carrington. Best practices for the characterization of hydrogen storage materials, 2008.

167. Z. Wang, F.H. Yang, R.T. Yang. Enhanced Hydrogen Spillover on Carbon surfaces Modified by Oxygen Plasma. Journal of Physical Chemistry C, 114(2010):1601–1609.

168. H. Wu, X. Fan, J.L. Kuo, et al. DFT Study of Hydrogen Storage by Spillover on Graphene with Boron Substitution. Journal of Physical Chemistry C, 115(2011):9241–9249.

169. C. Zlotea，P. Moretto，T. Steriotis. A Round Robin characterization of the hydrogensorptionproperties of a carbon based material. International Journal of Hydrogen Energy, 34 (2009):3044-3057.

170. K. Kaneko, C. Ishii. Super high surface area determination of microporous solids. Colloids and Surface, 67(1992):203-212.

171. H.O. Pierson. Handbook of carbon, graphite, diamond, and fullerenes: properties, processing, and applications. 1993.

172. www.mic-instrument.com

173. S. Brunauer, P.H. Emmet, E. Teller. Adsorption of gases in multimolecular layers. Journal of the American Chemical Society, 60(1938):309–319.

174. M.M. Dubinin. Fundamentals of the theory of adsorption in micropores of carbon adsorbents–characteristics of their adsorption properties and microporous structures. Carbon, 27(1989):457–467.

175. S.J. Gregg, K.S.W. Sing. Adsorption, surface area and porosity. 2nd ed. Academic Press, London, 1982.

176. K Kaneko. Specific intermolercular structures of gases confined in carbon nanospace. Carbon, 38(2000):287-303.

Conclusion

Le stockage de l'hydrogène dans des charbons actifs préparés, caractérisés et optimises à l'IJL a donc fait l'objet de cette thèse. L'objectif principal était de développer des matériaux dont les propriétés d'adsorption sont réversibles et à même de s'approcher au plus prêt des objectifs de stockage définis par l'US DOE pour 2015, soit 5.5% massiques. Dans cette optique, quatre étapes ont été successivement suivies : (1) l'étude et la compréhension des conditions expérimentales de préparation de ces adsorbants ; (2) l'optimisation de leur texture poreuse pour le stockage d'hydrogène ; (3) l'étude des corrélations entre capacité de stockage d'hydrogène et paramètres texturaux (aire spécifique, volumes poreux et distributions de tailles de pores) ; (4) l'étude du dopage des matériaux par de l'azote et des nanoparticules métalliques.

Les paramètres de contrôle de la porosité, nature de l'agent d'activation, rapport massique agent activant/précurseur (W), température (T), et vitesse de chauffe ont été étudiés. Les meilleurs adsorbants ont été obtenus par activation des anthracites avec KOH. Nous avons montré que les aires spécifiques et les volumes de micropores augmentent linéairement avec la température et la quantité d'agent activant jusqu'à un plateau, au-delà duquel des valeurs moindres sont obtenues. Ces deux variables expérimentales sont les plus importantes et gouvernent la texture des adsorbants et donc leurs performances pour le stockage d'hydrogène. La vitesse de chauffe a, en revanche, un effet négligeable du moins dans la gamme de valeurs explorée. L'analyse statistique a bien confirmé que les grandeurs W et T sont significatives pour optimiser un adsorbant pour l'hydrogène. Nous avons développé un modèle quadratique sur la base des paramètres W^2, W, T^2 et T, qui peut être utilisé pour prédire la capacité d'hydrogène d'un anthracite activé dans telle ou telle condition.

La méthodologie de surface de réponse (RSM) a notablement aidé à produire des charbons actifs optimisés, conduisant à des capacités de stockage jusqu'à 6.6% en masse d'adsorbant à 77K et 4 MPa. Cette performance a été obtenue avec un charbon préparé avec W = 4 et T = 1023 K. L'analyse de variance a montré par ailleurs que le rapport massique KOH/anthracite, W, est le seul paramètre significatif lorsque

l'activation chimique est conduite à des valeurs de T et de W dans les gammes 998 – 1048 K et 2 – 4, respectivement.

Des corrélations entre la capacité de stockage et la texture poreuse ont été établies expérimentalement pour de nombreux charbons actifs. La capacité de stockage a ainsi été trouvée directement proportionnelle à la surface spécifique BET, tant que la valeur de celle-ci n'est pas supérieure à sa valeur théorique limite de 2630 m^2/g. En accord avec ce résultat, la capacité de stockage est également proportionnelle au volume microporeux. L'évolution de la quantité d'hydrogène adsorbée par 14 charbons actifs, dont des matériaux commerciaux, a été ajustée en fonction des volumes poreux, découpés selon 4 gammes de tailles de pores (< 0.5, 0.5 – 0.7, 0.7 – 2 et > 2 nm) en utilisant une expression polynômiale. Nous avons pu montrer que, pour obtenir des capacités de stockage supérieures à 3% en masse, la présence de pores plus larges que 0.7 nm était nécessaire. Ce résultat n'est pas en contradiction avec la taille optimale de pore, proche de 0.7 nm, qui avait été suggérée par d'autres auteurs. Il exprime simplement que, pour augmenter les performances en stockage, il faut davantage développer la porosité et l'aire spécifique, ce qui ne peut se faire qu'au travers d'un élargissement de la distribution de tailles de pores.

Le dopage par de l'azote ou des nanoparticules métalliques est une stratégie pour tenter d'améliorer les performances en stockage d'hydrogène d'un charbon actif donné. Trois charbons présentant des surfaces spécifiques comprises entre 2450 et 3200 m^2/g ont été dopés par des nanoparticules de palladium à différents taux de charge, dans la gamme 1.3 – 10.0 % massiques. Nous avons vu que la taille des particules correspondantes dépendait du taux de Pd mais également de l'aire spécifique des charbons de départ, les plus petites particules étant obtenues aux faibles taux de charge dans les substrats de surface élevée. Les plus hauts taux de charge ayant peu d'influence sur la distribution de tailles de pores du support carboné, nous en avons déduit que les particules de Pd, plus grandes, restaient à confinés sur la surface externe des grains de charbon actif. A 298K et jusqu'à 1 MPa, la quantité

d'hydrogène adsorbée est proportionnelle à la quantité de Pd. A plus haute pression, elle dépend surtout du volume microporeux, aussi l'addition de Pd n'apporte guère d'amélioration. A 77K, la capacité de stockage dépend fondamentalement de la texture poreuse, et par conséquent la présence de Pd est défavorable. Elle réduit en effet non seulement le volume microporeux accessible, mais elle augmente la masse de l'adsorbant, réduisant davantage encore sa capacité massique. En dopant les matériaux avec de l'azote entre 4 et 7% en masse, l'aire spécifique et le volume microporeux diminuent. Les résultats montrent alors que ce type de dopage a un impact négatif sur les performances en stockage d'hydrogène.

Des capacités de stockage jusqu'à 6.6 % en masse de l'adsorbant ont été mesurées à 77K et 4 MPa. Cette valeur est l'une des plus élevées parmi celles qui ont été rapportées dans la littérature. En comparaison, le fameux charbon commercial MAXSORB-3 a stocké « seulement » 5.8 % dans les mêmes conditions. Nos matériaux ont par ailleurs donné des capacités de 1.0 % massique à 298K et 20 MPa. Nous avons pu montrer que ces performances supérieures sont dues à la fois à une aire spécifique plus élevée et à une distribution de tailles de pores décalée vers les plus petites largeurs.

Ces travaux sont actuellement approfondis de par les travaux d'une seconde thèse en cours sur le même thème.

Résumé

Cette thèse présente la préparation, la caractérisation et l'évaluation en termes de capacité de stockage d'hydrogène de charbons actifs optimisés pour cette application. L'objectif était de développer des matériaux qui puissent atteindre ou approcher la capacité de stockage visée par le Département Américain à l'Energie pour 2015, soit 5.5 % en masse du système de stockage. Dans ce but, les recherches rapportées ici se sont focalisées sur : (1) l'étude et la compréhension des conditions expérimentales de préparation de ces adsorbants ; (2) l'optimisation de leur texture poreuse pour le stockage d'hydrogène ; (3) l'étude des corrélations entre capacité de stockage d'hydrogène et paramètres texturaux (aire spécifique, volumes poreux et distributions de tailles de pores) ; (4) l'étude du dopage des matériaux par de l'azote et des nanoparticules métalliques. Des capacités de stockage égales à 6.6 % en masse de l'adsorbant à 77K et 4 MPa d'une part, et de 1.0 % massique à 298K et 20 MPa d'autre part, ont été obtenues dans ce travail, parmi les plus élevées qui aient été rapportées dans la littérature.

Mots-clés: Charbon actif; Stockage d'hydrogène; Adsorption; Analyse statistique; Dopage.